# Galaxies and supermassive black holes evolving in a secular universe

**Mauricio Cisternas**

Max-Planck-Institut für Astronomie

Heidelberg 2011

**Dissertation in Astronomy**

submitted to the

Combined Faculties of the Natural Sciences and Mathematics

of the Ruperto-Carola-University of Heidelberg, Germany,

for the degree of

Doctor of Natural Sciences

presented by

**Mauricio Cisternas**

born in Santiago, Chile

Oral examination: November 15$^{th}$, 2011

# GALAXIES AND SUPERMASSIVE BLACK HOLES EVOLVING IN A SECULAR UNIVERSE

REFEREES: DR. KNUD JAHNKE

PROF. DR. JOCHEN HEIDT

# ABSTRACT

Most massive galaxies host a supermassive black hole (BH), that had most of its mass built up throughout bright periods of vigorous accretion, during which it is referred to as an active galactic nucleus (AGN). In the local universe it has been observed that BH mass ($M_{\mathrm{BH}}$) follows tight correlations with various properties of the galactic bulge in which it resides. This led to the currently popular "co-evolution" picture, in which most present-day galaxies went through at least one active phase in the past, during which a link between galaxy and BH gets established. However, more robust observational constraints are required on how galaxy and BH related at earlier times, and which mechanism is responsible for triggering these BH growth phases. This thesis studies a large sample of AGN out to $z \sim 1$ from the COSMOS survey, selected from their X-ray emission and imaged in finest detail with the *Hubble Space Telescope*, allowing the study of growing BHs together with their host galaxies. We present new constraints on the ratio of BH mass to *total* galaxy stellar mass ($M_*$) over the last 7 Gyr for 32 type-1 AGN. We show that the $M_{\mathrm{BH}} - M_*$ ratio at $z \sim 0.7$ is consistent with the local relation between BH mass and galactic *bulge* mass. For these galaxies to obey the local relation only a redistribution of disk-to-bulge mass is needed, likely driven by passive secular evolution.

We then tackle and answer a 30-year old question: what is the relevance of major mergers and interactions as triggering mechanisms for AGN activity? We visually analyze the morphologies of 140 AGN out to $z \sim 1$ looking for signatures of recent mergers, and compare them with a control sample of over 1200 matched inactive galaxies. We find that the merger fraction of the AGN host galaxies is statistically identical to the corresponding inactive galaxy population, at roughly 15%. Together with the fact that the majority of the AGN host galaxies are disk-dominated, unlikely relics of a recent major merger, these results are the strongest evidence to date that secular evolution rather than major merging has dominated BH fueling at least since $z \sim 1$, and that BHs and galaxies have, for the last 7 Gyr, evolved in a secular universe.

# ZUSAMMENFASSUNG

Die meisten massereichen Galaxien enthalten in ihrem Zentrum supermassereiche Schwarze Löcher (BH), die den Großteil ihrer Masse in Phasen starker Akkretion aufbauen. Das während dieser Zeit hell leuchtende Zentrum wird aktiver Galaxienkern genannt (AGN). Beobachtungen im lokalen Universum zeigen eine enge Korrelation zwischen der Schwarzlochmasse und verschiedenen Eigenschaften des stellaren *Bulges* der Galaxie. Diese Erkenntnis führte zur Einführung des populären Szenarios der "Ko-Evolution", in dem die meisten der heutigen Galaxien mindestens eine aktive Wachstumsphase durchleben wärend der eine Verbindung zwischen der Galaxie und dem schwarzen Loch hergestellt wurde. Um das Verhältnis von BH und Galaxien zu frühen kosmologischen Zeiten weitergehend zu untersuchen und die Mechanismen und Auslöser des gemeinsamen Wachstums herauszufinden werden jedoch robustere Einschränkungen durch Beobachtungen benötigt. Diese Arbeit analysiert eine große Stichprobe von AGN bis hin zu $z \sim 1$ aus dem COSMOS *Survey*. Die Objekte wurden durch Röntgenstrahlung selektiert und im höchster räumlicher Auflösung mit dem Hubble Weltraumteleskop beobachtet, was eine Untersuchung wachsender BHs und Galaxien ermöglicht. Wir präsentieren neue Einschränkungen des Verhältnisses zwischen Schwarzlochmasse ($M_{BH}$) und totaler stellarer Masse ($M_*$) während der letzten 7 Milliarden Jahre für 32 Typ-1 AGN. Wir zeigen, dass das Verhältnis $M_{BH} - M_*$ bei $z \sim 0.7$ konsistent ist mit der lokalen Beziehung zwischen BH und der Masse in der stellaren Auswölbung. Damit diese Galaxien die lokale Relation befolgen wird nur eine Umverteilung von stellarer Masse aus der Scheibe in den *Bulge* benötigt, wahrscheinlich ausgelöst durch passive langfristige Prozesse.

Desweiteren beantworten wir eine 30 Jahre alte Frage: Welche Rolle spielen Verschmelzungen von Galaxien vergleichbarer Größe (*major merger*) als Auslöser für die AGN-Aktivität? Dafür analysieren wir die Morphologie von 140 AGN bis $z \sim 1$ in Bezug auf Anzeichen für kürzliche Verschmelzungen und vergleichen diese mit einer Kontrollstichprobe von über 1200 von Masse und Typ her ähnlicher inaktiver Galaxien. Der Anteil der verschmelzenden Galaxien beider Proben ist statistisch ununterscheidbar und liegt bei etwa 15%. Zusammen mit der Tatsache, dass die Mehrheit der AGN beinhaltenden Galaxien scheibendominiert sind, und daher als Relikte eines kürzlichen *major merger* nicht in Frage kommen, sind diese Ergebnisse heute der stärkste Beweis dafür, das mindestens seit $z \sim 1$ langfristig ablaufende Prozesse und nicht *major merger* das Wachstum von Schwarzen Löchern bestimmte. Über die letzten sieben Milliarden Jahre entwickelten sich folglich Schwarze Löcher und Galaxien in einem säkularen Universum.

# CONTENTS

# CHAPTER 1

## INTRODUCTION

**The widely accepted Lambda Cold Dark Matter ($\Lambda$CDM) paradigm of structure formation predicts a hierarchical cosmogony: initially small dark matter haloes will continuously merge to produce larger structures. As a natural consequence, "baryonic" galaxies hosted by these haloes will also evolve through merging. Galaxies will go through at least one active phase, in which the supermassive black holes known to exist in the centers of most massive galaxies will experience most of their growth. The correlation between the properties of these black holes and their host galaxies gave rise to a picture of co-evolution between them. Here we give a brief historical overview of some of our current knowledge about the universe, galaxies and black holes, to set the stage for the work presented in this thesis.**

## 1.1  Our hierarchical universe

At least until the late 16th century, the accepted cosmological paradigm placed the Earth at the center of the universe, with the other planets, the Sun, and stars rotating around it, as shown in the illustration in Figure 1.1. A lot has changed since then[1]. Today, not only do we know that the Earth is actually rotating around the Sun, a star a hundred times larger in size and five orders of magnitude more massive than our

---

[1]Nevertheless, the public understanding of science has proved to be hard to reform. National studies in the United States during the late 90s found that 1 in 5 American adults believed that the Sun rotates around the Earth (Miller 2004).
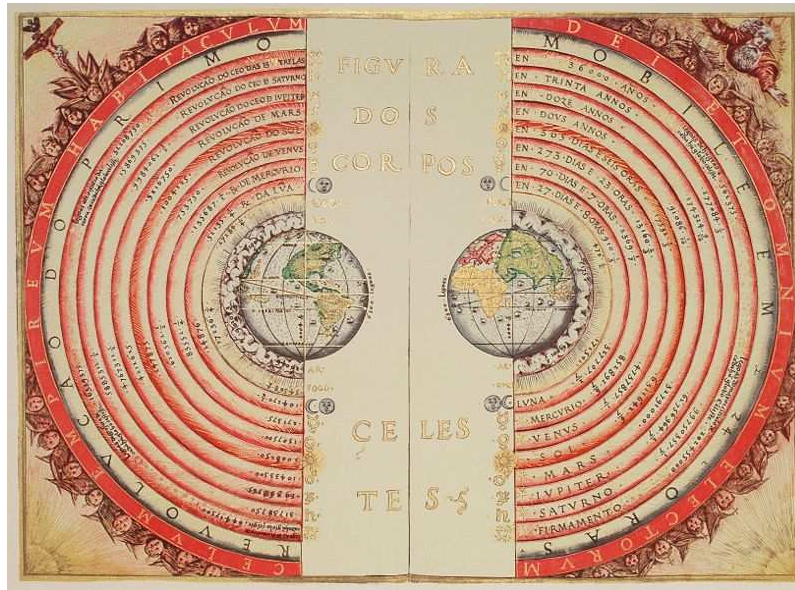
**Figure 1.1:** The accepted cosmological paradigm until the early 1700s. An illustration of the geocentric model of the universe from 16th century cosmographer Bartolomeu Velho's *Cosmographia*, depicting the Earth in the center, and everything else rotating around it.

planet, but we also know that as a star it is a fairly small-sized one, and only one among 300 billion other stars that make up a flattened disk-like structure known as the Milky Way, our Galaxy. We have also come to learn that some of the bright nebulae observed in the night-sky, such as Andromeda, were not part of the Milky Way but rather other galaxies in their own right, as inferred by Hubble (1929) by estimating their distance from us. The Milky Way together with roughly 30 other galaxies in the neighborhood forms a gravitationally-bound group known as the Local Group, which in turn is only a small group among many other groups and clusters made up of thousands of other galaxies which together constitute the Virgo Supercluster, one among millions of other superclusters.

As if our place in the universe has not been already minimized enough over the last 400 years, during the 20th century we came to know that ordinary visible matter accounts for only 1/5 of the overall mass budget of the universe, with the rest being non-baryonic dark matter–its existence already predicted early on by Zwicky (1933). Only after becoming aware that matter, ordinary and dark altogether, makes up just over 1/4 of the *total* energy density of the universe –the rest corresponding to an unknown force responsible for driving the expansion of the universe to which we refer to as dark energy (Riess et al. 1998; Perlmutter et al. 1999)– did we get a

slightly clearer picture of the present-day paradigm.

The cosmological principles state that our universe is homogenous and isotropic, i.e., there is no preferred location, and on large scales it is homogenous in all directions. In the current standard "ΛCDM" model, our expanding universe is largely dominated (73%) by dark energy, denoted as the cosmological constant Λ. Cold Dark Matter on the other hand, accounts for roughly 23% of the remaining energy density, but makes up most of the matter density of the universe. While the exact non-baryonic particles that compose dark matter are still unknown (for a review, see Feng 2010), a few things are certain: it emits no electromagnetic radiation, travels at slow speeds, and is collisionless. The ΛCDM model successfully explains the cosmic microwave background (Smoot et al. 1992; Komatsu et al. 2011) as well as the observed large scale galaxy clustering (e.g., Peacock 1991; Padilla & Baugh 2003; Percival et al. 2007).

In the current paradigm, large-scale structure originated from initially small primordial density fluctuations amplified by gravity (e.g., Peebles 1980). These initial perturbations are thought to be random quantum fluctuations from the pre-inflationary era magnified by the exponential expansion of the universe (Hawking 1982). While at very early times after inflation the growth of these density fluctuations is believed to have been linear, as time goes by and the mass scales increase we enter a non-linear regime of gravitational collapse (Zel'Dovich 1970; Press & Schechter 1974). These overdense, virialized regions grow hierarchically, from the bottom-up: larger dark matter potential wells –haloes– form later from the accretion and mergers of smaller progenitors.

Large-scale numerical simulations (e.g., Springel et al. 2005b) have been successful in following the non-linear evolution of these initial perturbations and have been able to reproduce the observed distribution of matter in the universe, assuming that light emitted by baryonic matter traces the invisible dark matter. Baryonic matter in the form of gas will follow the dark matter halo gravitational potential, and will subsequently cool and collapse to the center of the halo, leading to the formation of stars and subsequently galaxies (White & Rees 1978). Unlike modeling the large scale distribution of dark matter, following the evolution of ordinary matter is much more complex. Baryonic matter can undergo a wealth of different processes and interactions: among other things, it can cool, heat up, be shocked, and can react to pressure gradients and magnetic fields. A numerical model that fully describes all these processes at small scales soon becomes infeasible due to numerical resolu-

tion limitations, and hence alternative recipes such as "semi-analytical" models have been successful in reproducing empirical luminosity functions and trends in color and morphology of galaxies (e.g., Kauffmann et al. 1993; Cole et al. 1994; Kauffmann et al. 1999; Somerville & Primack 1999). These models follow the merging histories of the dark matter haloes, and separately use simple analytic recipes to trace the evolution of the baryonic matter within them. Thanks to their flexibility, semi-analytic models have been able to overcome many failed initial attempts at reproducing observations, such as the faint-end slope of the luminosity function, and the steep break in the massive-end of the galaxy mass function. Specifically, in the latter case, models predicted an excess of massive galaxies and therefore a mechanism to suppress the continuous cooling of gas was required to keep more stars from forming. Feedback from supernova explosions alone did not have the necessary energy output to suppress gas cooling to the necessary level (Benson et al. 2003). However, the inclusion of the feeback from active galactic nuclei (AGN) in the galaxy formation recipes did seem to provide the necessary energy needed to regulate the cooling processes and star formation (Silk & Rees 1998), reproducing the observed massive end of the galaxy mass function (e.g., Croton et al. 2006; Bower et al. 2006). Since then, AGN have been thought to possibly play a central role in galaxy evolution.

## 1.2   Active Galactic Nuclei: What are they?

Today we refer to an actively accreting supermassive black hole (BH) in the center of a galaxy as an AGN. Surrounding the BH, the accretion disk will be heated up to extreme temperatures from the enormous friction of the infalling matter, converting kinetic energy into heat. The energy output is such that it can outshine the galaxy by a few orders of magnitude and, astonishingly, the AGN "engine" will be contained within the order of a mere hundred AU[2].

Active galaxies were already unknowingly observed in the early 20th century, as Fath (1909) and Slipher (1917) noted unusually strong emission lines in the spectra of the spiral galaxy NGC 1068, shown in the top panel of Figure 1.2 together with its optical image. It was Seyfert (1943) who selected six galaxies with particularly luminous central regions and studied their optical spectra, finding that all of them had very bright emission lines, therefore realizing that these were a whole different class of objects. As more of these "Seyfert galaxies" were observed, Khachikian & Weedman

---

[2]The radius of a typical spiral galaxy is on the order of 10 kpc, with 1 pc = 206,265 AU.
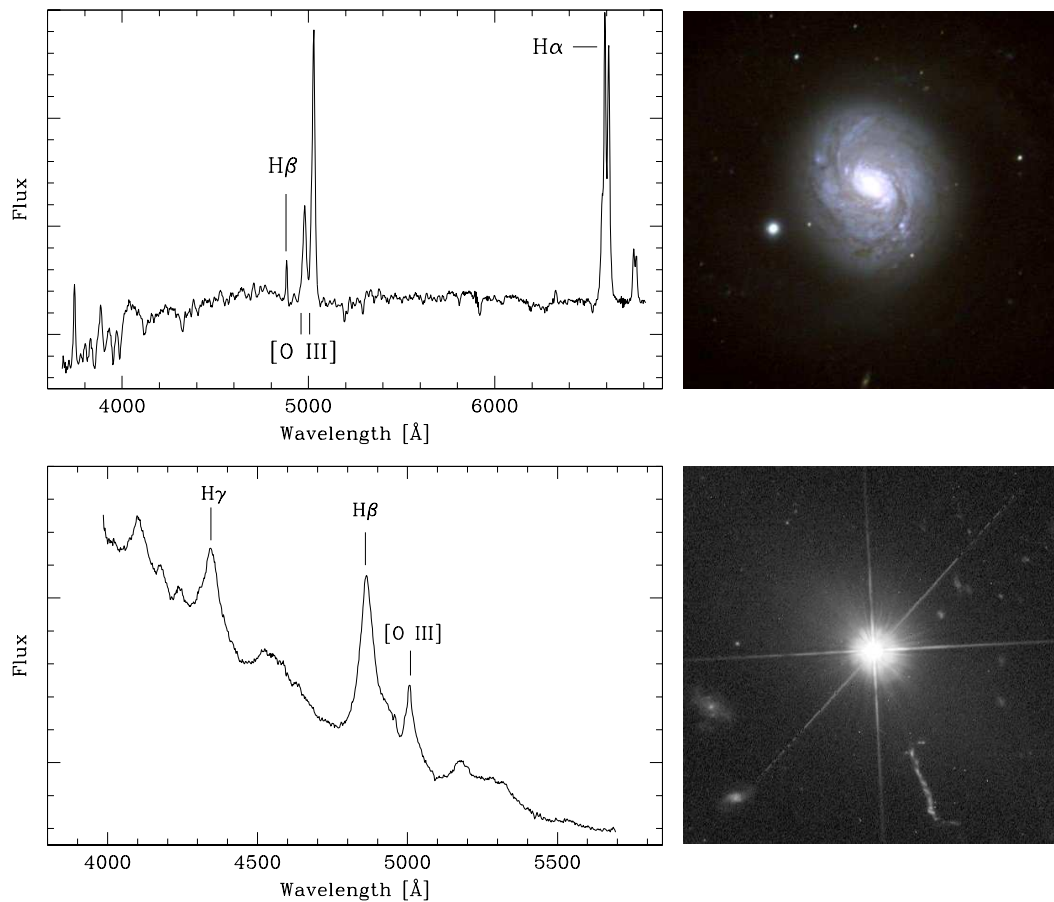
**Figure 1.2:** Firsts of their kind: Optical spectra and images of the Seyfert galaxy NGC 1068, the first active galaxy ever to be classified as such (top), and 3C 273, the first quasar ever to be recognized (bottom). On the left, the optical spectra showing some of the prominent emission lines, in arbitrary flux units (data drawn from Moustakas & Kennicutt 2006; Boroson & Green 1992). On the right, a color composite image of the Seyfert galaxy NGC 1068, and an *HST*/WFPC2 image of 3C 273. *Credit: NOAO/AURA/NSF (NGC 1068) and NASA/J. Bahcall (3C 278).*

(1974) noted that among them, there were two subclasses. This classification is based on the emission lines present in their spectra: type-1 sources are those that feature both broad and narrow emission lines, while those that only show narrow lines are referred to as type-2. Not so long after though, Osterbrock (1978) suggested that type-1 and type-2 Seyfert galaxies were intrinsically the same, but for the latter the broad line region was obscured by a dusty torus, consistent with the average lower luminosities of type-2 Seyferts with respect to type-1s–hence giving the first idea of

geometrical unification. Later, Antonucci & Miller (1985) provided evidence that the polarization spectrum of the type-2 Seyfert NGC 1068 looked like a type-1, which led to the current classical line of sight unification paradigm[3] (Antonucci 1993; Urry & Padovani 1995) shown in Figure 1.3. In this model the central nucleus, made up of a BH and its accretion disk, is surrounded by a dusty torus. If we happen to see the nuclei through the torus, we will be observing a type-2, whereas if we observe the system face-on, we get a type-1. This unification scheme also accounts for other phenomena such as blazars, a subclass of AGN thought to have its relativistic jets pointed close to the direction of the line of sight.

Quasars, the very luminous side of the AGN family, have been generally regarded as exotic objects. They were initially detected in the late 1950s, during the bloom of radio astronomy in the aftermath of World War II. Some of the scientists involved in radar technologies during wartime applied their expertise to continue the pioneering work of Jansky during the 1930s. This led to a handful of radio surveys of the sky, which thanks to their reasonable resolution were able to relate radio detections with resolved optical sources. Remarkable initial radio surveys such as the third Cambridge catalog (3C, Edge et al. 1959; Bennett 1962) detected a number of sources which could be immediately related with resolved galaxies from their positions in the sky. Other radio sources were found to match objects that looked like stars on optical images, but which puzzlingly, showed spectral properties not resembling any known type of star, in particular broad emission lines at unknown wavelengths (Matthews & Sandage 1963). It was soon after this that Schmidt (1963) identified the redshifted Balmer series at $z = 0.16$ in the spectra of the radio source 3C 273, irrefutable evidence of its extragalactic origin. Its spectrum and optical image are shown in the bottom panels of Figure 1.2. Additional evidence followed from Greenstein & Matthews (1963), who identified a number of emission lines for 3C 48 as being at the even higher redshift $z = 0.37$. The most notable implication from the distances derived from the redshifts was that these sources were tremendously luminous, a hundred times intrinsically brighter than an average galaxy.

Before too long, it was understood that Seyfert galaxies and quasars were not independent classes but rather two extremes on a continuous sequence in luminosity of a

---

[3]The classical geometric unification is still a matter of debate. More complex models have been proposed, such as the wind-cone structure by Elvis (2000). The inclusion of accretion rate as another "axis" in the current AGN unification models has been introduced by Trump et al. (2011), who find intrinsically different accretion rates between type-1 and type-2 AGN. Aditionally, Ramos Almeida et al. (2011b) argue that the dust tori of both types of AGN are different, with type-2 tori having more clumps and lower optical depths than type-1 tori.
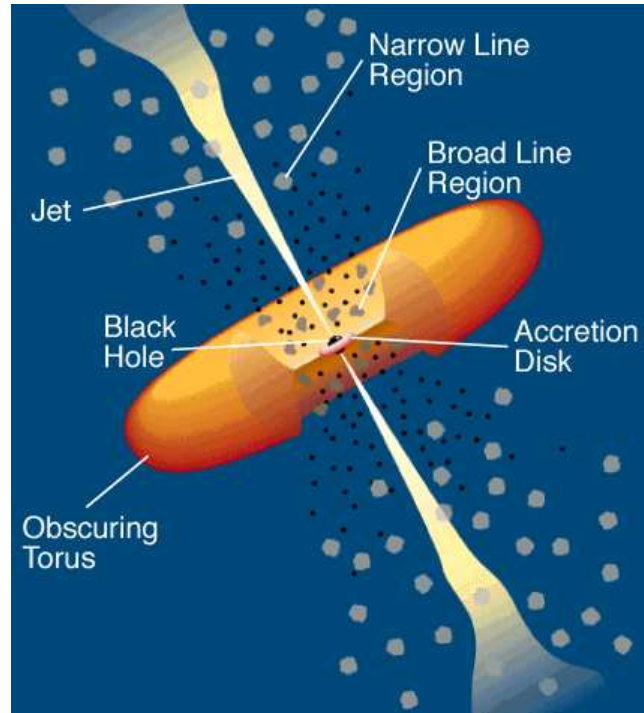
**Figure 1.3:** Classical line of sight unification model, explaining the existence of type-1 and type-2 objects, and showing the main components of an AGN (not to scale). In the case of type-1 AGN, we directly observe the BH and its accretion disk shown in the center, as well as the broad line region close to them. For type-2s, the inner regions are likely obscured by the dusty torus (Antonucci 1993; Urry & Padovani 1995).

single class (Weedman 1976). This was a sensible assumption based on the properties they shared: both quasars and the nuclei of Seyfert galaxies had broad emission lines in their spectra and showed flux variability (Schmidt 1969; Fitch et al. 1967). Perhaps the most important common feature among AGN is that they are bright X-ray sources (Elvis et al. 1978); to this day, this remains one of the most efficient ways to select clean samples (e.g., Mushotzky 2004) and study their luminosity evolution (Ueda et al. 2003).

## 1.3    Co-evolution of galaxies and black holes

At first, AGN were regarded as an intriguing phenomenom. Important clues about their actual physics came early on, from Woltjer (1959) who hinted that Seyfert

galaxies might just be a phase every galaxy went through, and from Hoyle & Fowler (1963) who proposed that the energy source of quasars was of gravitational origin, presumably from the collapse of very massive objects under their own extreme gravitational potentials. As early as 1965, Zel'Dovich & Novikov mentioned the possible involvement of massive black holes, and Lynden-Bell (1969) suggested that quasars grew by gas accretion and that there were many "dead" quasars dormant in local inactive galaxies.

Today, our knowledge in this respect has progressed significantly: it is now well established that all local galaxies with a significant bulge component host a supermassive black hole (e.g., Kormendy & Richstone 1995; Richstone et al. 1998). Even our own, the Milky Way, has a BH known as Sgr A* (e.g., Schödel et al. 2002; Ghez et al. 2003). The BH ubiquity paradigm comes as a direct consequence of the discovery of tight correlations between the BH mass and various properties of galactic bulges[4], including luminosity (Kormendy & Richstone 1995; Magorrian et al. 1998), stellar velocity dispersion (Ferrarese & Merritt 2000; Gebhardt et al. 2000; Tremaine et al. 2002), stellar mass (Marconi & Hunt 2003; Häring & Rix 2004), and light concentration (Graham et al. 2001). The central BH is thought to be a relic of a quasar phase the galaxy went through (Lynden-Bell 1969; Richstone et al. 1998), during which the bulk of the BH mass, in the range $M_{\mathrm{BH}} = 10^6 - 10^{9.5} M_\odot$, was built up (Soltan 1982; Yu & Tremaine 2002; Marconi et al. 2004; Shankar et al. 2004). Altogether, the likely scenario is that every massive galaxy went through at least one quasar phase.

Subsequent observational evidence suggested that quasars might play a major role in the evolution of galaxies. The quasar luminosity density evolved in a similar way as both the star formation rate (SFR) of the universe out to $z \sim 4$ (Boyle & Terlevich 1998) as well as the number density of starburst galaxies out to $z \sim 2$ (Sanders & Mirabel 1996; Dickinson 1998). Put together with the BH-galaxy scaling relations, the appealing co-evolution picture was born (e.g., Kauffmann & Haehnelt 2000; Volonteri et al. 2003; Wyithe & Loeb 2003). A physical mechanism, namely AGN feedback, was often invoked by models of galaxy formation to explain the observed correlations and at the same time to solve some of the problems the field was dealing with (e.g., Granato et al. 2004; Di Matteo et al. 2005; Hopkins et al. 2006a, 2007; Somerville et al. 2008). The massive energy output from the central

---

[4]An increased scatter in the BH-bulge correlations has been observed below $M_{\mathrm{BH}} \sim 10^7 M_\odot$ (Greene et al. 2010), suggesting that the universality of the correlations may hold true only above a certain mass threshold.

active BH was enough to shut down star formation and therefore self-regulate its growth (Silk & Rees 1998).

While a physically coupled growth of galaxy and BH provides an attractive paradigm for the observed scaling relations, the aforementioned models do not work from first principles but rather use "sub-grid" prescriptions, i.e., simple recipes to incorporate baryonic processes in the calculations. In addition, no direct observational evidence of AGN feedback has been found to date. This led to Peng (2007) to try a different approach, based on a much more basic process: galaxy merging. In a thought experiment, he developed a "toy model" with the sole premise that when galaxies merge, their masses as well as that of their BHs add up, and that the galaxy mass function has a Schechter (1976) shape, i.e., the number of objects decreases with increasing mass and has a steep break at the very-massive end. He showed that, physics aside, a low-scatter linear mass scaling relation can be reproduced by galaxy merging from an initially uncorrelated distribution of galaxies in the $M_* - M_{BH}$ plane. In his model, for a tight correlation to arise, five or more major mergers were needed per galaxy, though it was initially unclear whether that was a realistic assumption. Jahnke & Macciò (2011) followed-up this idea, this time using realistic dark matter halo merger trees, and incorporating simple recipes for the global star formation and BH accretion rates, as well as for the disk-to-bulge conversion during mergers. In their work, they managed to reproduce the observed local $M_{*,bulge} - M_{BH}$ relation, showing that while AGN feedback is a possible element in galaxy evolution, it is not required to justify the observed coupling between properties of BHs and galactic bulges.

Theoretical models have found different solutions to reproduce the observed present-day universe. This is a "degeneracy", which can only be solved with further empirical evidence. Unfortunately, the local scaling relations *alone* cannot tell us much about the physical nature of the coupling between galaxy and BH. It exists *today*, but, did it always look like this? Was it different at earlier times? This question has a direct implication for the proposed coupling: do BHs and galaxies grow together, or do they grow independently?

## 1.3.1    Scaling relations beyond the local universe

The local scaling relations serve as a parameter constraint for the co-evolution models, i.e., *by design* they are able to reproduce the BH-galaxy correlations in good

agreement with observations. But once at $z > 0$ the situation is far from clear: there are disagreements among the models and robust observational constraints are scarce. From the theoretical side, different models predict different trends of evolution with redshift (e.g., Granato et al. 2004; Croton 2006; Robertson et al. 2006; Hopkins et al. 2006b; Booth & Schaye 2011). Observationally, our ability to recover both BH mass and the properties of the bulge is particularly limited, and very different methods have been employed.

Perhaps the most widely used method to estimate BH masses at $z > 0$ is from the broad emission line widths from single epoch AGN spectra. The BLR size, estimated from reverberation mapping of nearby active galaxies (e.g., Peterson 1993; Peterson et al. 2004), has been found to correlate with the continuum luminosity (Kaspi et al. 2000). Therefore, under the assumption that the BH gravitational potential produces the widths of the permitted emission lines, a set of scaling laws can lead to BH mass measurements.

Regarding galaxy properties, e.g., bulge stellar velocity dispersion ($\sigma_*$), a variety of results can be found in the literature: Shields et al. (2003) and Salviander et al. (2007) have used narrow [O III] and [O II] lines to measure $\sigma_*$. The former found that the relation between $M_{\mathrm{BH}}$ and $\sigma_*$ out to $z \sim 3$ is consistent with the local value, while the latter found that for a fixed value of $\sigma_*$, the $M_{\mathrm{BH}}$ was larger by 0.2 dex at $z \sim 1$. Shen et al. (2008) used the stellar absorption spectra of the host galaxies to measure $\sigma_*$ for a large sample of ~900 type-1 AGN out to $z \sim 0.4$, and found no evolution with respect to the local relation. Another group intensively probed the redshift windows $z = 0.36, 0.57$, measuring the host stellar velocity dispersion using high signal-to-noise ratio spectra (Treu et al. 2004; Woo et al. 2006; Treu et al. 2007; Woo et al. 2008). They reported strong evolution, finding smaller $\sigma_*$ for a given $M_{\mathrm{BH}}$ when compared to the local relation. At much higher redshift ($z > 3$), the CO lines have been used to estimate the velocity dispersion of the galaxies (Walter et al. 2004; Shields et al. 2006; Ho 2007), and again a strong evolution was found, pointing to a scenario in which BHs grew significantly faster and earlier than their host spheroids.

Photometric decomposition techniques on galaxy images have been employed to estimate masses and luminosities of AGN host galaxies, in general finding clear evolution at $z > 1$ (Peng et al. 2006a,b; McLure et al. 2006; Schramm et al. 2008; Decarli et al. 2010; Bennert et al. 2011). On the other hand, Jahnke et al. (2009) found no evolution in the ratio of BH mass with respect to *total* galaxy mass for a sample of 10 type-1 AGN at $z \sim 1.4$. Even so, since their objects featured a disk component, their

result still allowed for evolution with respect to *bulge* mass. A different technique was applied by Merloni et al. (2010), who used a large multiwavelength coverage to fit individual AGN and host galaxy components to the observed spectral energy distributions (SEDs) of 89 type-1 AGN. They found that out to $z \sim 2.2$, the host galaxies are much less massive for a given BH mass when compared with the local value, i.e., a strong positive evolution.

Finally, a groundbreaking approach was shown recently by Inskip et al. (2011), who for the first time directly measured the dynamical mass of a luminous quasar at $z = 1.3$ from gas kinematics. They found that the bulge mass of this particular source is consistent with the local relation within the scatter.

From the above it is possible to conclude that, while there are many hints pointing towards less-massive bulges for a given $M_{BH}$ at earlier cosmic times, it is still unclear whether the BH-galaxy relation evolves, the normalization changes with redshift, or if there is just a much larger scatter. Even at $z < 1$ there is a disagreement, and hence it is important to look for other observational clues that tell us about the growth of galaxies and BHs.

## 1.3.2   AGN fueling mechanisms

As mentioned earlier, AGN activity and star formation rate are related as both experience a similar increase at earlier cosmic times. Both share the need of cold dense gas, ideally deprived of nearly all its angular momentum so that it can condense to form stars and be able to reach the central regions to feed the BH. What mechanism can bring copious amounts of gas from kpc to sub-pc scales, close to the very center of the galaxy?

It was already suggested from the pioneering simulations by Toomre & Toomre (1972) that major gravitational interactions between galaxies could be an efficient way of transporting material to the central regions. Strong torques will be exerted on the gas content of a galaxy undergoing a merger or interaction, which will result in most of its angular momentum being removed, leaving the gas free to start falling to the central regions of the galaxy (e.g., Hernquist 1989; Barnes & Hernquist 1991, 1996; Mihos & Hernquist 1996; Springel et al. 2005a; Cox et al. 2006; Di Matteo et al. 2007; Cox et al. 2008).

From the observational point of view, the launch of *HST* radically changed the way of
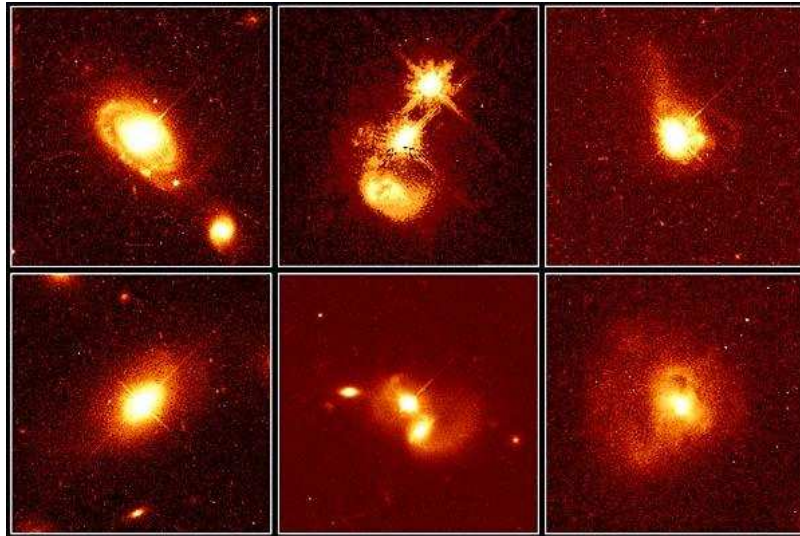
**Figure 1.4:** Selected quasars imaged with *HST*/WFPC2. These were among the first space-based observations of quasar host galaxies in which, thanks to the superb resolution, it was possible to discern interaction signatures as well as close companions. *Credit: J. Bahcall/M. Disney/NASA.*

studying quasars. Before there was no convincing observational "proof" of a quasar host galaxy, but now it was possible to resolve their host galaxies and close environments with unprecedented resolution. Early *HST* imaging studies (e.g., Disney et al. 1995; Bahcall et al. 1997) found many cases of quasars with close companions, as well as highly distorted host galaxies or ongoing merger events, therefore making an explicit case for a "merger-AGN" connection. A selection of these *HST*/WFPC2-imaged quasars is shown in Figure 1.4, in which it is possible to appreciate ongoing interactions (center panels) as well as peculiar galaxies, possibly wrecked due to an earlier merger event (right side panels).

These initial studies were followed by many others presenting further cases of interacting AGN host galaxies, providing additional *circumstantial* evidence in support of this scenario (e.g., Canalizo & Stockton 2001; Zakamska et al. 2006; Canalizo et al. 2007; Urrutia et al. 2008; Bennert et al. 2008). While the merger-induced AGN activity picture is appealing, the evidence is inconclusive for the establishment of a causal merger-AGN connection. In general, no proper comparison was performed against the "background level" of merger activity, i.e., the merger fraction of normal, inactive galaxies. Merging galaxies abound, but the vast majority do not concurrently host a bright quasar. In this respect, a significant improvement was made by

Dunlop et al. (2003), who compared their quasar sample against the quiescent galaxy population, and found no structural differences. Other recent studies have employed large *HST* programs, in which it is possible to study large samples of AGN in parallel with inactive galaxies from the same dataset, and have found no particular difference in the structural parameters of both samples (e.g., Grogin et al. 2005; Gabor et al. 2009).

Since the evidence for major galaxy encounters triggering AGN is indefinite, it is relevant to consider the alternatives. Secular processes, i.e., those that require much longer than a dynamical time to be relevant, have been claimed to be able to lead to gas inflows, bulge growth, and BH fueling (for reviews, see Kormendy & Kennicutt 2004; Wada 2004; Martini 2004b; Jogee 2006). These mechanisms can be both external, (e.g., minor mergers, prolonged gas accretion) and internal (e.g., bar instabilities, collisions of giant molecular clouds, supernova explosions). Even though these processes have been generally related to Seyfert galaxies only (e.g., Simkin et al. 1980; Taniguchi 1999; Knapen et al. 2000; Hopkins & Hernquist 2009), it is still an open question whether they could potentially be relevant for the triggering of higher luminosity AGN.

## 1.4   The COSMOS survey

Extragalactic astronomy studies have greatly benefited from sky surveys. For example, the Sloan Digital Sky Survey (SDSS,  Abazajian et al. 2003) generated an unprecedented wealth of knowledge on galaxy evolution (e.g., Blanton et al. 2003; Baldry et al. 2004) and the large scale structure (e.g., Percival et al. 2007) of the local universe. On the other hand, *HST* deep surveys such as the Hubble Deep Field (HDF, Williams et al. 1996), Ultra Deep Field (UDF, Beckwith et al. 2006) and the Great Observatories Origins Deep Survey (GOODS, Giavalisco et al. 2004) have provided highly detailed imaging at high redshifts, albeit on very narrow fields.

Statements on the evolution of galaxies and BHs require large well-defined samples of AGN and host galaxies, spanning a significant range in cosmic time and ideally from a large area of the sky. In this respect, the Cosmic Evolution Survey[5] (COSMOS,  Scoville et al. 2007a) meets all the requirements to provide such a sample. The COSMOS survey features the largest contiguous area ever imaged with Ad-

---

[5]http://cosmos.astro.caltech.edu/

vanced Camera for Surveys (ACS) onboard *HST* (Scoville et al. 2007b; Koekemoer et al. 2007). The location of the 1.64 deg$^2$ field, close to the celestial equator, allows access from several major space and ground-based observatories, enabling a large multiwavelength coverage from X-ray to radio from supplementary observational projects.

One of the most effective ways of finding AGN is to make use of the X-ray emission from the accreting BHs (e.g., Mushotzky 2004). Complete coverage of the whole COSMOS field in X-rays was achieved with the *XMM-Newton* (XMM-COSMOS, Hasinger et al. 2007; Cappelluti et al. 2009) through 55 pointings with a total exposure time of ~1.5 Ms. The XMM-COSMOS catalog features ~1800 bright ($L_X >$ $10^{42}$ erg s$^{-1}$) X-ray point-like sources, which had their corresponding optical counterparts associated based on a likelihood ratio technique (Brusa et al. 2007). Ancillary spectroscopic and photometric surveys (Trump et al. 2007, 2009a; Lilly et al. 2007; Salvato et al. 2009; Ilbert et al. 2009) led to accurate redshifts and subsequent confirmation of ~1000 AGN as well as classification of their spectral type (Brusa et al. 2010).

Altogether, COSMOS provides the ideal data set for significant improvements in our understanding of galaxies and BHs to be made. In this thesis we will study a large sample of X-ray selected AGN as well as inactive galaxies from COSMOS, both with space-based imaging and multiwavelength photometry, by far the best sample of its kind to date.

## 1.5   Thesis overview

In this thesis we investigate the mechanisms that drive the evolution of galaxies and BHs from the "second half" of cosmic time, i.e., since redshift $z \sim 1$. As the only way to study BHs beyond the local universe is when they are actively accreting, we will use a large, clean X-ray-selected AGN sample from the COSMOS survey to study their evolution as well as that of their host galaxies. This thesis is arranged as follows: In Chapter 2, we present a robust method to perform photometric decomposition of *HST*/ACS images of type-1 AGN and host galaxies by forward modeling the individual components. In Chapter 3, we use 32 type-1 AGN with available virial BH mass estimates to investigate the evolution of the relation between BH mass and total galaxy mass out to $z = 0.9$, and discuss the implication of our findings. In

Chapter 4, we establish the relevance of major galaxy mergers as an AGN triggering mechanism. From a sample of X-ray selected AGN out to $z = 1$, we visually analyze their host galaxy morphologies looking for distortions and merging signatures, and compare them with the merger fraction of the equivalent inactive galaxy population. We discuss our results, and summarize the work presented in this thesis in Chapter 5.

# CHAPTER 2

## DECOMPOSITION OF ACTIVE GALACTIC NUCLEI AND THEIR HOST GALAXIES

**Due to the extreme amounts of light emitted by active galactic nuclei, photometric studies of the properties of active galaxies, in particular type-1 AGN, are constrained by the accuracy with which one can separate the emissions from the active nucleus and its host galaxy. In this chapter we use high-resolution *HST*/ACS imaging to perform a two-component image-decomposition of our sample of type-1 AGN to successfully recover their host galaxies. We explain the considerations involved in getting a converging model as well as the reliability of this technique.**

## 2.1 How to describe galaxies and active black holes?

When studying active galaxies, ideally one wants to isolate the emission of the active nuclei from that of its host galaxy with the minimum loss of information, in order to accurately characterize their photometric or structural properties.

In the current accepted AGN-unification model (Antonucci 1993; Urry & Padovani 1995), type-1 sources represent a direct view of the accretion disk, heated by the immense friction of the infalling matter spiraling into the supermassive black hole. Due to its dimensions, of the order of $10^{-3}$ pc, there is no current way of resolving this very bright structure even for nearby active galaxies. Therefore, it will always

---

This chapter has been adapted from Cisternas et al. (2011a)

show up as a point source, with its size limited by the PSF. Because of this bright nucleus, it is understandable that analyzing the host galaxies of type-1 AGN has been historically a highly complicated task. The point source can be as bright as, and frequently outshine, the host galaxy, and therefore our ability to recover the host galaxy will be mainly determined by the size and accuracy with which we can characterize the PSF.

The goal of this Chapter is to present the state of the art in terms of automated photometric AGN-host galaxy decomposition. One way to carry out this task is the so-called peak-subtraction method, previously employed in studies attempting to recover the host galaxies of bright quasars (Sánchez et al. 2004; Jahnke et al. 2004b). Basically, this approach consists of scaling a well-characterized PSF to the peak of the quasar central flux, and subsequently subtracting it from the quasar image. Because the peak of the flux will also include a contribution from the underlying host galaxy, this method will inevitably lead to an oversubtraction in its central regions. Nonetheless, it is a robust lower limit and simple to implement, and can be a reasonable assumption for bright quasars in which the flux contrast in the central regions should indeed be quite high. On moderately luminous AGN, however, the contrast levels are less extreme, and hence subtracting a peak-scaled PSF would substantially damage the resulting host galaxy. For these kind of sources, a more accurate and sophisticated decomposition can be achieved by fitting simultaneously a PSF and an analytical model to account for the AGN and its host galaxy respectively. In this study, we will show how this can be done through forward modeling of our data. We will extensively use the two-dimensional fitting code GALFIT (Peng et al. 2002, 2010), which given a functional form will find the best combination of parameters that represent the two components through a $\chi^2$ minimization. This is particularly useful when one is interested in the physical properties of the host galaxy because, depending on the functional form chosen, we can recover estimates of its size, shape, flux, elongation, and orientation. Below we present our choice on how to parameterize both point source and host galaxy. We opt to use GALFIT over other fitting algorithms available on the market such as GIM2D (Simard et al. 2002), as it has been shown that in comparison the former runs significantly faster, and performs better when dealing with multiple close companions (Häussler et al. 2007). Moreover, the latter was mainly conceived to perform bulge-disk decompositions and lacks the flexibility offered by GALFIT.

### 2.1.1 Parameterizing a galaxy

In photometric studies, the spatial information contained in galaxy images can be exploited by using analytic functions to describe the surface brightness profiles. Widely used functional forms include the $r^{1/4}$ law better known as the de Vaucouleurs (1948, 1953) profile, associated with elliptical galaxies, spheroids, and classical bulges, and the exponential profile (Patterson 1940; de Vaucouleurs 1959; Freeman 1970), a good description for galactic disks. An illustration of these two basic classes is shown in Figure 2.1. The left panels show an elliptical (top) and a disk-dominated galaxy (bottom) from the COSMOS *HST*/ACS imaging. To the right, their respective surface brightness plots are shown, in which the open circles correspond to the data, and the solid lines show the corresponding de Vaucouleurs and exponential profiles. It can be seen that both are very good representations of the data, for the latter only outside the central regions due to the presence of the galactic bulge.

While these functions can account for the two most rudimentary morphological types, not all galaxies are either pure spheroids or pure disks, e.g., as the galaxy shown in the bottom panel of Figure 2.1. Therefore, a much more versatile and useful functional form is given by the Sérsic (1968) profile,

$$\Sigma(r) = \Sigma_e \, e^{-\kappa \left[((r/r_e)^{1/n}) - 1\right]} \tag{2.1}$$

where $r_e$ is the effective radius of the galaxy, and $\Sigma_e$ is the surface brightness at $r_e$. The power-law index $n$ will be coupled to $\kappa$ so that $r_e$ always encloses half of the total luminosity. The Sérsic profile is simple, yet powerful: the parameter $n$ will form a continuous sequence of shapes, going from a concentrated profile at low values, to a shallower profile as it increases. As a generalization it includes the previous two cases, with $n = 4$ being the de Vaucouleurs profile, $n = 1$ being the exponential disk profile.

### 2.1.2 Modeling the active nucleus

A key aspect of the AGN-host galaxy decomposition is the choice of an accurate PSF, both for modeling the AGN itself and for deconvolving the light distribution from the host galaxy. Even though the space-based *HST* provides much more stable PSFs compared to ground-based telescopes, instrumental effects are still important. The position of the target within the detector (spatial PSF variation) and the temperature dependence of the focus along different orbits (temporal PSF variation) can lead
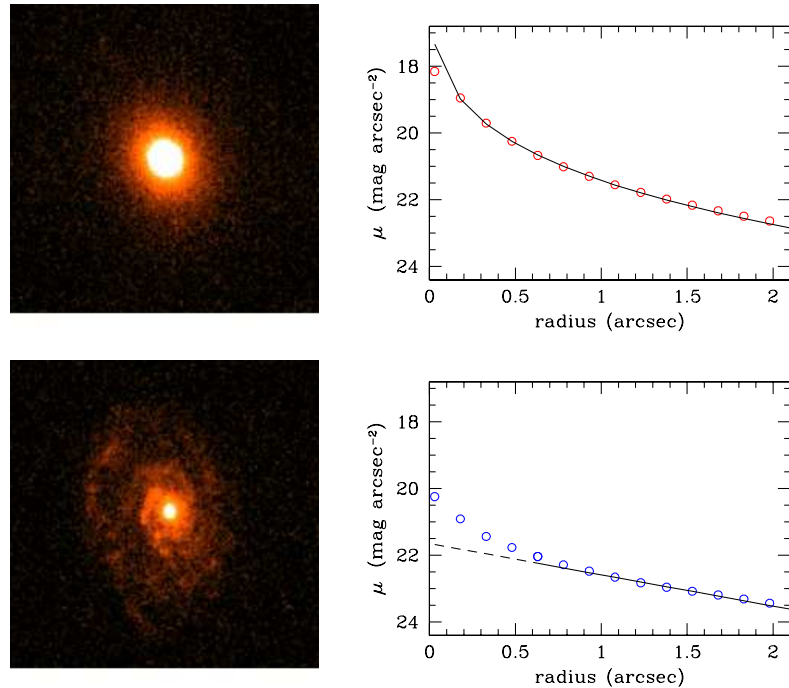
**Figure 2.1:** Example of the two basic morphological classes. The left panels show an elliptical (top) and a disk-dominated galaxy (bottom) from the COSMOS *HST*/ACS imaging. On the right, their respective surface brightness plots. The open circles correspond to the data and the solid lines show the corresponding de Vaucouleurs and exponential profiles. For the latter case, we show as a dashed line the regime in which the exponential profile stops being a good representation of the data. The cutouts are $6'' \times 6''$ .

to discrepancies between the PSFs from the observations and the ones used for the analysis (e.g., Krist 2003; Rhodes et al. 2007; Kim et al. 2008). This yields systematic errors in the image decomposition which can be critical for bright AGN with a high contrast to the galaxy, and have an immediate impact on the derived host galaxy properties.

Other studies with large *HST* coverage such as the Galaxy Evolution from Morphology and SEDs survey (GEMS, Rix et al. 2004) in the Chandra Deep Field South (CDF-S, Giacconi et al. 2001), have found that spatial variations dominate with respect to other sources, and can account to up to 20% of rms flux difference among individual pixels (Jahnke et al. 2004b; Sánchez et al. 2004). These studies concluded that, rather than using a single average PSF for the subsequent analyses, it was more sensible to build individual PSFs from isolated stars that lie close to each source of
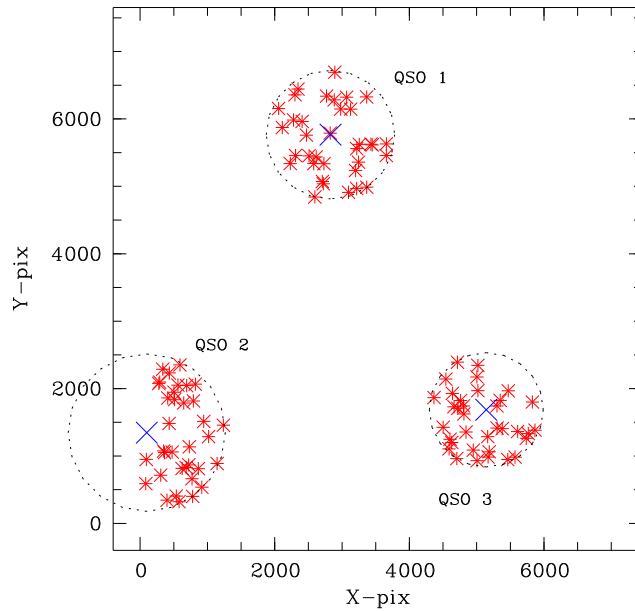
**Figure 2.2:** An illustration of the PSF creation process. For a given type-1 AGN (blue crosses), the closest ~30 stars (red asterisks) in terms of pixel position within the ACS detector in which they were observed are selected, to produce a local, time-averaged PSF.

interest in both focus value and spatial position. In a similar way, the COSMOS survey provides us with the opportunity to minimize these spatial and temporal effects by using stellar PSFs from stars observed under the same conditions as our targets.

First, we account for the different focus values with which each of the tiles that make up the COSMOS field were observed. Different foci result from thermal fluctuations which cause a change in the primary-to-secondary mirror spacing. Therefore, using the focus values computed by Rhodes et al. (2007), we select only those tiles that have a similar focus as the one of the source of interest. From there, we choose the closest ~30 stars at $\leq 40''$ in terms of pixel position within the ACS detector. Figure 2.2 illustrates the PSF creation process.

While with these considerations we are creating the most precise estimates of real PSFs that our data allows for, the individual stars still show some mismatch, especially in the central pixels. We therefore produce rms frames for each PSF stack to quantify these mismatches. As described in the following section, the modeling of the AGN will require a weight to be assigned to the individual pixels, and these rms

images are essential for this purpose.

## 2.2    Decomposing the type-1 AGN sample

From the previous section we have all the ingredients to correctly characterize both active nuclei and host galaxies. In this section we present the current standard in terms of photometric decomposition of type-1 AGN. We first describe how to employ the fitting code GALFIT to model and decouple the individual components in the image by finding the best combination of parameters for the Sérsic function and PSF. We explain all the relevant considerations necessary to obtain not only a successful fit, but also one with a physical meaning. We then explain how we applied GALFIT on our whole sample by integrating it in a custom-built pipeline to fully automate the decomposition.

### 2.2.1    The COSMOS type-1 AGN sample

The COSMOS 2 deg$^2$ field was observed with *XMM-Newton* for a total exposure time of ~1.5 Ms through 55 pointings, at the average vignetting-corrected depth of 40 ks (Hasinger et al. 2007; Cappelluti et al. 2009). For these X-ray point sources, optical counterparts were associated using the likelihood ratio technique (Brusa et al. 2007, 2010). From the X-ray catalog consisting of ~1800 sources, we draw a parent sample of ~550 sources classified as type-1 AGN from spectroscopic surveys (Trump et al. 2007, 2009a; Lilly et al. 2007) revealing broad emission lines, and from spectral energy distribution (SED) fitting (Capak et al. 2007; Salvato et al. 2009; Ilbert et al. 2009).

For the photometric modeling we are going to present, we require the best image quality available, and hence we are going to take advantage of the high-resolution *HST* imaging of the COSMOS field. These observations comprise 583 orbits using the Advanced Camera for Surveys (ACS) with the F814W (broad *I*-band) filter (Koekemoer et al. 2007). The imaging data feature an oversampled scale of 0.″03/pixel. We make an initial flux cut and only consider optical counterparts brighter than $I_{F814W} = 24$.

We restrict our sample to the redshift range $z \sim 0.3 - 1.0$. For the majority of our final

sample, we used high-confidence spectroscopic redshifts, while for the rest (20%), we used photometric redshifts by Salvato et al. (2009). The lower redshift cut is chosen due to the low number of AGN below $z \sim 0.3$, and also to avoid working with saturated sources. The upper limit arises because the F814W filter is shifted into rest-frame UV for sources above $z \sim 1$. At this regime, the bright active nucleus starts to dominate due to its blue color, outshining the host to larger extents, and severely increasing the systematic uncertainties of the overall modeling procedure.

This selection yields 83 type-1 AGN, with a median redshift of $z \sim 0.8$, and a median X-ray luminosity in the 2-10 keV energy band of $L_X \sim 10^{43.6}$ erg s$^{-1}$.

## 2.2.2   Modeling with GALFIT

To accurately disentangle the individual flux contributions of the AGN and its host galaxy, we perform a rigorous two-dimensional parametric modeling with GALFIT. As illustrated before, we reduce each system down to a two-component model: a PSF to represent the AGN and a Sérsic light profile to account for the host galaxy. GALFIT is designed to minimize the $\chi^2$ using the Levenberg-Marquardt downhill-gradient method (Press et al. 1992), iteratively modifying the input fitting parameters and comparing them with the data image. Once a best-fit model has been achieved, the nucleus model can be then subtracted from the original image, leaving us with the solely emission from the host galaxy plus some residuals.

As mentioned before, while mainly distinguishable because of their disk, spiral galaxies usually feature a bulge component that fails to be totally addressed with a single exponential profile. Additionally, they can feature other nonaxisymmetric structures such as prominent bars. GALFIT allows, and is very efficient at, fitting multiple components of a single galaxy. Many studies investigating structural properties of galaxies through image decomposition techniques have indeed characterized these galactic substructures by the means of multi-component modeling (e.g., Civano et al. 2010; More et al. 2011). However, at our resolution and S/N it has been shown that it is sufficient with a single-component model to account for the host galaxy rather than a more complex, multi-component one, as shown by simulations addressing the bulge+disk+AGN decomposition problem (Sánchez et al. 2004; Simmons & Urry 2008; Kim et al. 2008).

To perform the fit of a given input data image, GALFIT requires the user to provide

(i) a PSF image, which will be given by the specifically-created local PSF described in the previous section, and (ii) a sigma image, which will be used to assign relative weights to the individual pixels, which is essential for the $\chi^2$ minimization process.

In our case, the sigma image will be based on a variance map, constructed considering, not only the contributions from the readout noise of the detector and the sky background, but also the fact that our final ACS science images were oversampled from $0\!\!''05$/pixel to $0\!\!''03$/pixel using MultiDrizzle (Koekemoer et al. 2002) to combine the different exposures dithered to different positions. Therefore, for the creation of the variance frames we also take into account the pixel area conversion from the drizzling process, as well as the weight image produced by MultiDrizzle, in which each given pixel will contain the effective number of pixels and integration times that contributed to that drizzled pixel.

Fitting simultaneously a PSF and a Sersic profile involves 10 free parameters for GALFIT to modify in each iteration: apart from position (x and y) and integrated magnitude in both cases, the Sersic profile includes the effective radius $r_e$, the power-law index $n$, the axis ratio $b/a$, and the position angle. Attempting to get a successful fit without an initial prior would be tedious and risky: due to GALFIT's design, it can happen that it converges to a best-fit solution that represents a local minimum rather than the global one, and also that the best-fit solution runs into unrealistic non-physical parameters due to imperfect match between model and data. Therefore, an appropriate initial guess of the parameters to be fitted is recommended to get a faster and converging model with GALFIT. We opt to run Source Extractor (SExtractor, Bertin & Arnouts 1996) on our images to generate, in a fast and automatic way, rough estimates of the free parameters mentioned before. A detailed description of the considerations taken on this step are given in the following subsection.

Running GALFIT produces an image block containing the original data image, the model, and a residual map. Figure 2.3 shows three examples of the decomposition process applied on real type-1 AGN with *HST*/ACS imaging data from the COSMOS survey. From top to bottom, the three components of the image block described before, followed by the surface brightness profile showing the original data as open circles, and the best-fit PSF and Sersic models as the solid and dashed lines respectively. At the bottom, the resulting host galaxy images, made by subtracting the best-model PSF from the original type-1 AGN science image.
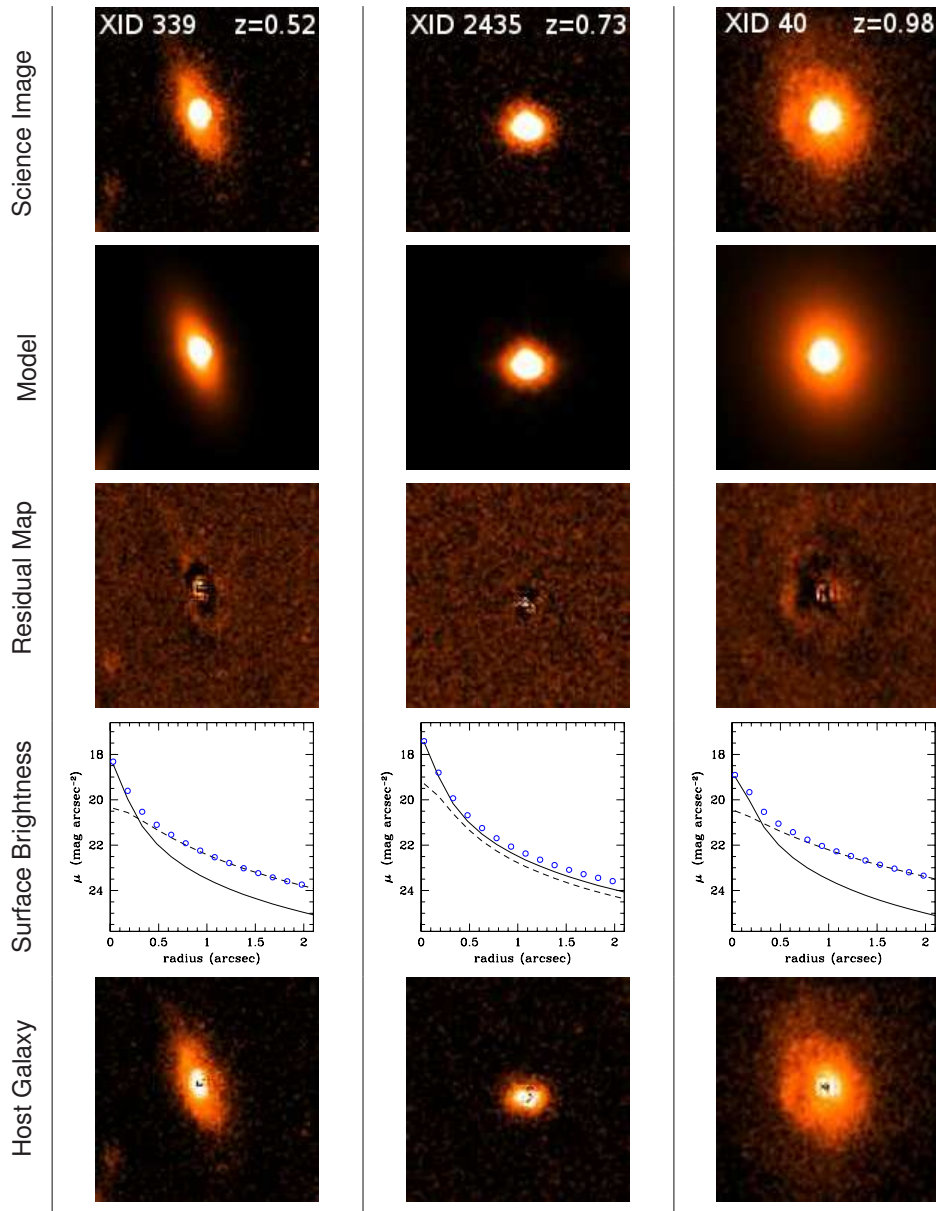
**Figure 2.3:** Examples of the AGN-host galaxy decomposition for three different objects, with their original XMM-Newton identifiers (Cappelluti et al. 2009) and redshifts indicated at the top. From top to bottom: The original science images, the best models produced by GALFIT from the two-component fitting, the residual maps showing the features not represented by the model, the surface brightness profiles showing the data (open circles), best-fit PSF (solid line), and Sersic galaxy model (dashed line), and the nucleus-subtracted host galaxy. The cutouts encompass the same physical scale, roughly 22 kpc × 22 kpc.

### 2.2.3   Batch fitting of the sample

While GALFIT is an extremely powerful tool for the decomposition we intend to perform on our sample of type-1 AGN, it was not conceived for the batch fitting of multiple images in an automatic way. In this context, we created our own pipeline in IDL to automate the process described before using a similar approach as that of GALAPAGOS described in Häussler et al. (2007). The creation of such a pipeline has to take care of many aspects: accurate characterization of the source of interest within the image cutout, effectively deal with additional objects in the vicinity, prevent missing faint sources or wrongly deblending single large sources due to different sizes and brightness levels, among others. Below we detail a few relevant considerations:

**Two setups for SExtractor.** Due to the redshift range spanned, our objects feature different sizes and surface brightness levels. If on top of that, one considers the neighboring objects that fall in the cutout image, it is understandable that not a single configuration of SExtractor will successfully characterize all the objects of the sample. If one uses a source detection configuration focused on the small, faint objects, the larger galaxies will be over-deblended. On the other hand, if one increases the flux and area thresholds to avoid the over-deblending, the smaller object will never be found. Hence, we adopt a "hot and cold" approach as in Häussler et al. (2007) and prepare two configurations for SExtractor. We first run a "cold" configuration to characterize the bright/large objects without over-deblending, and then we run a "hot" configuration, optimized to detect faint/small objects. As we found by experience, just two configuration parameters were needed to assure successful detections on our data set with a detection threshold of $5\sigma$ above the background rms: (i) the minimum number of pixels above threshold to trigger a detection `DETECT_MINAREA`=70/30, and (ii) the minimum flux contrast between peaks for deblending `DEBLEND_MINCONT`=0.05/0.005 for the cold/hot configurations respectively.

**Three alternatives for *n*.** Before we mentioned the possibility that some parameters converge to unrealistic values due to GALFIT's design. To have a broader range of options in case this happens, we run our pipeline using three alternatives for the Sersic index *n*: it runs as a free parameter, but also fixed to a $n = 1$ exponential disk, and to $n = 4$ de Vaucouleurs profile. With this we are "forcing" GALFIT to find a reasonable set of parameters for the likely cases of a disk-dominated or purely bulge-dominated galaxy. This will be very handy for the cases in which the free-*n* case is not sufficiently constrained and runs out of boundaries.

**Representative Sigma Images.** As mentioned earlier in this Chapter, GALFIT requires a sigma image to give relative weights to the individual pixels, for which we could initially use the corresponding variance map. However, this variance map is not enough: it does not account for the intrinsic PSF rms error, inherent from averaging over many stars, and hence does not reflect the true weights of the pixels that contain point-source flux. In order to "relax" the constraints over the PSF, we need to propagate this uncertainty to the overall sigma image[1].

While in principle this looks like a simple task, we are required to scale the PSF rms error according to the expected AGN contribution to the overall flux, and therefore we need to have an initial measure of the AGN-to-total ratio. This will be worked out by performing two runs of GALFIT for every case. First, we do a pass with GALFIT using the non-corrected sigma images to get an idea of the AGN-to-total ratio. This estimates can then be used to scale the PSF rms errors, propagate them to the overall sigma images, so then we are able to run GALFIT again with new, more precise, weights.

**Dual AGN in a single host galaxy.** Regarding double-nucleus sources, which could need a dedicated modeling, we only found one object in our sample. This is also consistent with the visual inspection from Civano et al. (2010), who specifically looked for double-nucleus AGN on the *Chandra* observations of the COSMOS field (C-COSMOS; Elvis et al. 2009), which feature higher point source sensitivity. We checked for this particular source (Figure 4.2, bottom left), for which our method removes the brightest of the two nuclei. The other point source is significantly fainter and does not dominate the overall galaxy brightness, hence not requiring a more complex decomposition.

With all these considerations, below we give a step-by-step description of the pipeline. Given a list of type-1 AGN, with their respective $256 \times 256$ pixel cutouts, sigma images, and local PSFs with their rms errors, our pipeline worked as follows:

1. To begin with, it runs the IDL procedure `CNTRD`, adapted from the `DAOPHOT` photometry package. This will yield a list of accurate centroids for each of our sources. The cutouts are roughly centered on the AGN itself, which is why we require a more exact centroid determination.

2. Then, it runs SExtractor on the cutouts, and from these identifies the primary

---

[1]GALFIT by design cannot accept any additional model uncertainties or else the algorithms would be become too non-linear for its $\chi^2$-minimization loop.

source based on the proximity to the centroid determined earlier. In the same
way, it characterizes any secondary object extracted. If no primary source was
detected, the pipeline runs SExtractor again, but this time optimized to find
smaller objects.

3. GALFIT runs based on an input file which specifies how many sources to fit,
   which parametric function to use on them, and more importantly, the initial
   guesses on their free parameters. Therefore, the next step is to use the param-
   eters estimated by SExtractor to create a GALFIT starting file for each object.
   The pipeline will write the parameters for each of the models: the x and y po-
   sitions will be those determined with `CNTRD`, the starting magnitudes will be
   given by SExtractor's `MAG_BEST`, and for the Sersic fit only, a rough size will
   be given by `FWHM_IMAGE`, the axis ratio $b/a$ comes from `B_WORLD/A_WORLD`,
   and the position angle will be `THETA_IMAGE`. As mentioned before, three dif-
   ferent GALFIT parameter files will be created for every object: two with the
   power-law index fixed, and the other as a free parameter, with a starting value
   at $n = 2$. Any additional secondary source will be fitted as a free-index Sersic
   model with its starting guesses also derived by SExtractor.

4. With the input files created, the pipeline proceeds to make a first run of GAL-
   FIT to get an estimate of the scaling factor to be applied on the *rms* of the PSF.
   Then, the rms uncertainty is propagated as $\sigma_{AGN} = \sqrt{\sigma_{Data}^2 + (f \cdot \sigma_{PSF})^2}$ to
   create a more truthful weights on the pixels of the AGN image.

5. GALFIT runs again as in step 4, and this time producing a model-AGN sub-
   tracted data image, i.e., the AGN host galaxy.

6. After the modeling, the data is uploaded to a web-interface for a more efficient
   inspection.

This setup is designed to run without any further intervention. In the event of an
unsuccessful fit, the program will write down the object name and proceed with
the next one. Running the three Sérsic setups in parallel threads on a multi-core
workstation the modeling of the type-1 sample can be completed within 2 hours.

### 2.2.4   Results

For each object in our sample, among the resulting models from the three Sérsic cases, the one with the least $\chi^2$ will be the one closer to the original data image in terms of pixel-by-pixel values. Nevertheless, to choose the right model we expect our best fit candidate to have sensible resulting parameters, so that the solution has also a physical meaning. We require our host galaxy model: (1) not to be too concentrated or too shallow, meaning a half-light radius between 2.5 pixels $< r_e < 100$ pixels, (2) not to diverge to extreme elongations, therefore to have $b/a > 0.5$, and (3) to have its Sérsic index within $0.5 < n < 8$, for the free $n$ case. We interpret that if the values run away from these boundaries, GALFIT did not manage to model the underlying galaxy but instead could be accounting for uncertainties in the PSF or the galaxy model mismatch.

An example of the typical output, displayed as a web-based interface to aid the inspection of the models, is shown in Figure 2.4. The stand-alone image on the left corresponds to the original science cutout, with its *XMM*-ID, redshift, and box dimensions. Next to it, from left to right, the $n =$ free, 1, and 4 fitting results in which from top to bottom the model, the nucleus subtracted host, and the residual map images are displayed. Below them, the relevant parameters of the fitted host galaxy. The lowest $\chi^2$ value gets highlighted in green, in the same way as the resulting parameters that have unrealistic values get highlighted in red.

Table 2.1 shows a summary of the modeling process. Considering the 3 runs for each of the 87 type-1 AGN modeled, GALFIT crashed only in 4 opportunities, although this happened with 4 different objects, hence there was always a reasonable solution among the 2 remaining models It is not surprising that the free-$n$ models ran into unphysical solutions more frequently: the additional degree of freedom means a higher degeneracy of "best" solutions available, with some of these having unphysical parameters. This could result in higher chances of GALFIT running into local $\chi^2$ minima and not getting out.

The model with the least $\chi^2$ is chosen between those that comply with the sanity check. If the model with the free Sérsic index is chosen among the 3 cases, we reassign the index and model it as follows: (1) if $n < 2$ then $n = 1$, (2) if $2 \leq n \leq 3$ then $n = 2.5$, and (3) if $n > 3$ then $n = 4$. This will group the galaxies into rough automatic morphological classes, from which we have that 57,5% have $n < 2$, 33,3% have $n > 3$, and the remaining 9.2% have an intermediate $n$.
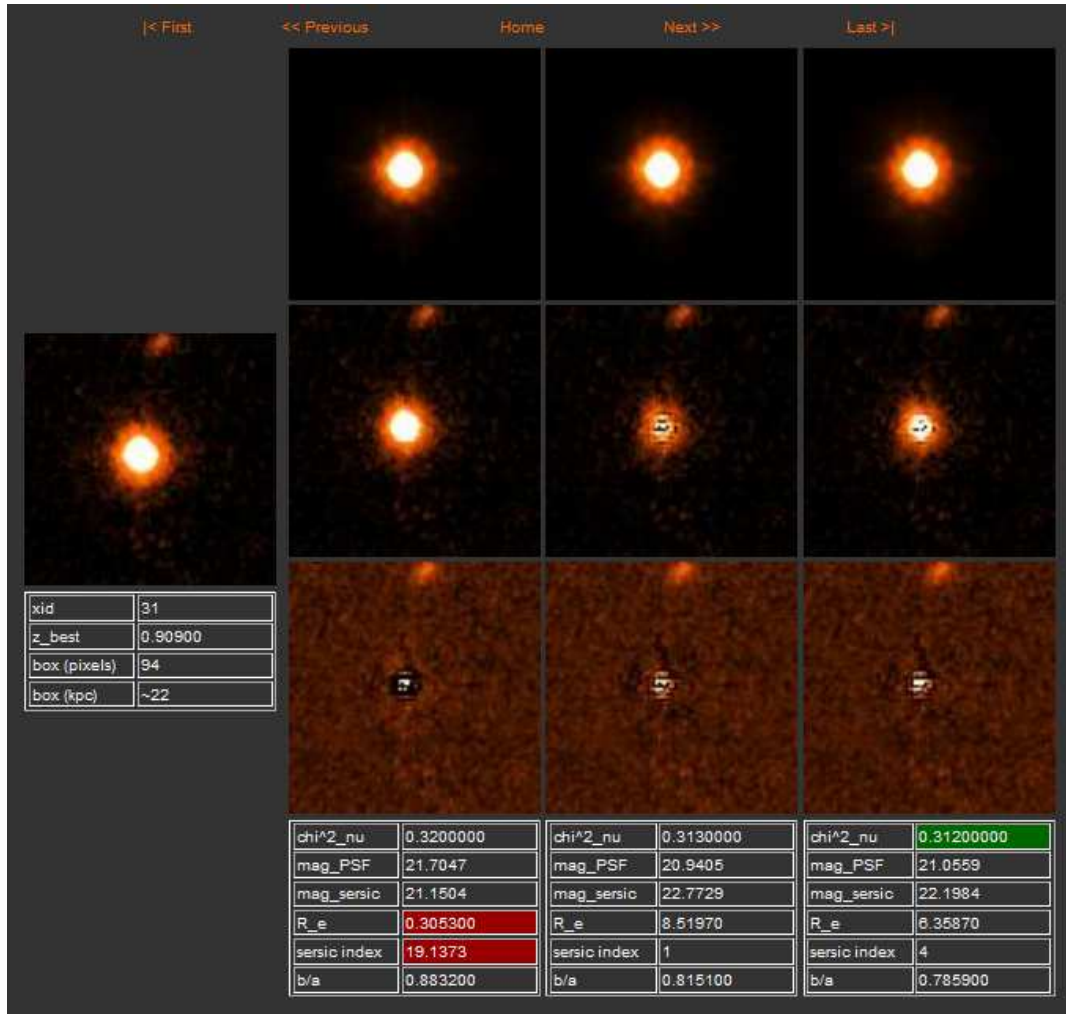
**Figure 2.4:** A screenshot of a typical output displayed on our web-based interface, created to ease the inspection of our resulting models. The stand-alone image on the left corresponds to the original science cutout, with its XMM-ID, redshift, and box dimensions. Next to it, from left to right, the $n$ =free, 1, and 4 fitting results, in which from top to bottom the model, the nucleus subtracted host, and the residual map images are displayed. Below them, the relevant parameters of the model host galaxy, highlighting the best $\chi^2$, and the parameters that ran out of boundaries.

## 2.3 Photometric reliability of the image decomposition

We have successfully employed our nucleus removal technique on our sample of type-1 AGN to recover their underlying host galaxies. Our thorough procedure em-

**Table 2.1:** Summary of the GALFIT modeling outcome.

| Sérsic index | $n$=free | | | $n = 1$ | $n = 4$ |
|---|---|---|---|---|---|
| Unsuccessful fits[a] | 1 | | | 2 | 1 |
| Unphysical $r_e$[b] | 14 | | | 0 | 5 |
| Unphysical $b/a$[b] | 0 | | | 0 | 0 |
| Unphysical $n$[b] | 19 | | | ... | ... |
| | $n < 2$ | $2 \leq n \leq 3$ | $n > 3$ | | |
| Best model | 16 | 8 | 5 | 34 | 24 |

[a] GALFIT crashed, returning no solution.
[b] See text for our definition of sensible values for $r_e$, $n$, and $b/a$.

ployed the widely used parametric fitting code GALFIT on a custom-built pipeline to automate the task. While we have taken many considerations, the simple visual inspection of the resulting host galaxies shows that many of them had an oversubtracted center, as indicated by negative residuals. In the same way, it is possible that those that do not reveal residuals could have been undersubtracted, i.e., the best-fit PSF had less flux than the actual AGN, leaving *positive* residuals. An empirical assessment of the significance of the residuals and potential systematic biases in photometry is mandatory in these kind of studies.

In order to evaluate the performance of our procedure, and the impact on the recovered host galaxies, we will simulate a sample of type-1 AGN from a starting point of real galaxies and stars, both from the very same *HST*/ACS COSMOS data set. Stars will be added as fake active nuclei on top of inactive galaxies, matching the host-to-nucleus contrast level as in our original sample. We will run the pipeline on the "mock" type-1 sample to remove their fake nucleus, and compare the properties of the host galaxies before and after the subtraction. This will give us a definite measure of the precision of our procedure, and on any bias that it may be introducing on our host galaxies.

## 2.3.1   Simulating type-1 AGN host galaxies

We require that our mock sample follows the properties of our original sample in terms of signal-to-noise ratio (S/N) and host-to-nucleus contrast level (H/N). Rather
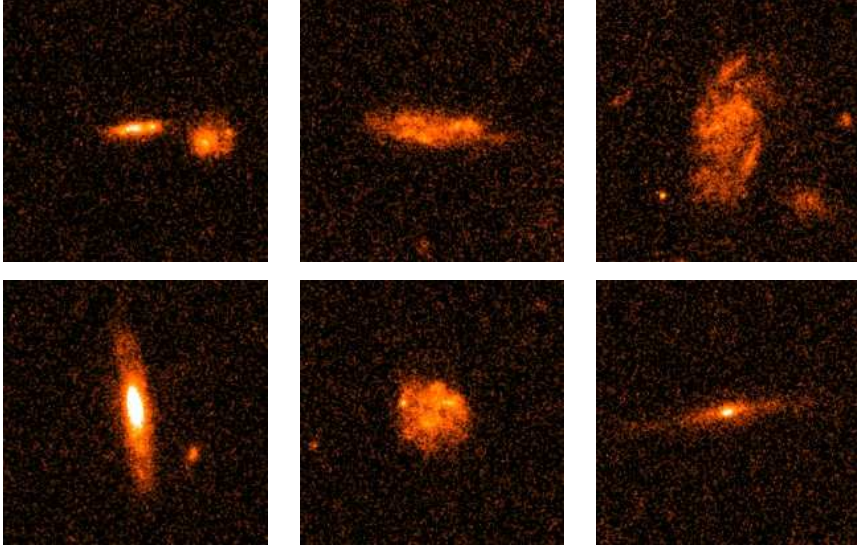
**Figure 2.5:** Examples of galaxies that were rejected from the initial inactive galaxy sample due to either being bulgeless, irregular, and/or an edge-on disk. These are unlikely counterparts for potential type-1 AGN host galaxies. The cutouts are $6'' \times 6''$ .

than creating ideal galaxies with added noise to test our decomposition pipeline, we will use real data to create a large simulated type-1 AGN sample: we will select inactive galaxies from the COSMOS catalog and add stars as fake nuclei. Under the assumption that our modeling was to first order correct, we will match the S/N by using galaxies with similar apparent magnitudes and redshifts, and the stars to be added will be selected so that resulting H/N matches that of our original sample.

For each type-1 AGN host galaxy, we proceed by selecting 10 similar inactive galaxies from the COSMOS ACS catalog (Leauthaud et al. 2007), with available photometric redshifts from Ilbert et al. (2009). We consider the aperture photometry on the type-1 AGN hosts after the nucleus removal to select galaxies with a $I_{F814W}$ magnitude within a range of $\triangle I_{F814W} = 0.1$, and a photometric redshift within a range of $\triangle z = 0.05$. If not enough galaxies were found, the search ranges were increased by 10%, and another iteration was performed. For most AGN 1 or 2 iterations were needed to find the required number of inactive galaxies for each type-1 AGN host.

With the 830 inactive galaxies in hand, we remove galaxies that are unlikely to be AGN host galaxy counterparts *a priori* via an initial visual inspection. Such galaxies include: (1) bulgeless disks and irregulars, which would represent a low-mass population, having no corresponding partners on the AGN sample, and (2) edge-on disks,

| Galaxy | + | Star | = | Mock AGN | Mock host |
|--------|---|------|---|----------|-----------|
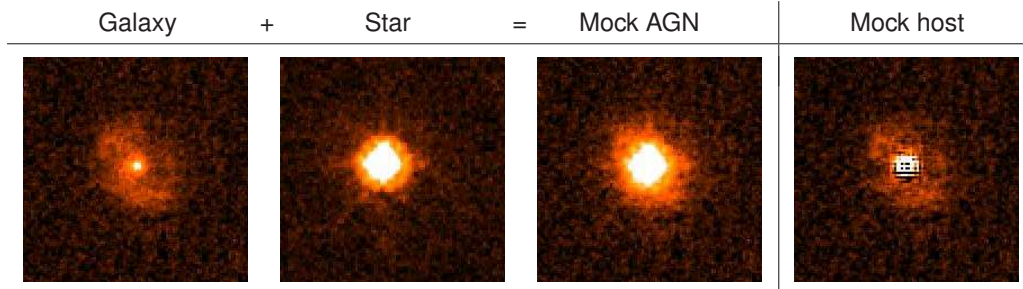


**Figure 2.6:** Illustrative example of the simulation of type-1 AGN host galaxies. On each case, a star is added to the galaxy to create a mock type-1 AGN system. The image decomposition procedure yields a host galaxy with some residuals, shown on the right.

which could in principle hold an AGN but this would be heavily obscured and therefore not be a type-1. The visual inspection resulted in 98 galaxies removed, from which some typical examples are shown in Figure 2.5.

In selecting stars, we will do so remaining true to the characteristic blue colors of the AGN. We perform an initial selection of stars from the COSMOS ACS archive by placing color cuts in $(B - V) < 0.75$ and $(V - R) < 0.95$. For each of the inactive galaxies, we look for stars that match the contrast level between the fluxes of the host and nucleus (H/N) of the corresponding AGN. With a matching star found, we simply add it over the centroid of the galaxy. Figure 2.6 shows an example of this procedure, in which a high-contrast type-1 AGN was created using a galaxy at $z \sim 0.8$.

## 2.3.2 Testing the impact of the AGN removal

We apply the same point source removal procedure as for the original type-1 AGN sample. Individual local PSFs are created exactly as before, and the light contributions of the star and the underlying galaxy are separated using our GALFIT-based pipeline. Figure 2.6 shows an example of the subtraction procedure on a simulated type-1 AGN, in which it is possible to observe side-by-side the original and recovered host galaxies. The resulting host galaxies will feature residuals in the center just as the original type-1 sample due to the mismatch between the added stars and the PSFs used on the modeling. With the exception of 5 unsuccessful fits, we are left with 727 simulated nucleus-subtracted AGN hosts that will give us an appropriate insight into the ability of our decomposition to recover the host galaxies.
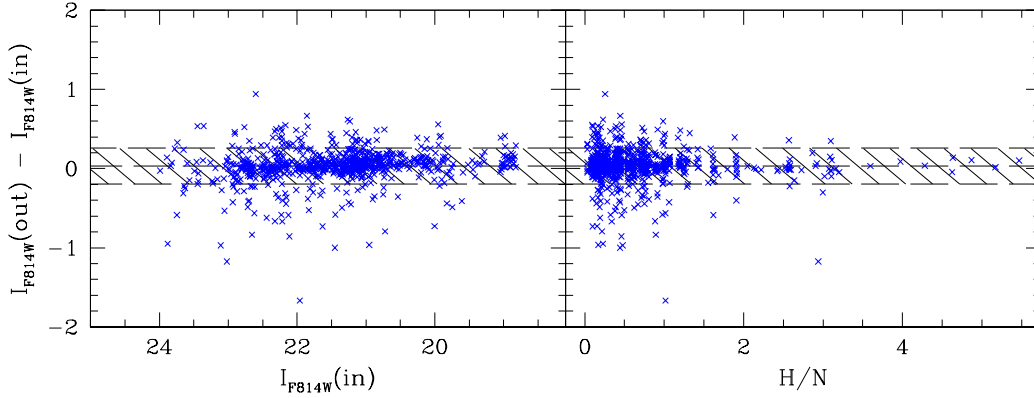
**Figure 2.7:** The difference in the observed magnitudes ($I_{F814W}$) of the comparison galaxies before (in) and after (out) the point source addition/subtraction. The left-hand panel plots this difference against the initial magnitude, and the right-hand panel against the host to nucleus flux ratio, H/N. The $1\sigma$ deviation away from the mean is 0.23 mag, indicated by the shaded area centered at 0.03 mag.

We have performed photometry on the mock AGN host galaxies before and after the addition/subtraction of the fake nucleus. We find that, on average, the galaxies are fainter by 0.03 mag after the subtraction, with a $1\sigma$ spread of 0.23 mag. Figure 2.7 shows the difference between the initial and recovered magnitudes for the hosts as a function of the initial magnitudes and H/N ratio for our control galaxies. Interestingly, there is no obvious correlation between the offset and the initial magnitudes of the galaxies. However, rather than a correlation with the brightness of the galaxy, the recovered values tend to be less exact for more compact galaxies and brighter active nuclei, as one would intuitively expect: smaller galaxies will overlap most of their flux with the central point source, making the decomposition more complex.

In total, these results show that this technique is trustworthy, as the offset found can be considered negligible. This implies that the decomposition is recovering the host galaxies with a very high precision, sufficient for the two science applications following in the next Chapters, and that the residuals observed only compromise a minute fraction of the overall flux.

## 2.4 Summary

In this chapter, we have presented and applied an image-modeling technique to de-compose nuclei and host galaxies of a sample of 87 type-1 AGN from the COSMOS survey. In summary:

1. We successfully modeled and decomposed the type-1 AGN sample. Using three alternatives for the Sérsic index for the host galaxy (fixed at $n = 1$ and $n = 4$, and as a free parameter), we produced a set of models for each AGN, from which we chose the best requiring reasonable structural parameters.

2. For each object, among the resulting models there was always a "realistic" solution. While for ~22% of the free-$n$ models the parameters ran into un-physical values, there was always a sensible solution from one of the fixed-$n$ cases.

3. We tested the accuracy of this technique by applying it on a simulated sample of 830 AGN host galaxies. We found that there is no significant systematic photometric error, and we are able to recover the host galaxy photometry with an accuracy of $0.03 \pm 0.23$mag.

As our technique proved trustworthy, we are ready to apply it on a scientific context: in Chapter 3 we will measure the luminosities of the AGN-subtracted host galaxies to estimate stellar masses, and in Chapter 4 we will perform a detailed analysis on their morphologies, free of point source contamination.

# THE RATIO OF BLACK HOLE MASS TO GALAXY MASS OVER THE LAST SEVEN BILLION YEARS

**In this chapter we investigate the behavior of the black hole mass to total stellar mass scaling relation out to $z \sim 0.9$ for 32 type-1 AGN. From our analysis we found that the $M_{\mathrm{BH}} - M_*$ ratio shows a zero offset with respect to the local relation for galactic bulge masses, as well as no evolution with redshift. Our results indicate that since $z \sim 0.9$ no substantial addition of stellar mass is required on the galaxy. Nevertheless, given that many of these galaxies show a disk component, their bulges are indeed undermassive. We conclude that for the last 7 Gyr the only mechanism required for these galaxies to obey the $z = 0$ relation is a redistribution of disk-to-bulge mass, likely driven by secular processes.**

## 3.1 Introduction

Over the last 15 years, tight correlations between various properties of galactic bulges and their central supermassive black holes have been discovered (e.g., Kormendy & Richstone 1995; Magorrian et al. 1998; Ferrarese & Merritt 2000; Gebhardt et al. 2000; Tremaine et al. 2002; Marconi & Hunt 2003; Häring & Rix 2004). While these correlations can be accounted for by a statistical convergence of typically several mergers per galaxy over cosmic time (Peng 2007; Jahnke & Macciò 2011), the

This chapter is based on Cisternas et al. (2011b)

observed coupling has often been taken as an indication of physically driven co-evolution (e.g., Kauffmann & Haehnelt 2000; Volonteri et al. 2003; Wyithe & Loeb 2003; Di Matteo et al. 2005).

A strong constraint for either globally or individually coupled growth of BH and stellar mass is the evolution of their scaling relations with redshift. Different theoretical models predict different levels of evolution (Granato et al. 2004; Robertson et al. 2006; Croton 2006; Di Matteo et al. 2008b), and observations which directly probe the physical mechanisms that regulate this co-evolution are scarce.

A handful of studies probing the scaling relations beyond the local universe have found a larger ratio of BH mass to bulge stellar mass (e.g., Walter et al. 2004; Peng et al. 2006a,b; Treu et al. 2007; Jahnke et al. 2009; Decarli et al. 2010; Merloni et al. 2010; Bennert et al. 2011), suggesting that BHs grow earlier than their host spheroids. Nevertheless, small number statistics and frequently ignored selection biases remain the main obstacles against additional evidence and more solid constraints.

In this chapter we explore the $M_{\mathrm{BH}} - M_*$ relation for 32 type-1 AGN in the redshift range $0.3 < z < 0.9$, with virial $M_{\mathrm{BH}}$ measurements. Stellar masses are computed by combining the host galaxy luminosities (accurately measured via high-resolution *HST*/ACS imaging) with a specially built mass-to-light ratio ($M_*/L$) based on a large sample of type-2 AGN, for which the masses have been estimated through a spectral energy distribution (SED) fitting.

## 3.2   Sample

Our parent sample of type-1 AGN has been drawn from the XMM-COSMOS survey catalog (Hasinger et al. 2007; Cappelluti et al. 2009), consisting of ~1800 bright X-ray sources. A detailed description of the accurate identification of their optical counterparts and multiwavelength properties is given by Brusa et al. (2010). Targetted spectroscopic observations with Magellan/IMACS (Trump et al. 2007, 2009a) and publicly available spectra from SDSS (Schneider et al. 2007) allowed the accurate classification of ~ 400 type-1 AGN. Within the redshift range $0.3 < z < 0.9$, we selected those with available virial $M_{\mathrm{BH}}$ estimates from Trump et al. (2009b), based on measurements of the width of the H$\beta$ line applied on the scaling relations of Vestergaard & Peterson (2006). This selection results in 32 type-1 AGN.

**Table 3.1:** Type-1 AGN Sample and Derived Host Galaxy Properties.

| Object (J2000) | $z$ | $\log M_{\mathrm{BH}}$[a] $(M_\odot)$ | Sérsic $n$[b] | $F814W_{\mathrm{Host}}$ (AB) | $\log L_{F814W}$[c] $(L_\odot)$ | $\log M_*$[d] $(M_\odot)$ |
|---|---|---|---|---|---|---|
| COSMOS J095817.54+021938.5 | 0.73 | 7.72 | 1.0 | 21.82 | 8.98 | 10.30 |
| SDSS J095819.88+022903.6 | 0.34 | 8.29 | 1.4 | 17.51 | 10.03 | 11.23 |
| COSMOS J095831.65+024901.6 | 0.34 | 8.08 | 1.4 | 19.33 | 9.29 | 10.65 |
| COSMOS J095840.61+020426.6 | 0.34 | 8.39 | 1.8 | 18.16 | 9.76 | 11.02 |
| COSMOS J095845.80+024634.0 | 0.35 | 7.39 | 2.8 | 19.70 | 9.16 | 10.54 |
| SDSS J095902.76+021906.5 | 0.34 | 8.66 | 4.0 | 17.81 | 9.91 | 11.14 |
| COSMOS J095909.53+021916.5 | 0.38 | 7.77 | 2.0 | 19.44 | 9.34 | 10.68 |
| COSMOS J095928.31+022106.9 | 0.35 | 7.24 | 1.0 | 18.41 | 9.68 | 10.95 |
| COSMOS J100002.21+021631.8 | 0.85 | 8.29 | 4.0 | 19.63 | 9.99 | 11.07 |
| SDSS J100012.91+023522.8 | 0.70 | 8.15 | 4.0 | 19.01 | 10.07 | 11.17 |
| COSMOS J100014.55+023852.7 | 0.44 | 7.79 | 4.0 | 20.05 | 9.23 | 10.57 |
| COSMOS J100017.54+020012.6 | 0.35 | 7.59 | 2.3 | 19.98 | 9.07 | 10.47 |
| SDSS J100025.25+015852.2 | 0.37 | 8.58 | 4.0 | 19.75 | 9.21 | 10.57 |
| COSMOS J100028.63+025112.7 | 0.77 | 8.49 | 4.0 | 20.13 | 9.70 | 10.86 |
| COSMOS J100029.69+022129.7 | 0.73 | 8.03 | 1.0 | 19.58 | 9.87 | 11.01 |
| COSMOS J100033.38+015237.2 | 0.83 | 8.07 | 1.1 | 20.42 | 9.65 | 10.81 |
| COSMOS J100033.49+013811.6 | 0.52 | 8.01 | 4.0 | 20.49 | 9.21 | 10.54 |
| COSMOS J100037.29+024950.6 | 0.73 | 7.41 | 1.0 | 21.65 | 9.05 | 10.36 |
| SDSS J100043.15+020637.2 | 0.36 | 8.07 | 4.0 | 17.44 | 10.10 | 11.28 |
| COSMOS J100046.72+020404.5 | 0.55 | 7.75 | 0.7 | 18.89 | 9.91 | 11.08 |
| COSMOS J100058.71+022556.2 | 0.69 | 7.91 | 1.0 | 20.61 | 9.42 | 10.66 |
| COSMOS J100118.52+015543.0 | 0.53 | 8.22 | 1.0 | 19.58 | 9.59 | 10.84 |
| COSMOS J100141.09+021300.0 | 0.62 | 7.35 | 3.4 | 20.82 | 9.24 | 10.53 |
| COSMOS J100146.49+020256.7 | 0.67 | 7.73 | 4.0 | 20.27 | 9.52 | 10.75 |
| COSMOS J100202.22+024157.8 | 0.79 | 8.24 | 1.0 | 21.24 | 9.29 | 10.53 |
| COSMOS J100205.03+023731.5 | 0.52 | 8.38 | 4.0 | 18.54 | 9.99 | 11.15 |
| COSMOS J100212.11+014232.4 | 0.37 | 7.70 | 1.8 | 20.02 | 9.09 | 10.48 |
| COSMOS J100218.32+021053.1 | 0.55 | 8.61 | 1.9 | 18.50 | 10.06 | 11.20 |
| COSMOS J100230.06+014810.4 | 0.63 | 7.50 | 1.0 | 20.20 | 9.49 | 10.73 |
| COSMOS J100230.65+024427.6 | 0.82 | 7.82 | 2.3 | 20.54 | 9.59 | 10.77 |
| SDSS J100232.13+023537.3 | 0.66 | 8.19 | 1.8 | 19.36 | 9.87 | 11.03 |
| COSMOS J100243.96+023428.6 | 0.38 | 8.25 | 4.0 | 18.15 | 9.86 | 11.08 |

[a] Uncertainty quoted as 0.4 dex (Trump et al. 2009b).
[b] Selected from the fixed ($n =1,4$) and free fits.
[c] As defined in Equation (3.1).
[d] Total propagated uncertainty is 0.35 dex.

A fundamental part of our analysis of the AGN host galaxies is based on the *HST*/ACS imaging of the COSMOS field (Scoville et al. 2007b; Koekemoer et al. 2007); this is therefore an ideal redshift range. As mentioned previously, beyond $z = 1$, the F814W filter shifts to restframe UV, where the point-like AGN starts to dominate the overall light distribution, making it highly difficult to resolve its host galaxy.

In Table 3.1 we summarize the sample, including the properties derived in the following sections.

## 3.3 AGN host galaxy masses

We infer the stellar masses for our 32 type-1 AGN host galaxies under the generally accepted unified AGN model (Antonucci 1993; Urry & Padovani 1995), in which type-1 and type-2 sources correspond to different viewing angles of the same phenomena. While recent observational evidence shows that AGN type depends on accretion rate as well as orientation (Trump et al. 2011), at $z \sim 1$ and moderate X-ray luminosities the host galaxies of both types of AGN show equivalent properties (Ammons et al. 2011).

We use a $M_*/L$ especially built from a large sample of type-2 AGN host galaxies with stellar masses derived from a thorough SED fitting. To quantify the light of the type-1 AGN hosts we model and remove the flux contribution of the AGN, utilizing high-resolution *HST*/ACS imaging with the F814W filter and $0.''03$/pixel sampling. The motivation for this approach is the simplicity and strength of the technique, which might prove extremely useful for cases in which the spectral coverage on the host galaxy is limited or even non-existant.

### 3.3.1 Assessing a characteristic AGN mass-to-light ratio

With the goal of estimating stellar masses for our type-1 AGN host galaxies, we need to construct realistic $M_*/L$ distributions. AGN hosts have characteristically young stellar populations different from the general population (Kauffmann et al. 2003; Sánchez et al. 2004; Jahnke et al. 2004a,b), and are drawn from the bright-end of the galaxy luminosity function (Zakamska et al. 2006).

With this in mind, we build a $M_*/L$ from a large sample of type-2 AGN, also from

the COSMOS survey. Type-2 AGN have the advantage that the bright nucleus is highly obscured, leaving the host galaxy almost free of contamination from AGN light. This allows us to exploit the vast ground-based multiwavelength photometry from COSMOS to accurately model the host galaxy SED, providing well-determined stellar masses.

Our sample of spectroscopically confirmed type-2 AGN (Trump et al. 2009a; Bongiorno et al. 2010) consists of 199 sources at $z \sim 0.2 - 0.9$. While the AGN contribution to the overall SED is minimal, for the sake of accuracy a large grid of composite galaxy+AGN models were used to find the best fit template most fully representing the type-2 system (Bongiorno et al. in prep). Stellar masses were derived from the SEDs, assuming a Chabrier initial mass function (IMF). Comparison of these stellar masses with fits of just a single galaxy template (Ilbert et al. 2010) shows an agreement within 0.1 dex, indicating that within the uncertainties the AGN contribution is negligible.

We require an observable quantity common to both our type-1 and type-2 samples. For this we define an instrumental, partially k-corrected luminosity based on the photometry from the *HST*/ACS imaging with the F814W filter,

$$L_{F814W} = 4\pi \cdot d_L^2 \cdot f_{F814W} \cdot (1 + z)^{-1} \qquad (3.1)$$

where $f_{F814W}$ is the aperture corrected flux and $d_L$ is the luminosity distance. The $(1 + z)^{-1}$ term accounts for the bandpass shifting.

In order to determine a relation between $M_*/L$ and both redshift and luminosity, and to reduce the covariance between the two variables, we perform a variance-weighted least squares bivariate fit of the form

$$\log M_*/L_{F814W} = A \cdot z + B \cdot \log(L_{F814W}/L_0) + C, \qquad (3.2)$$

where $\log(L_0/L_\odot) = 8.2$ corresponds to the minimum value of the luminosity. Fitting this function to our 199 type-2 AGN host galaxies, using the propagated uncertainties from both $M_*$ and $L_{F814W}$ to weight each object, results in the coefficients $A = -0.25 \pm 0.12$, $B = -0.21 \pm 0.08$, and $C = 1.67 \pm 0.11$.

Figure 3.1 shows $M_*/L$ for the type-2 AGN sample (filled circles) as a function of redshift (left panel) and luminosity (right panel) and in comparison to ~40000 inactive galaxies with $I < 23$ from the COSMOS catalog (Ilbert et al. 2009). The latter
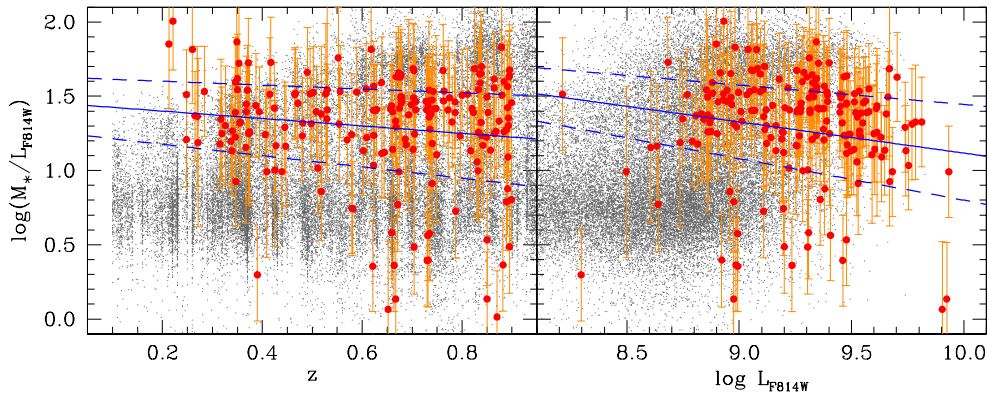
**Figure 3.1:** Mass-to-light as a function of redshift (left panel) and luminosity (right panel) for the type-2 AGN sample, plotted as the filled circles. The dots correspond to ~40,000 inactive galaxies with $I < 23$ from the COSMOS catalog (Ilbert et al. 2009), shown for comparison. The solid lines are the projections of the best-fit plane from Equation (3.2) at the median luminosity and redshift values respectively. The typical $1\sigma$ errors on the fit are marked by the dashed lines.

separate into the usual red sequence and blue cloud with different $M_*/L$. The solid lines are the projections of the best-fit plane from Equation (3.2) at the median luminosity and redshift values respectively. The typical $1\sigma$ errors on the fit are marked by the dashed lines.

## 3.3.2   Type-1 AGN host luminosities

Analyzing type-1 AGN host galaxies remains complicated due to the bright nucleus which can dominate the galaxies' light emission. Nevertheless, high-resolution *HST*/ACS imaging allows us to perform two-dimensional decomposition by modeling the AGN and its host galaxy as a point-spread function (PSF) and a Sérsic (1968) profile respectively using GALFIT (Peng et al. 2002). Further multi-component modeling of the host galaxy (i.e., bulge+disk) has been shown not to be efficient at our resolution and S/N levels (Sánchez et al. 2004; Simmons & Urry 2008; Kim et al. 2008). The precision of the AGN-host galaxy decomposition strongly depends on the PSF of choice to be supplied to GALFIT. Thanks to the large COSMOS *HST*/ACS area, we can account for instrumental and temporal variations by building specific PSFs for each object by averaging its nearest ~30 stars (Jahnke et al. 2004b). For
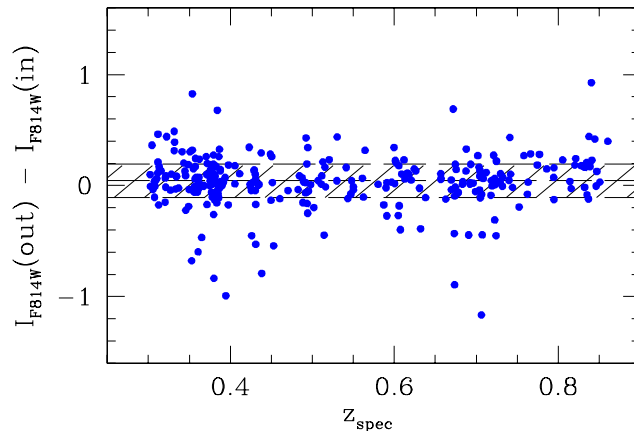
**Figure 3.2:** Difference in the observed magnitudes ($I_{F814W}$) of the comparison galaxies before (in) and after (out) the point source addition/subtraction, as a function of redshift. The $1\sigma$ deviation away from the median is 0.15 mag, indicated by the shaded area centered at 0.01 mag.

each object, we perform several GALFIT runs with three alternatives for the Sérsic index $n$: fixed to a $n = 1$ exponential profile, to a $n = 4$ de Vaucouleurs profile, and also as a free parameter. The best model is chosen based on a combination of the least $\chi^2$ and a sanity check on the resulting parameters. We require our galaxy model to have a half-light radius between 2.5 and 100 pixels, i.e., not unphysically large or concentrated; to have a realistic elongation, implying $b/a > 0.5$; and for the free $n$ case not to run outside the range 0.5–8. After subtraction of the best-model PSF, we are left with the host galaxy emission plus some residuals.

As we already showed in Chapter 2, the image decomposition technique is trustworthy and does not affect in any significant way our host galaxy photometry. Nevertheless, since our findings showed that there is no major global effect on the *whole* type-1 sample, it might be convenient to check whether for this particular subsample there is any larger effect. Depending on the morphologies, compactness, and brightness of the galaxies, it may be that this subsample gets affected differently. Therefore, we check for the impact of the decomposition on a comparison sample specifically matching out type-1 subsample. For each type-1 host we select 10 inactive galaxies from the COSMOS catalog matching both in redshift and apparent magnitude. To each comparison galaxy we add a star as a fake active nucleus, keeping the contrast between host and nucleus of the corresponding type-1 system. We model and remove

the point source as for the original AGN, and perform photometry on the comparison galaxies before and after the procedure. Figure 3.2 shows the difference between the initial and recovered magnitudes for the hosts as a function of redshift. We find only a modest offset of $0.04 \pm 0.15$ mag, for which we correct our type-1 host galaxy photometry as well as its error budget. The host galaxy flux will be used to estimate the luminosity as in equation (3.1), which is subsequently applied to our derived $M_*/L$ relation from equation (3.2) to estimate the masses. The resulting luminosities and stellar masses are presented in Table 3.1. The uncertainty in the photometry together with the errors on the fitting coefficients result in a total stellar mass uncertainty of 0.35 dex.

## 3.4  Results and discussion

The $M_{\mathrm{BH}}$–$M_*$ relation for our 32 type-1 AGN is shown in Figure 3.3 in three redshift intervals. As a reference, we compare our measurements with the local relation between BH and bulge mass (Häring & Rix 2004), given by

$$\log M_{\mathrm{BH}} = 1.12 \log M_* - 4.12 \tag{3.3}$$

shown as the solid line together with its scatter of 0.3 dex, indicated by the dashed lines. The vast majority of our sources (30/32) fall directly within the uncertainties of the $z = 0$ relation, *but with their total instead of bulge stellar mass*. Our sample presents a median offset perpendicular to the local relation of $\Delta\log(M_{\mathrm{BH}}/M_*) = 0.01 \pm 0.03$, consistent with zero. In Figure 3.4 we show the offset of each object as a function of redshift. Interestingly, no trend is observed in the offset as a function of increasing redshift. Nevertheless, to check for traces of redshift evolution in our sample we force a fit to a function of the form $\Delta\log(M_{\mathrm{BH}}/M_*) = \delta\log(1 + z)$ to our data, again using a weighted least squares method. We find a best fit with $\delta = 0.02 \pm 0.34$ (solid line), in practice undistinguishable from the $\Delta\log(M_{\mathrm{BH}}/M_*) = 0$ line at this redshift range, and consistent with zero evolution within the scatter.

### 3.4.1  Mass function bias

As the observed offset from the local relation is not redshift-dependent, its origin still needs unveiling: selection effects or pure random scatter?
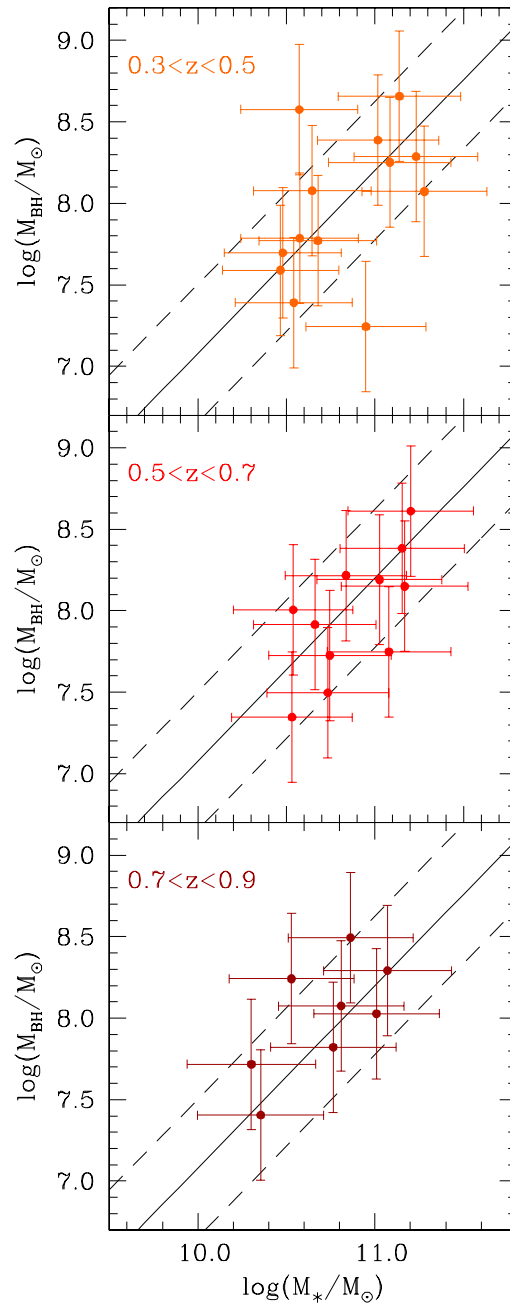
**Figure 3.3:** BH mass versus total galaxy stellar mass scaling relation for our sample of 32 type-1 AGN, shown in three arbitrary redshift bins. For comparison, the best fit local relation for bulge mass as in Equation 3.3 is shown (solid line), along with its 0.3 dex scatter (dashed lines).

It has been pointed out in the literature (Salviander et al. 2007; Treu et al. 2007; Lauer et al. 2007; Merloni et al. 2010; Decarli et al. 2010) that selection effects have to be taken into account when trying to infer the intrinsic scaling relations from the observed data, else a false signal of evolution could be perceived. While local studies select their samples of inactive galaxies based on galaxy properties ($M_*$, $L$, $\sigma_*$), at higher redshifts the samples are selected based on AGN luminosity and hence BH mass, implying that for a given $M_{\rm BH}$ there is a range of potential stellar masses $M_* \pm dM_*$ due to an intrinsic cosmic scatter $\sigma_\mu$. If the expected $M_*$ for a given $M_{\rm BH}$ happens to be in the steep massive part of the galaxy stellar mass function $\phi(M_*)$ there will be a much higher probability of retrieving a less massive galaxy, which automatically translates into a positive measured offset in $M_{\rm BH}/M_*$.

As in Merloni et al. (2010), we quantify the bias based on the result derived by Lauer et al. (2007). Assuming that the local relation from Häring & Rix (2004) holds true within the redshift range probed here, and that $\sigma_\mu$ is not too large, the offset as a function of $M_{\rm BH}$ due to selection effects can be approximated as[1]

$$\Delta \log(M_{\rm BH}/M_*) \approx \sigma_\mu^2 \left[ \frac{d \ln \phi(M_*)}{d \log M_*} \right]_{M_*(M_{\rm BH})} \tag{3.4}$$

where the galaxy mass is given simply by $\log M_* = (\log M_{\rm BH} + 4.12)/1.12$, and $\phi(M_*)$ is the galaxy mass function from the S-COSMOS survey at $z \sim 0.5$ (Ilbert et al. 2010). In Figure 3.5 we show the offset of our sources from the local relation as a function of $M_{\rm BH}$, as well as the expected offset due to the mass function bias from Equation (3.4) for two different values of $\sigma_\mu$: 0.3 (solid line) and a more conservative 0.5 (dashed line), which is a good representation of the range of intrinsic scatter estimates in the local relation (Gültekin et al. 2009).

It is clear that even for the likely $\sigma_\mu = 0.3$ case the mild positive offset at the high-$M_{\rm BH}$ end can be explained by the expected mass function bias, while the effect is small for the lower-mass half of our sample. This reaffirms that no signs of evolution are present with respect to total galaxy mass out to $z \sim 0.9$.

---

[1]Note that in the derivative, Merloni et al. (2010) used $\log \phi(M_*)$ instead of the correct $\ln \phi(M_*)$.
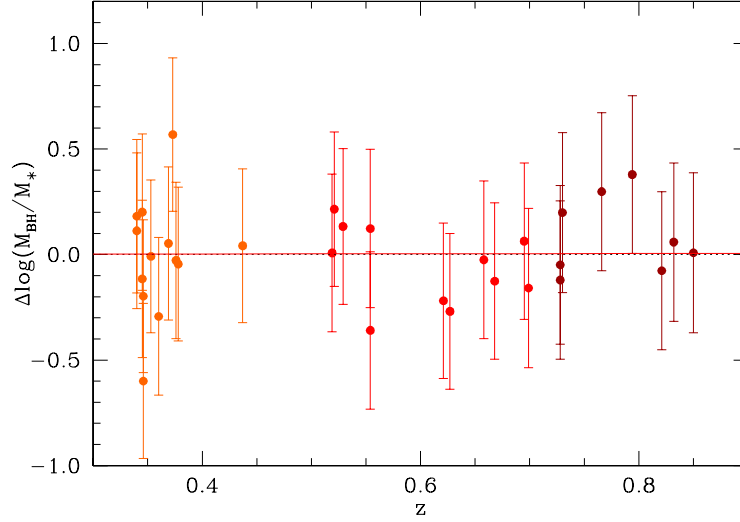
**Figure 3.4:** Perpendicular offset from the local relation (dotted line) as a function of redshift. Fitting a redshift evolution of the form of $\Delta\log(M_{BH}/M_*) = \delta(1 + z)$ yields $\delta = 0.02 \pm 0.34$, shown as the solid line.
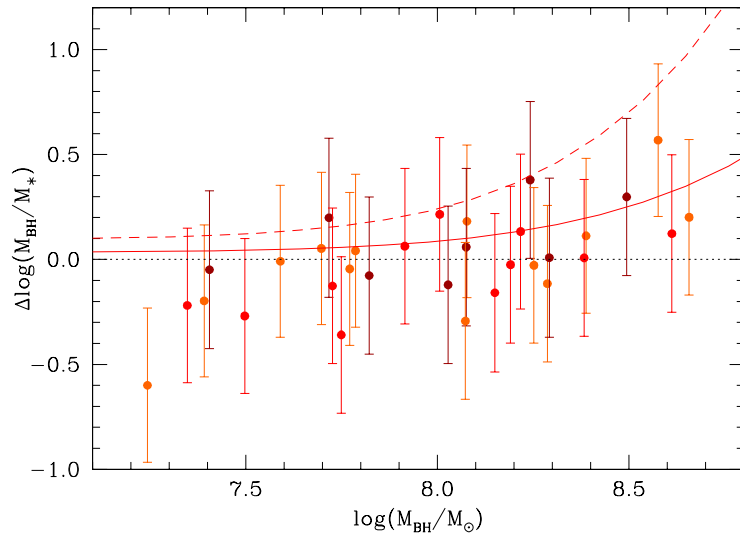


**Figure 3.5:** Offset from the local relation as a function of BH mass. The expected mass function bias from Equation (3.4) is shown for two different cases of intrinsic cosmic scatter: 0.3 dex (solid line), and 0.5 dex (dashed line).

### 3.4.2 No significant $M_{BH}$ and $M_*$ growth down to $z = 0$

Although our objects are in general agreement with the local $M_{BH}/M_*$ ratio, they are still observed $3 - 7$ Gyr before $z = 0$. What constraints can be inferred for their subsequent evolution, both in stellar and BH mass?

From the perspective of the ongoing BH growth, we can estimate the increase in $M_{BH}$ using the Eddington accretion rate $\dot{M}_{Edd}$, i.e., the mass accretion rate required to sustain the Eddington luminosity $L_{Edd}$, given by

$$\dot{M}_{Edd} \approx 2.2 \cdot 10^{-1} \, M_8 \, M_\odot \, \mathrm{yr}^{-1} \tag{3.5}$$

where $M_8$ will be the mass of the object, in this case $M_{BH}$, in units of $10^8 M_\odot$. Therefore, during the current AGN episode: (i) Taking an average accretion rate $L/L_{Edd}$ of 0.1 for these sources at $z < 1$ (Trump et al. 2009b), and considering a remaining accretion period of half a typical observable AGN lifetime ($\sim$10 Myr) (e.g., Martini 2004a; Porciani et al. 2004), the increase of log$M_{BH}$ will be $\sim$0.001 dex. (ii) A definite upper limit on the subsequent BH growth can be given by considering the AGN lifetime derived from the number density of XMM-COSMOS AGN by Gilli et al. (2009). Out to $z \sim 1$ they compute an AGN duty cycle of 0.1, corresponding to an AGN lifetime of $\sim$1 Gyr. Using the same accretion rate as before, we estimate that our sources will *at most* grow 0.09 dex in BH mass due to accretion. This implies that these sources will hardly move in the upward direction of the $M_{BH}$–$M_*$ plane.

Concurrently, we can give upper limits to the stellar mass increase due to star formation in these galaxies. Based solely on the average specific star formation rates at this mass range (log$M_*$ = $10.2 - 11.2$ log $M_\odot$; Karim et al. 2011), from their respective redshift down to $z = 0$, in the most extreme case the increase will be a factor of 1.8 (or 0.25 dex). This ignores potential quenching mechanisms and is sufficient to show that we should not expect a significant change in stellar mass.

Regarding merger activity, the major merger rate (mass ratio >1:3) since $z \sim 0.5$ is low ($\sim$0.05 Mergers Gyr$^{-1}$; Hopkins et al. 2010) and should (i) not have a significant impact on the total galaxy mass of the ensemble, and (ii) major mergers will add similar mass fractions to both galaxy and BH.

Nevertheless, the true relevance of the overall, mainly minor merging activity will be in the subsequent bulge growth of these galaxies: The fact that the *total* stellar mass of our galaxies is already consistent with the local relation for galactic bulges at $z \sim 0.7$ means that, for them to obey the local relation by $z = 0$, their current total
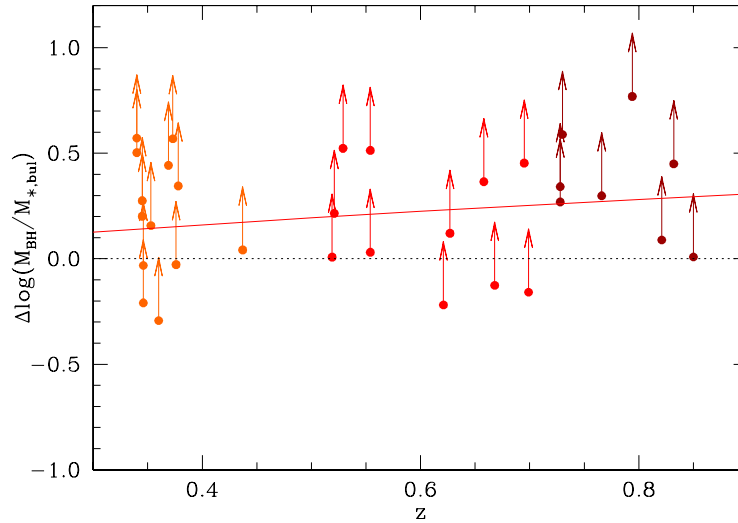
**Figure 3.6:** Perpendicular offset from the local relation (dotted line) as a function of redshift as in Figure 3.4, but considering the *bulge* mass upper limit of the galaxies (see text for our B/T definition). The solid line corresponds to a redshift evolution with $\delta = 1.15 \pm 0.34$.

mass should end up redistributed as bulge mass. Secular processes such as minor interactions and internal instabilities are the prevailing bulge-building mechanisms (Kormendy & Kennicutt 2004; Weinzirl et al. 2009; Parry et al. 2009). This also fits with recent evidence suggesting that major merging may not be relevant at triggering these AGN at $z < 1$ (e.g., Grogin et al. 2005; Gabor et al. 2009; Georgakakis et al. 2009; see Chapter 4). Altogether, this has the implication that over the last 7 Gyr no extreme mass growth is required to produce the local scaling relations. Instead a rather passive, non-violent secular evolution will drive the redistribution of mass into the bulge components.

With this in mind our results do not necessarily contradict previously reported evolution with respect to *bulge* properties in the redshift windows $z = 0.36, 0.57$ (e.g., Treu et al. 2007; Woo et al. 2008; Bennert et al. 2010). Based on our GALFIT modeling, we can make some basic assumptions to estimate the bulge-to-total mass ratio (B/T) of our galaxies: assuming a B/T upper limit of 0.3 and 0.6 for the galaxies with $n < 2$ and $2 < n < 3$ respectively, we can give a rough estimate of $M_{*,bul}$ at least for illustrative purposes. For the $n > 3$ case, we take an upper limit of B/T=1, as it corresponds to a bulge-dominated galaxy. According to this definition of $M_{*,bul}$, we show its offset as a function of redshift in Figure 3.6. Fitting the same functional form as before yields $\delta = 1.15 \pm 0.34$, an indication that our data permits an evolution

with respect to *bulge* mass, and in broad agreement with Treu et al. (2007).

## 3.5 Conclusions

A representative AGN host galaxy $M_*/L$ was used to estimate stellar masses for 32 type-1 AGN hosts at $0.3 < z < 0.9$. Combined with already available virial BH mass estimates, we studied the $M_{BH} - M_*$ scaling relation out to 7 Gyr lookback time covering the range $M_{BH} \sim 10^{7.2-8.7} \, M_{\odot}$, and extended recent studies probing the $z > 1$ regime (Jahnke et al. 2009; Merloni et al. 2010). In summary:

1. $M_*/L$ for intermediately luminous AGN at a given redshift and luminosity has scatter of only ~0.25 dex.

2. Within a 0.03 dex uncertainty in the mean, the *total* mass of our sources are consistent with zero offset from the $z = 0$ relation for galactic *bulges*.

3. No increase of the offset was found with redshift. Nevertheless, a forced fit to the functional form $\delta \log(1 + z)$ yields $\delta = 0.02 \pm 0.34$, confirming non-evolution.

4. We found that a positive observed offset exists in the observed value at high $M_{BH}$. When including the mass function bias upon inference of the intrinsic relation for our sample, we found that this selection effect accounts for the increasing offset with $M_{BH}$.

5. The fact that the majority of these galaxies are disk-dominated, together with the lack of evolution with respect to total $M_*$, implies that all mass to be found in the bulge at $z = 0$ is already present in the galaxy at the observed redshift, and the only process required is a redistribution of stellar mass from disk to bulge driven by secular evolution.

6. Our result allows an evolution of the bulge mass scaling relations: a simple assessment of B/T based on our GALFIT modeling indeed yields $\delta = 1.13 \pm 0.34$.

We presented a simple and solid technique to estimate stellar masses of type-1 AGN host galaxies when no high-resolution multiwavelength coverage is present. Our

work explicitly confirmed the expected non-evolution of the $M_{\mathrm{BH}} - M_*$ ratio out to $z$=0.9. The low levels of star formation, merger activity, and BH growth do not allow for any extreme evolution at these redshifts and secular processes must dominate any changes in the mass distributions and structures of galaxies.

# CHAPTER 4

## CHASING THE MAJOR MERGER—AGN CONNECTION

**In this chapter we set out to understand the relevance of major merging as an AGN triggering mechanism out to $z = 1$. Using the *HST*/ACS imaging from the COSMOS survey, we visually analyzed the morphologies of 140 X-ray-selected AGN looking for signatures of recent mergers, and compared them with a control sample of over 1200 matched inactive galaxies. We found that the merger fraction of the AGN host galaxies is statistically the same as that of the equivalent inactive galaxy population, roughly a 15%. Together with the fact that the majority of the AGN hosts are disk-dominated, an unlikely relic of an old major merger, our results are the strongest evidence to date that rather than major merging, secular evolution dominanted black hole fueling for the last 8 Gyr.**

## 4.1   Introduction

There is a general agreement that supermassive black holes (BHs) lie at the centers of nearly all galaxies, or at least those with a bulge component. Additionally, strong correlations exist between the BH mass and various properties of the galactic

---

This chapter has been adapted from Cisternas et al. (2011a). While the logical flow among Chapters 3 and 4 is as it is being presented in this thesis, the actual temporal order was the opposite. At the time the work for Chapter 4 was carried out, the final XMM-COSMOS catalogs were not out, and hence the available sample of type-2 AGN was smaller. Therefore, a different method to estimate stellar masses was emploeyd in Section 4.4.2. We tested for any fundamental differences, finding that both methods agree within ≲0.15 dex, concluding that it did not merit reviewing the mass estimates.

bulge (e.g., Kormendy & Richstone 1995; Magorrian et al. 1998; Ferrarese & Merritt 2000; Gebhardt et al. 2000; Tremaine et al. 2002; Marconi & Hunt 2003; Häring & Rix 2004; Gültekin et al. 2009) While it has been recently proposed that these correlations are just the product of a statistical convergence of several galaxy mergers over cosmic time (Peng 2007; Jahnke & Macciò 2011), these correlations have often been interpreted as the signature of coupled evolution between the BH and its host galaxy (Kauffmann & Haehnelt 2000; Volonteri et al. 2003; Wyithe & Loeb 2003; Granato et al. 2004; Hopkins et al. 2007; Somerville et al. 2008).

Given that most galaxies are believed to have undergone a quasar phase, and that the central BH represents a relic of this event (Lynden-Bell 1969; Richstone et al. 1998), the co-evolution picture is naturally very appealing even while some aspects of it remain unclear. It has been suggested that most of the mass of the BH is built up during the brightest periods of this quasar phase (Soltan 1982; Yu & Tremaine 2002). If there is such a connection between the growth of the BH and its host galaxy, periods of quasar activity should occur alongside the growth of the bulge, and the mechanism that triggers the accretion onto a once quiescent BH, turning it into an active galactic nucleus (AGN), should be tightly linked with the overall evolution of the host galaxy. The nature of AGN triggering is therefore of key importance for our understanding of galaxy evolution in general.

According to the current paradigm of hierarchical structure formation, major mergers are a crucial element in the assembly and growth of present-day galaxies (e.g., Kauffmann et al. 1993; Cole et al. 2000; Somerville et al. 2001; Bell et al. 2006; Jogee et al. 2009; Robaina et al. 2010). A closer look into the behavior of simulated collisions between galaxies, beginning with the pioneering work of Toomre & Toomre (1972), suggests that gravitational interactions are an efficient way of transporting material toward the very center of a galaxy. Mergers and strong interactions can induce substantial gravitational torques on the gas content of a galaxy, depriving it of its angular momentum, leading to inflows and the buildup of huge reservoirs of gas in the center (Hernquist 1989; Barnes & Hernquist 1991, 1996; Mihos & Hernquist 1996; Springel et al. 2005a; Cox et al. 2006; Di Matteo et al. 2007; Cox et al. 2008).

From early on, major mergers have been related to observations of powerful nuclear starbursts (Gunn 1979), and connections with quasar activity were made soon after. Stockton (1982), in a study of luminous quasars with close companions, suggested that these neighboring galaxies could be survivors of a strong interaction with the

quasar. Further observational studies came to support this picture: more cases of quasars with close companions were found, and post-merger features were detected in the host galaxies, whenever it was possible to resolve them (e.g., Heckman et al. 1984; Gehren et al. 1984; Hutchings et al. 1984, 1988; Stockton & Ridgway 1991; Hutchings & Neff 1992). The merger–quasar connection scenario gained strength with the discovery of the ultraluminous infrared galaxies (ULIRGs). More than 95% of these were found in a merging state, some of them hosting an AGN. This led to the scenario in which ULIRGs and quasars were part of the same chain of events (Sanders et al. 1988a,b; Sanders & Mirabel 1996; Surace et al. 1998; Surace & Sanders 1999; Surace et al. 2000; Canalizo & Stockton 2000, 2001).

With the advent of *HST*, deep imaging of AGN host galaxies at higher redshifts became possible with unprecedented resolution. Many observational studies of luminous AGN found a high rate of merging signatures in their hosts and detected the presence of very close companions, which before *HST* could not be resolved (e.g., Bahcall et al. 1997; Canalizo & Stockton 2001; Zakamska et al. 2006; Urrutia et al. 2008). At the same time, deeper imaging of AGN host galaxies that were initially classified as undisturbed revealed post-merger features not previously detected, both from space-based (Canalizo et al. 2007; Bennert et al. 2008) and ground-based observations (Ramos Almeida et al. 2011a).

There is, however, one major caveat for most of the studies listed above: almost none of them made use of, or had the access to, an appropriate control sample of inactive galaxies; such a control sample is essential for discerning if the merger rate is in fact enhanced with respect to the "background level", i.e., the merger rate of inactive galaxies. Only Dunlop et al. (2003) compared their statistically complete sample of quasars against the quiescent galaxy population, finding no difference in the structural parameters between samples, as well as no enhancement in the large-scale disturbances. Even if not explicitly, this showed a clear divergence from previous studies regarding the merger-AGN connection scenario, and agreed with the very low frequency of post-merger signatures observed on Seyfert galaxies and low-luminosity AGN (Malkan et al. 1998; Schade et al. 2000).

A new era of large *HST* programs now offers the potential for resolving this discrepancy. The imaging of larger, contiguous fields has yielded a large number of objects, making it possible to study AGN hosts at space-based resolution, and at the same time to compile a control sample of non-active galaxies. Initial studies using *HST* imaging by Sánchez et al. (2004) with the Galaxy Evolution from Mor-

phologies and SEDs survey (GEMS, Rix et al. 2004) and by Grogin et al. (2005) with the Great Observatories Origins Deep Survey (GOODS, Giavalisco et al. 2004) found no evidence for an enhancement in merging signatures of AGN hosts over control galaxy samples. If merger activity does not play a major role in AGN triggering, other methods to produce gas inflows, build up the bulge, and fuel the BH should also be of importance. Alternate secular mechanisms—minor interactions, large scale bars, nuclear bars, colliding clouds, supernova explosions—can also lead to angular momentum removal and gas inflows from different scales to the central regions (for reviews, see Kormendy & Kennicutt 2004; Wada 2004; Martini 2004b; Jogee 2006). While these processes have usually been related to Seyfert galaxies and low-luminosity AGN (e.g., Simkin et al. 1980; Taniguchi 1999; Knapen et al. 2000; Hopkins & Hernquist 2009), they could potentially play a larger role than usually reckoned for more luminous AGN as well. Although the results from the GEMS and GOODS surveys are highly intriguing, the field sizes of ~0.22 deg$^2$ and ~0.08 deg$^2$ respectively were still too small for definitive conclusions to be drawn. A suitably larger sample would be required to turn these appealing hints into statements.

In this context, we tackle this long-standing issue by performing a comprehensive morphological analysis of a sample of X-ray-selected AGN host galaxies from the Cosmic Evolution Survey (COSMOS, Scoville et al. 2007a), the largest contiguous area ever imaged with the *HST* (Scoville et al. 2007b; Koekemoer et al. 2007). Our goal is to disentangle the actual relevance and predominance of major galaxy mergers from the other suggested mechanisms for the fueling of the BH.

In the past, targeted high-resolution imaging of AGN hosts has only been possible for small samples, while extensive ground-based surveys with large samples have lacked of the necessary resolution to perform detailed morphological studies at moderate redshifts. Earlier results from the detailed analysis by Gabor et al. (2009), where the morphologies of ~400 AGN host galaxy candidates from the COSMOS field were parameterized, showed that these had an asymmetry distribution consistent with that of a control sample of inactive galaxies, and lacked an excess of companions, already suggesting that major interactions were not predominant among AGN as a triggering mechanism. Here we use the largest sample of optically confirmed X-ray-selected AGN ever imaged at *HST* resolution from the COSMOS survey and perform a visual inspection of the morphologies of the host galaxies. We opt for a visual analysis of our galaxies over an automatic classification system because of the inherent problems and incompleteness of the latter in identifying mergers, even for some obvious cases, as cautioned by recent studies probing both methods (Jogee et al. 2009; Kartaltepe

et al. 2010). To establish the relevance of our findings, we compare the AGN hosts to a matching sample of inactive galaxies from the same exact data set.

## 4.2 Sample selection

We will perform our analysis on a complete sample of X-ray selected optically confirmed type-1 and type-2 AGN from the COSMOS field.

We use the sample previously described in Chapter 2, i.e, X-ray selected AGN confirmed as type-1 from spectroscopic surveys and from spectral energy distribution (SED) fitting (e.g., Trump et al. 2009a; Lilly et al. 2007; Salvato et al. 2009; Ilbert et al. 2009). We additionally include a subsample of X-ray selected type-2 AGN, based on those used by Gabor et al. (2009) drawn from a parent sample of ~300 narrow emission line objects (Trump et al. 2007, 2009a). Restricting ourselves to the redshift range $z \sim 0.3 - 1.0$, our selection yields 83 type-1 and 57 type-2 AGN.

In this chapter, we analyze the morphological properties of the AGN host galaxies. For this, we take advantage of the high-resolution imaging of the COSMOS field with the *HST*. These observations comprise 583 orbits using the Advanced Camera for Surveys (ACS) with the F814W (broad *I*-band) filter (Koekemoer et al. 2007). The imaging data feature an oversampled scale of $0\rlap{.}''03$/pixel. Although the ACS survey of the COSMOS field is highly homogeneous, the exact depth achieved is dependent on the angle of the telescope with the Sun at the time of the observations (Leauthaud et al. 2007). Ninety six out of the 575 pointings were made with an angle smaller than a critical value of $70°$, leading to a slightly shallower image. The limiting surface brightness levels above the background for the pointings made with an angle with the Sun larger and smaller than the critical value are ~23.3 mag arcsec$^{-2}$ and ~22.9 mag arcsec$^{-2}$ respectively.

Figure 4.1 shows the X-ray luminosity distribution of our sources in the 2-10 keV energy band. The values were obtained mainly from those calculated by Lusso et al. (2010) and are complemented with those by Mainieri et al. (2007). The median of our distribution lies at $L_X = 10^{43.5}$ erg s$^{-1}$, which means that we are probing a reasonably luminous representative AGN sample. For reference, in Figure 4.1 we also show the X-ray luminosity distribution of the type-1 AGN subsample only, which dominates the overall distribution and has a slightly brighter median $L_X$ ($10^{43.6}$ erg s$^{-1}$) than the type-2 subsample ($10^{43.3}$ erg s$^{-1}$).
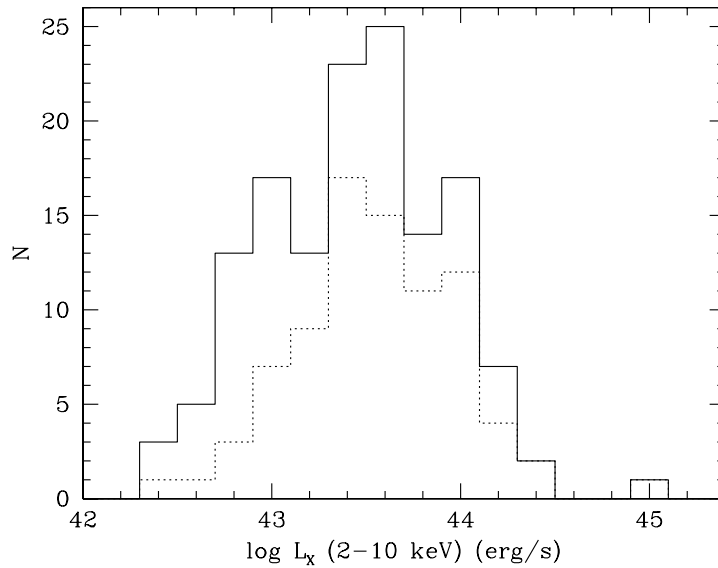
**Figure 4.1:** The X-ray luminosity distribution of our sample in the 2-10 keV energy band (solid line). For reference, we also show the distribution of the type-1 AGN subsample only (dotted line).

## 4.3   Methodology

In this chapter we analyze the morphologies of a sample of AGN host galaxies and of a control sample of inactive galaxies using high-resolution *HST*/ACS single *I*-band images. In the following subsections we explain how we built the comparison sample (hereafter CS), the motivation of choosing a visual inspection over an automatic method, and the classification scheme used.

As discussed in Chapter 2, analyzing the host galaxies of type-1 AGN is complex due to the presence of the bright active nucleus in the images, that can outshine the host galaxy to different extents. Therefore, our two-dimensional decomposition of the AGN and its host galaxy will prove once again essential for our analysis.

### 4.3.1   Comparison sample

The large number of galaxies available from the COSMOS *HST* observations provides us with the unique opportunity of building a control sample from the same data

set that we draw our AGN from. For our study, we require the control sample to permit us elaborate a comparison regarding distortion features. On this respect the most relevant parameter is the signal-to-noise ratio (S/N), hence we construct the comparison sample by selecting inactive galaxies matching each AGN both in apparent $I_{F814W}$ magnitude and photometric redshift. This is both required and sufficient since (1) the S/N determines the visibility of the merger signatures, and (2) while the stellar masses might differ slightly (factors of ~2 at the same distance and brightness), the mass dependence on the merger rate is not strong, with only a modest increase for higher masses (Bundy et al. 2009).

We proceed as in Chapter 2, in which we built a mock type-1 AGN sample from real inactive galaxies, but this time including the type-2 subsample as well: For each AGN host galaxy we select 10 similar comparison galaxies drawing information from the COSMOS ACS and photometric catalogs (Leauthaud et al. 2007; Ilbert et al. 2009). We require each comparison galaxy to have an $I_{F814W}$ magnitude within a range of $\triangle I_{F814W} = 0.1$, and a photometric redshift within a range of $\triangle z = 0.05$. We increased the search ranges by 10% when not enough matching galaxies were found in the catalog. An average of 1.8 iterations per AGN host were needed to complete the required number of inactive galaxies. For the case of the type-1 AGN subsample, the magnitudes of the host galaxies after the removal of the active nucleus are used for the selection of the control sample. For the type-2 subsample, at $L_X \sim 10^{43.5}$ erg s$^{-1}$ and $z < 1$, it is reasonable to assume that on these absorbed sources the AGN contribution to the bulk of the optical/IR light is negligible, and it arise mainly form the host galaxy (e.g., Bundy et al. 2008; Silverman et al. 2008). In the same fashion, we manually removed unlike AGN host galaxy candidates from the selected comparison sample; because of the correlation between BH mass and bulge mass, it is improbable that bulgeless and irregular galaxies host a supermassive black hole. For the type-1 subsample we remove the edge-on disks that due to the large obscuration towards the center, would prevent the detection as a broad line AGN.

Finally, the construction of the control sample for the type-1 AGN requires an additional effort. The nucleus removal process usually leaves residuals in the center which certainly affect any blind classification, making the type-1 AGN host galaxies readily discernible from the control sample. We account for this issue by exploiting our knowledge on creating mock type-1 AGN host galaxies. As in section 2, we mock up our selected inactive galaxies as AGN by adding a star in the center as a fake active nucleus, and then apply the same subtraction procedure as for the original type-1 AGN, attempting to make the two samples indistinguishable. As we showed

before, any effects on the selection of the comparison sample due to flux variations caused by the nucleus subtraction process can be neglected.

Our final comparison sample consists of 1264 galaxies in total. The $I_{F814W}$ and redshift distributions of the resulting type-1 and type-2 comparison samples are consistent with being drawn from the same parent distribution as the AGN subsamples, even after the removal of the unlikely counterparts described above. A Kolmogorov-Smirnov test on each couple of $I_{F814W}$ and redshift distributions confirms with probabilities > 38% that the AGN and control samples are consistent among each other (in general < 5% is used to show that two distributions differ).

### 4.3.2   Visual classification

Merger events come in many different flavors due to the large parameter space involved (e.g., merger stage, viewing angles, mass ratio, and gas fractions). Sometimes they can be obvious at first sight, but some others can be very subtle, or simply undetectable at the sensitivity of the observations. At our redshift range and image resolution, it has been shown that automatic classification methods to identify mergers tend to miss several obvious cases, and cannot compete with visual inspection (Jogee et al. 2009; Kartaltepe et al. 2010). On the other hand, when the numbers involved are over the tens of thousands, visual classification becomes impractical[1] and an automatic approach would be needed. General measurements of structural parameters that can be correlated with some physical process have proven to be a good compromise (e.g., Reichard et al. 2009using the lopsidedness as a tracer of merging and star formation).

Considering the above, in this chapter we opt to identify merger and interaction signatures visually. The number of objects we are dealing with allows us to do so (~1400 in total), and the image quality deserves a detailed case-by-case examination.

These visual studies can be subjective. In our case, the absolute fraction of merging galaxies measured by visual classifiers will depend on their own experience and background, and hence it is plausible that they can differ substantially among each other. Nevertheless, any personal scale and criteria each classifier uses will be ap-

---

[1]With the notable exception of the citizen-based Galaxy Zoo project (Lintott et al. 2008, http://www.galaxyzoo.org).

plied equally on both samples, active and inactive galaxies. Therefore, a key quantity on our study will be, more than the absolute fractions of merging galaxies, the difference *between* the merging fractions measured by a given classifier. If we instead focus on how each individual classifier perceives one sample *compared to* the other, by considering the differential between the merging fractions of active and inactive galaxies, this subjectiveness can be accounted for. Furthermore, the consistency of this study is improved by (1) using ten independent human classifiers to add statistical robustness and (2) mixing both samples of active and inactive galaxies so that the classification is actually blind and therefore does not favor either the AGN hosts or the inactive galaxies.

We break the classification down into two parameters.

1. *Hubble type.* We attempt to state whether the host galaxy belongs to one of the two basic morphological classes: bulge or disk dominated.

2. *Distortion class.* We define three classes regarding the degree of distortion of the galaxy as follows.

   (a) *Dist-0.* Galaxies that appear undisturbed, smooth and/or symmetric, showing no interaction signatures. This also applies to cases where the small diameter of the galaxy does not allow a detailed analysis. We pay particular attention to self-induced asymmetries such as dust lanes or star-forming regions, which are usually seen as small clumps in well-resolved spirals.

   (b) *Dist-1.* Here we include objects with mild distortions. This could be due to a minor merger for example, but at the same time could also be because of low S/N. This interaction class is a "gray zone" in which most of the discrepancies in the classification between the 10 people arise.

   (c) *Dist-2.* Strong distortions, potential signs for ongoing or recent mergers. This class mainly includes galaxies which have highly disturbed morphologies or show visible signatures of strong interactions, such as large tidal tails, arcs, debris, etc. Double-nucleus systems also fall into this category.

For the visual inspection, the classifiers had access to FITS images which they could re-scale in order to look for high-contrast and subtle features that may have not showed up at an arbitrary brightness scale.
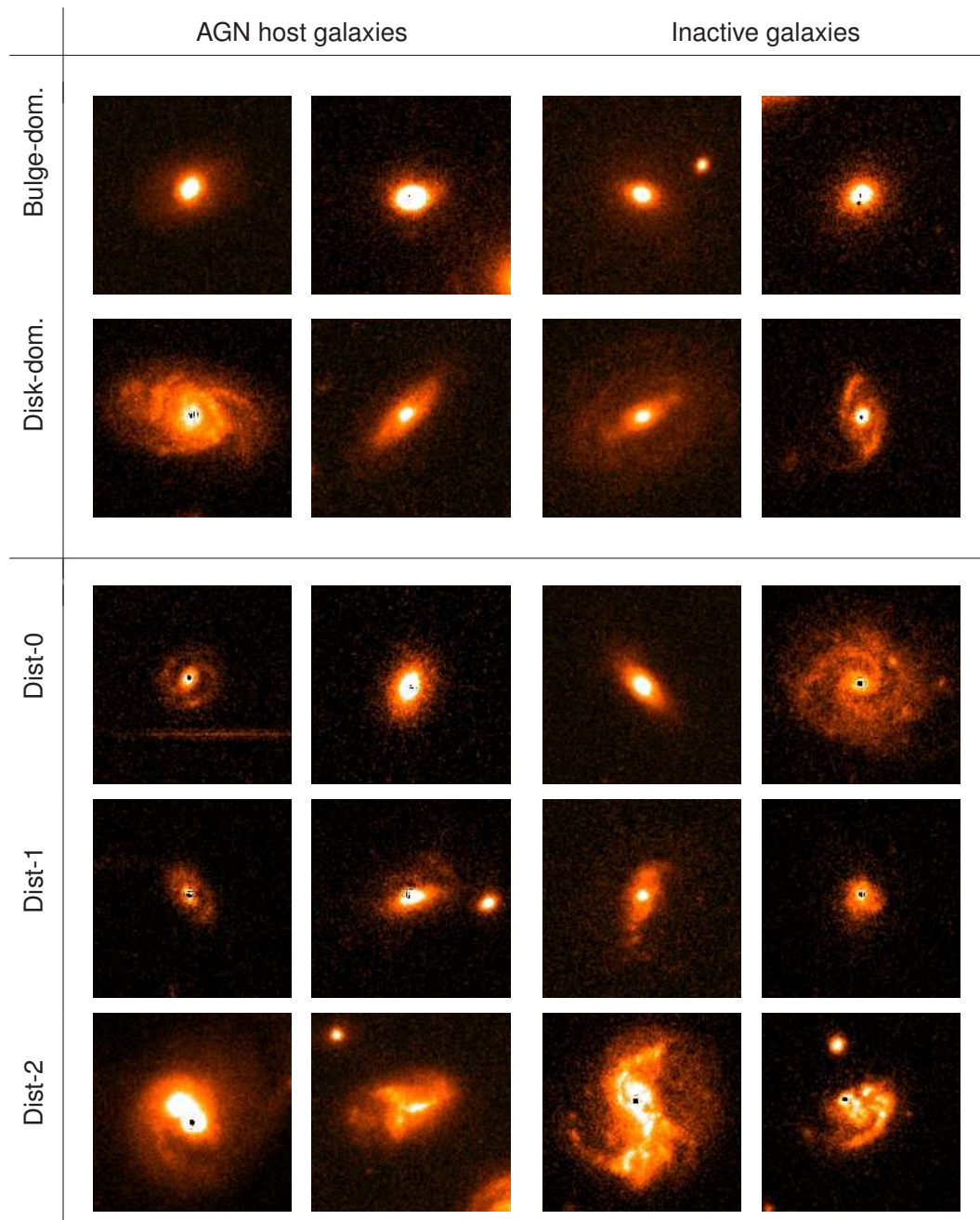
**Figure 4.2:** Example galaxy images arranged into different morphological (upper rows) and distortion (lower) classes with 100% agreement between the independent classifiers. The cutouts are $4''8 \times 4''8$. Black residuals at the center of some of the galaxies are residuals from the point source removal.

## 4.4   Results

The results from the visual classification by 10 people[2], for both Hubble type and
distortion classes, are shown in Table 4.1. For the different distortion classes, we
show the difference between samples (hereafter $\Delta$) as the distortion fraction of the
AGN minus that of the control sample. The results are weighted according to the
number of objects classified by each person[3] and used to calculate the mean frac-
tions, $\mu$, which we also display in Table 4.1. Figure 4.2 shows examples of active
and inactive galaxies which were classified with 100% agreement, arranged into the
different Hubble type and distortion classes.

### 4.4.1   Perception of the Hubble type

No morphology priors are applied in the selection of our comparison sample, with
the minor exception of the pruning of irregulars and edge-on disks as described in
Section 2.3.1. In order to test whether the samples are consistent regarding their mor-
phological composition, we compare the AGN and comparison samples in Table 4.1.
Although the mean values show a high dispersion due to the large discrepancies
between classifiers, the results for the AGN and comparison samples are in good
general agreement for each classifier.

The large fraction of disk-dominated galaxies, in particular in the AGN sample, is
interesting. To verify if this could be due to systematic bias by the classifiers, we
will use two independent parametric estimators of the morphological type available
at hand. First we compare the results from our GALFIT models chosen earlier, which
we extended to our type-2 subsample as well as to its comparison galaxies. We
identify sources as bulge- or disk-dominated if the best-fit results from GALFIT had
Sérsic indices of $n = 4$ and $n = 1$ respectively. The rest of the galaxies fell between
the two. As a second test, we look up the results for our comparison sample from
the Zurich Estimator of Structural Types (ZEST, see Scarlata et al. 2007 for details),
in which the structure of thousands of COSMOS galaxies was quantified through

---

[2]The 10 classifiers were: Mauricio Cisternas, Katherine Inskip, Knud Jahnke, Jeyhan Kartaltepe,
Anton Koekemoer, Thorsten Lisker, Aday Robaina, Marco Scodeggio, Kartik Sheth, and Jonathan
Trump.

[3]Each classifier looked at a minimum of ~200 galaxies from the combined sample. For each
classifier the samples were shuffled, to assure that even if all of them decided to look at 200 galaxies,
they would be looking at different objects. On average, each galaxy was classified $6.3 \pm 1.0$ times.

**Table 4.1:** Results from the Visual Analysis by the 10 Classifiers.

| Classifier | MC | KI | KJ | JK | AK | TL | AR | MS | KS | JT | $\mu$ |
|---|---|---|---|---|---|---|---|---|---|---|---|
| $N_{AGN}$ | 140 | 140 | 140 | 140 | 22 | 40 | 57 | 140 | 38 | 98 | … |
| $N_{type-1}$ | 83 | 83 | 83 | 83 | 22 | 40 | 0 | 83 | 19 | 41 | … |
| $N_{type-2}$ | 57 | 57 | 57 | 57 | 0 | 0 | 57 | 57 | 19 | 57 | … |
| $N_{CS}$ | 1264 | 1264 | 1264 | 1264 | 177 | 357 | 537 | 1264 | 357 | 903 | - |
| **Hubble type** | | | | | | | | | | | |
| $Bulge_{AGN}$ | 25.7% | 51.4% | 31.4% | 20.0% | 40.9% | 55.0% | 29.8% | 43.6% | 26.3% | 37.8% | 35.2% ± 11.0% |
| $Disk_{AGN}$ | 74.3% | 48.6% | 68.6% | 80.0% | 59.1% | 45.0% | 70.2% | 56.4% | 73.7% | 62.2% | 64.8% ± 11.0% |
| $Bulge_{CS}$ | 24.6% | 43.3% | 29.6% | 25.2% | 47.5% | 54.3% | 29.4% | 43.6% | 17.9% | 40.5% | 34.3% ± 9.5% |
| $Disk_{CS}$ | 75.4% | 56.7% | 70.4% | 74.8% | 52.5% | 45.7% | 70.6% | 56.4% | 82.1% | 59.5% | 65.7% ± 9.5% |
| $N_{CS}$ | 1264 | 1264 | 1264 | 1264 | 177 | 357 | 537 | 1264 | 357 | 903 | - |
| **Distortions** | | | | | | | | | | | |
| $Dist-0_{AGN}$ | 62.9% | 43.6% | 48.6% | 56.4% | 50.0% | 47.5% | 56.4% | 47.4% | 55.1% |  | 54.2% ± 7.5% |
| $Dist-0_{CS}$ | 65.5% | 47.3% | 60.1% | 63.0% | 67.8% | 51.5% | 58.5% | 51.5% | 61.2% |  | 59.9% ± 7.6% |
| $\Delta_{Dist-0}$ | –2.6% | –3.7% | –11.6% | –6.5% | –17.8% | –4.0% | –2.1% | –4.2% | –6.1% |  | –5.6% ± 3.5% |
| $Dist-1_{AGN}$ | 24.3% | 26.4% | 45.0% | 32.9% | 40.9% | 40.0% | 30.0% | 50.0% | 16.3% |  | 30.8% ± 9.3% |
| $Dist-1_{CS}$ | 22.4% | 28.3% | 34.2% | 26.9% | 19.2% | 34.2% | 33.5% | 39.2% | 17.8% |  | 27.5% ± 6.5% |
| $\Delta_{Dist-1}$ | 1.9% | –1.9% | 10.8% | 6.0% | 21.7% | 5.8% | –3.5% | 10.8% | –1.5% |  | 3.2% ± 5.7% |
| $Dist-2_{AGN}$ | 12.9% | 30.0% | 6.4% | 10.7% | 9.1% | 12.5% | 7.0% | 2.6% | 28.6% |  | 15.0% ± 8.8% |
| $Dist-2_{CS}$ | 12.1% | 24.4% | 5.7% | 10.1% | 13.0% | 14.3% | 6.0% | 9.2% | 20.9% |  | 12.6% ± 6.5% |
| $\Delta_{Dist-2}$ | 0.8% | 5.6% | 0.7% | 0.6% | –3.9% | –1.8% | 1.1% | –6.6% | 7.6% |  | 2.4% ± 3.5% |

**Notes.** We indicate the number of objects classified by each person and individually for each type-1 and type-2 subsample, as well as for the comparison sample (CS). For the distortion classifications, we include the difference between samples as $\Delta_{Dist-x} = Dist-X_{AGN} - Dist-X_{CS}$. For each category, we include the mean, $\mu$, and its dispersion, weighted according to the number of objects classified by each person.

**Table 4.2:** Comparison of our mean Hubble type classification with that of parametric estimators of galaxy morphologies

| | $\mu$[a] | GALFIT[b] | ZEST[c] |
|---|---|---|---|
| Bulge$_{AGN}$ | 35.2% | 25.7% | ... |
| Disk$_{AGN}$ | 64.8% | 55.0% | ... |
| Bulge$_{CS}$ | 34.3% | 41.2% | 19.6% |
| Disk$_{CS}$ | 65.7% | 43.5% | 67.8% |

[a] Weighted mean of the 10 classifications (as in Table 4.1).
[b] Percentages over 100% of the samples. The rest of the objects had an intermediate Sérsic index (with $2 \leq n \leq 3$, see Chapter 2 for details).
[c] Percentages over 100% of the comparison sample. The remaining galaxies were classified as irregulars (11.3%) by ZEST, and a few did not make it to the catalog (1.2%).

a principal component analysis over a combination of Sérsic index and five non-parametric diagnostics. The ZEST results show the fractions of galaxies classified either as bulges or disks. Of the remaining fraction classified as neither, the majority (11.3%) was classified as irregulars, most likely due to the lack of sensitivity of these automatic classification schemes to peculiar systems such as interacting galaxies; this is consistent with the observed fraction of highly distorted comparison galaxies. Sixteen galaxies, accounting for the remaining 1.2%, did not make it into the catalog.

Table 4.2 shows both of these tests along with the weighted mean fractions for comparison. It is clear that the numbers from these tests follow the trend seen in the visual classification. These tests provide a lower limit to the fraction of disks, with > 55% of our AGN sample being hosted by true disks.

## 4.4.2 The distortion fractions

Our prime interest lies in the observed difference in distortion fractions *between* samples of active and inactive galaxies. The absolute values in distortion fractions determined by the 10 classifiers are of lesser interest since the internal calibration for the three distortion classes differs between the classifying individuals. Since any subjectiveness will be applied equally to both active and inactive samples, using the

differences in the distortion fractions instead of absolute levels removes the person-to-person calibration differences and allows an unbiased interpretation.

Considering that the merging signatures we were looking for could sometimes be faint and weak, we address the potential loss of sensitivity to such features due to the slightly shallower limiting magnitudes for ~17% of the pointings (i.e., those with Sun-angles of <70°). For each person, we have also carefully analyzed the results by dividing their classified sample into sources with sun-angles either side of this critical angle. We find that there is no statistically significant difference in the distortion fractions as a function of Sun-angle. In addition, as the assignment of individual objects to either a deep or shallow field is effectively random, and given that the AGN distortion fractions are compared directly with those of a comparison sample selected from the same data set (and thus with the same limiting surface brightness issues), the overall impact on our results of any bias toward smaller distortion fractions in the shallower fields would in any case be negligible.

The objects that fell into the Dist-2 class were those which presented the strongest distortions, and hence signatures of a major interaction, for each individual classifier As any difference in recent major merger incidence would show itself in this class, we will focus on the Dist-2 results here.

### 4.4.2.1   Combining 10 classifications

In table 4.1 we have already listed the Dist-2 fractions for all classifiers, their mean values, and also the mean of the difference in Dist-2 fractions between the AGN and comparison samples. This permits the following initial assessment under the assumption of Gaussian errors: the difference (2.4%) is below the uncertainty of 3.5%, and hence it is not significant.

Nevertheless, since the error distribution is in fact *not* Gaussian but follows a *binomial* distribution (according to the number of distorted galaxies in a sample of given size) it is important that we use the correct combination of results in order to give answers to the two main questions: (1) Is there a genuine difference between the fractions of strongly distorted AGN hosts and inactive galaxies, and (2) with the given sample size, what difference in distortion fractions between samples can we actually rule out at a given confidence level—in this case we chose 95%. The first question asks whether the given dataset shows an enhanced AGN distortion fraction or not. The second question probes the discriminative power of this sample, and allows us to
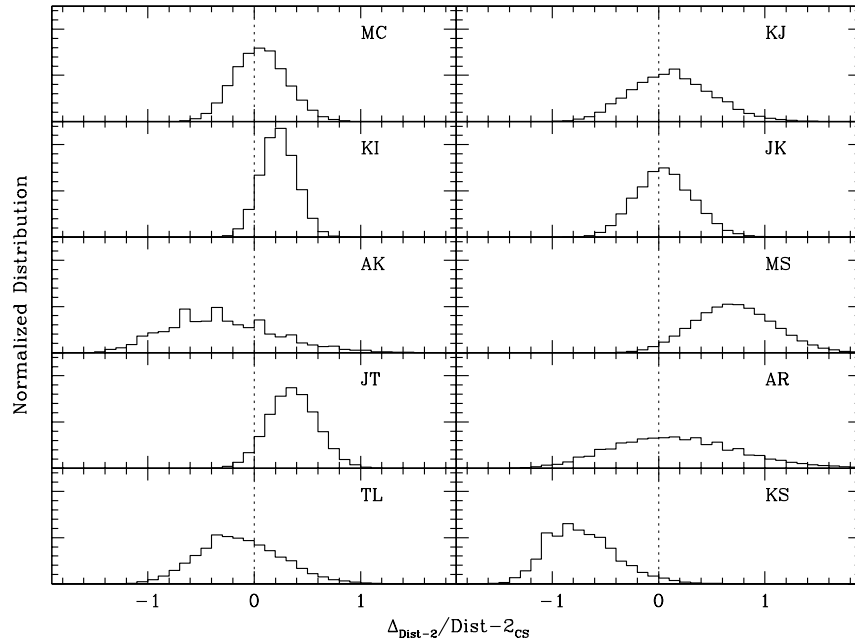
**Figure 4.3:** Distributions of the difference in the Monte Carlo sampled distributions of Dist-2 fractions between the AGN and control samples for the ten classifiers. For each distribution, a deviation from zero difference (dotted line) towards positive values indicates a higher fraction of distorted active galaxies, whereas a deviation towards negative values shows a higher fraction of distorted inactive galaxies.

gauge the actual importance of a null-result in question (1), since a decreasing sample size means an increasing uncertainty in the distortion fractions and hence small samples have near zero discriminative power.

Using the correct binomial error statistics for the distortion fractions of AGN and inactive galaxies, we compute for each classifier the probability distribution for the difference $\Delta_{Dist-2}$. This is done in the following way: (1) individially for each classifier, we Monte Carlo sample their pair of Dist-2 binomial probability distributions for the AGN and comparison samples separately, (2) we compute the difference between these randomly sampled values, (3) we repeat this process one million times for each classifier which yields 10 distributions for $\Delta_{Dist-2}$, (4) we normalize these probability distributions by the Dist-2$_{CS}$ values measured by each person as shown in Table 4.1, in this way removing any bias applied by each classifier's personal scale (Figure 4.3), and (5) now in "differential" space, where we are insensitive to between-person scatter, we combine these 10 distributions by co-adding their histograms, weighted by
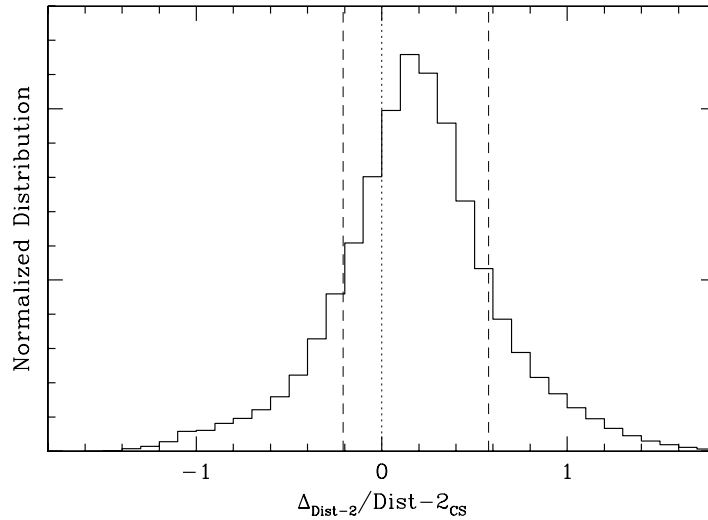
**Figure 4.4:** Combined posterior probability distribution of the difference of highly distorted galaxies between the AGN and control sample for the 10 classifiers. The central 68% confidence level is marked with vertical dashed lines, which shows that the histogram is consistent with zero difference (dotted line), ruling out any significant enhancement of merging signatures on our sample of AGN hosts with respect to the comparison sample of inactive galaxies.

the size of the sample each person classified[4].

The resulting probability distribution is shown in Figure 4.4. The histogram is fully consistent with zero difference, as indicated by the central 68% confidence interval denoted by the vertical dashed lines estimated by the areas at both ends, encompassing 16% each. This confirms the simple analysis from above: our study shows no significant difference between the fractions of strong distortions of AGN and inactive galaxies. Regarding the discriminative power of our sample, in Figure 4.5 we show the cumulative distribution of the Dist-$2_{AGN}$ fraction from Figure 4.4. The distribution shows that with 95% confidence the distortion fraction of AGN is in any case not larger than the inactive distortion fraction by a factor of 1.9, when considered relative to the mean distortion level found by the 10 classifiers (12.6%). Hence, the vast majority of AGN host galaxies at $z < 1$ with the given luminosities do not show signatures of having experienced a recent major merger.

---

[4]This represents a combined Bayesian posterior probability distribution with sample sizes as individual priors.
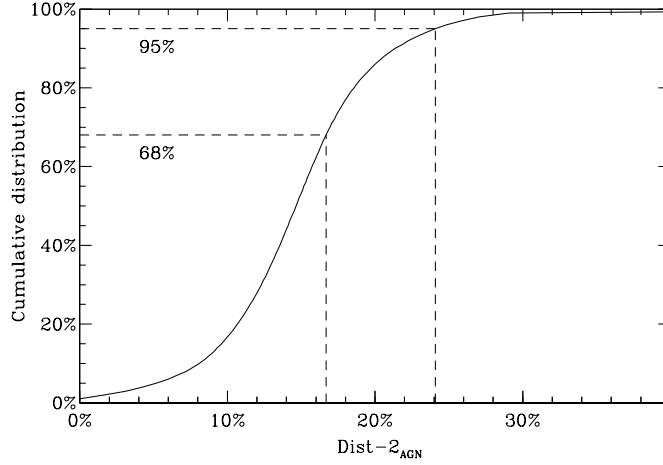
**Figure 4.5:** Cumulative distribution of the simulated Dist-$2_{AGN}$ fractions, showing the 68% and 95% confidence levels with the dashed lines. As mentioned in the text, this confirms with a 95% confidence that the highly distorted AGN fraction can *not* be larger than 24.08%.

#### 4.4.2.2 Mass dependency

Even if there is no overall difference between the fractions of highly distorted AGN and inactive galaxies, it is still interesting to look at the situation in mass-space, and investigate the possibility that an enhancement of the AGN merger fraction could be *hidden* because we consider the sample as a whole, regardless of stellar mass. Major merging is a key element in the assembly and evolution of massive galaxies (e.g., Bell et al. 2006; Lin et al. 2008; Bundy et al. 2009; van der Wel et al. 2009; Robaina et al. 2010), and in order to test if the fraction of highly distorted AGN host galaxies is significantly enhanced at the massive end (higher than $\sim 10^{10.5}\ M_\odot$), we have estimated stellar masses for our samples of active and inactive galaxies. We use the calibration from Bell & de Jong (2001) based on the Chabrier initial mass function. By obtaining the *V*-band luminosities:

$$L_V = 10^{-0.4(V-4.82)} \tag{4.1}$$

and assuming a common mass-to-light ratio from the rest-frame $(B - V)$ color, we derive stellar masses in solar units:

$$M_* = 10^{-0.728+1.305(B-V)} \times L_V \tag{4.2}$$

with all magnitudes in Vega zero point.
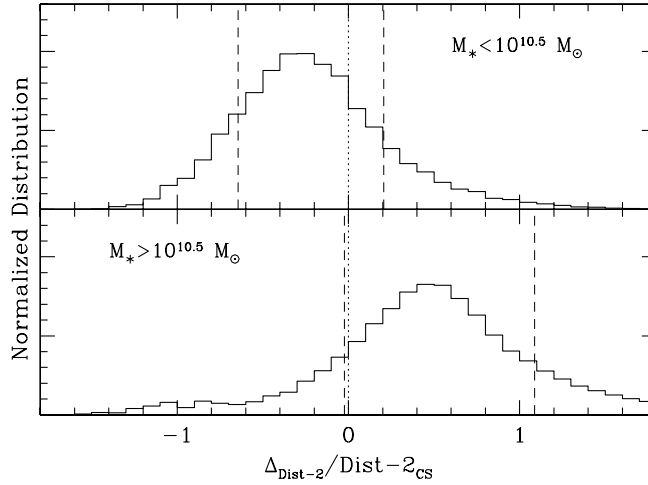
**Figure 4.6:** The combined differences in distortions of intermediate ($10^{9.3} < M_*/M_\odot < 10^{10.5}$; top panel) and massive ($10^{10.5} \leq M_*/M_\odot < 10^{11.7}$; bottom panel) galaxies are shown. In both cases, the central 68% confidence levels (dashed lines) are consistent with zero (dotted line).

For the inactive galaxies and the type-2 subsample we obtain rest-frame *B* and *V* from the photometric catalog by Ilbert et al. (2010). For the type-1 AGN, however, we cannot use that information because it includes the contribution from the luminous AGN. Therefore, we obtain the rest-frame *V*-band luminosities from the observed $I_{F814W}$ after the nucleus removal process and estimate the color term by computing the linear regression over the rest-frame $(B - V)$ colors as a function of redshift for the type-2 AGN. This yields the relation

$$(B - V)_{Vega} = 0.136\, z + 0.541. \tag{4.3}$$

The combined differences of highly distorted galaxies for two bins of stellar mass ($10^{9.3} - -10^{10.5} M_\odot$ and $10^{10.5} - -10^{11.7} M_\odot$) are shown in Figure 4.6. For both samples the ratio of galaxies occupying the massive bin is roughly 2:1 relative to the less massive one, hence we are dealing with very massive galaxies. Even if for the galaxies with stellar masses higher than $\sim 10^{10.5}\, M_\odot$ there is a modest enhancement in the distortion fraction of the AGN hosts over the control sample (Figure 4.6, bottom panel), it is again within the 68% confidence interval, i.e., it is not statistically significant. Therefore, it cannot be considered as an empirical proof of an enhancement at the massive end.

## 4.5   Discussion

From a detailed analysis of the results of our visual classification we showed that the fractions of heavily distorted active and inactive galaxies are consistent within the central 68% confidence interval and that the Dist-2 fraction of AGN host galaxies is less than twice that of the inactive galaxies at a 95% significance level, as shown in Figures 4.4 and 4.5, respectively. Putting these findings in context, provided that the duration of merger signatures and the visibility of the AGN phase overlap with each other, this indicates that there is no evidence that major merging plays a key role in the triggering of AGN activity in our sample. But what about the possible alternative scenario in which, in spite of a causal connection between merging and AGN triggering, we do not detect an enhancement of merger signatures in the AGN population due to a significant time lag between the interaction and the start of the AGN phase? Below we address this possible alternative interpretation and discuss the implications of our results.

### 4.5.1   Alternative interpretation: time lag between merging and the observability of the AGN phase

Appealing simulations of mergers between gas-rich galaxies state that the peak of star formation and quasar activity will occur during the final stages of the interaction, close to coalescence, within a more relaxed than distorted bulge-like remnant (Di Matteo et al. 2005; Springel et al. 2005a). In these models, during the first passage only modest starbursts are triggered and no major BH accretion occurs, and therefore the galaxies would not be detected as AGN. Furthermore, ad hoc models that include obscuration in galaxy mergers (Hopkins et al. 2005b) predict that, beginning from the early stages of the interaction, the AGN is "buried" for ~90% of its lifetime by large column densities, only revealing itself toward the end of the merger. However, all these models work with sub-grid prescriptions of BH accretion and fail to spatially resolve the actual accretion process by several orders of magnitude.

If there is indeed a substantial time lag after merging prior to the AGN activity becoming detectable, then the strong merging signatures we attempt to find could have already been washed out. Moreover, if AGN are obscured as the interacting galaxies coalesce, there could be a "contamination" population of undetected strong BH activity occurring within our control galaxies undergoing a major merger. Finally, a

third issue related to the obscuration plus time lag scenario is that the observed inter-actions that are occurring on a fraction (~15%) of our AGN host galaxies should be unrelated to the detected BH accretion—under the assumption of a large time lag we would not expect to see strong merging signatures.

Below we present three simple tests to address this possible alternative interpretation.

### I) AGN hosted by disks: Not a relic from a major merger

In the preceding text, we raised a possible alternative explanation for our results, that most major mergers could be missed because the time lag between merging and the observed AGN episode could be substantial, washing out the signatures that the *HST*/ACS resolution allows us to detect.

Models can provide us with some clues about the observability timescales during an interaction. For example, simulations of major mergers by Lotz et al. (2008) quantified that the strong signatures could still be detected 0.7 Gyr after the merger, by degrading their snapshots to the resolution of *HST* $z \sim 1$ imaging. Thus, in order to explain the observed zero distortion enhancement, a lag of at least 0.7 Gyr between coalescence and the visible phase of the AGN would be required for all galaxies[5]. It is, however, not straightforward to rely on these studies to discard the time lag issue; given the large number of parameters involved in determining how long a merger signature will remain visible, it is plausible that several late-stage mergers could have been missed. Although a merger between gas-rich galaxies can leave spectacular features for a long time, viewed from the wrong orientation they can be completely unnoticeable.

While it is difficult to assess the relevance for the timescale issue of major mergers being overlooked, we can be reasonably confident that the remnant will not look like a disk. Spheroidal and bulge-dominated galaxies are usually said to be formed as a result of major mergers (e.g., Toomre 1977; Barnes & Hernquist 1996; Cox et al. 2006). However, it has also been stated that disks can survive some major

---

[5]For example, see Schawinski et al. (2010) who make an extensive case of the time lag scenario. They propose an all-merger-driven AGN phase with a time lag of ~500 Myr for their sample of early-type galaxies at $z \sim 0.05$. Even if their result is mainly based on the interpretation of their data as a causal sequence of events (and is subject to alternative explanations), they caution that their particular sample only accounts for a very small fraction (~10%) of the overall AGN population found in the local universe.

mergers, especially if the progenitors are gas-rich (e.g., Barnes & Hernquist 1996; Springel & Hernquist 2005; Hopkins et al. 2009), nonetheless these kind of merger remnants have been argued to not lead to a large bulge growth and significant BH fueling (Hopkins & Hernquist 2009). Likewise, it has been argued that some gas-rich mergers can lead to the regrowth of the disk (Hopkins et al. 2009; Bundy et al. 2010). Even so, the timescales involved for such a process can be as much as an order of magnitude larger than the typical quasar lifetime of 1-100 Myr (e.g., Porciani et al. 2004; Hopkins et al. 2005b; Shen et al. 2007).

For the significant fraction of AGN hosted by disks found from our classification, we could safely say that the mechanism responsible for triggering those AGN was not a past major merger, suggesting also that since $z \sim 1$ alternative fueling methods seem to play a larger role than usually expected. Georgakakis et al. (2009), from a sample of X-ray-selected AGN, compared the luminosity function of their disk-hosted AGN against the analytic model of the X-ray AGN luminosity function for a stochastic accretion mode by Hopkins & Hernquist (2006). They showed that the model can reproduce the observations, but at the same time the overall number density of the observed disks was underpredicted, especially at high X-ray luminosities. On our sample of 140 AGN, 18 sources have $L_X \geq 10^{44}$ erg s$^{-1}$, from which 10 of their host galaxies were classified as disk dominated with an agreement $\geq 80\%$. This suggests that alternative BH fueling methods (i.e., those that do not destroy the disk) are not only more common on the overall AGN population at $z < 1$, but also much more efficient than the existing models predict.

**II) No veiled X-ray activity in merging galaxies**

The aforementioned models leave the possibility that we could be missing an important fraction of AGN due to gas and dust obscuration when a gas-rich major merger is taking place. Even though obscured AGN can still be detected through their hard X-ray emission (Hopkins et al. 2005a), it is possible that less luminous and highly obscured AGN lie below the detection threshold used to build the X-ray catalogs (Treister et al. 2004). The X-ray properties of such obscured objects have been successfully studied in the literature by the means of a stacking analysis of X-ray data (e.g., Daddi et al. 2007; Fiore et al. 2009). If obscured AGN are being missed, they should be preferentially found in merging galaxies. Therefore, in order to test this scenario and search for this potentially buried X-ray activity, we stack all the inactive galaxies regarded as highly distorted. Eighty-seven inactive galaxies fulfill our simultaneous criteria of being individually classified as either Dist-1 or Dist-2 with
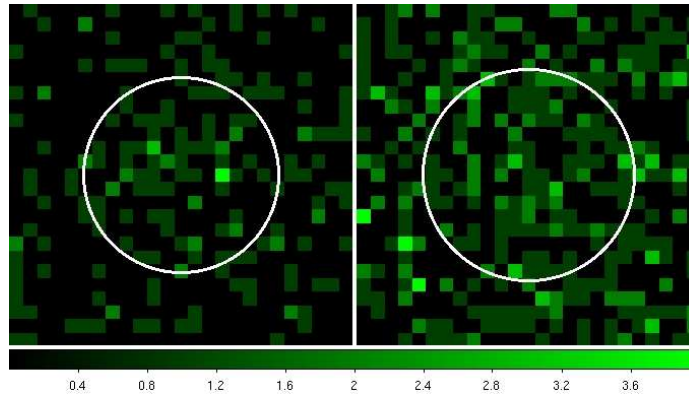
**Figure 4.7:** Stacked *Chandra* images of 45 inactive galaxies likely to be undergoing a major interaction, on the soft 0.5-2 keV (left) and hard 2-8 keV (right) energy bands, showing the average radii of the stacked sources as white circles. The cutouts are $12'' \times 12''$.

an agreement of $\geq 75\%$, and classified as Dist-2 with an agreement $\geq 65\%$.

For this analysis, we take advantage of the higher sensitivity of the *Chandra* observations of the COSMOS field (C-COSMOS; Elvis et al. 2009), compared with the *XMM-Newton* data. Even though *Chandra* covered only half of the field ($\sim 0.9$ deg$^2$), it has a flux limit three times below the *XMM-Newton* sensitivity, which makes the tradeoff in smaller coverage absolutely justifiable, considering that we want to detect possible X-ray sources below the XMM-COSMOS catalog sensitivity threshold.

For the stacking of the X-ray data, we used the CSTACK tool developed by Miyaji et al. (2008), which includes a detailed bootstrapping error analysis through 500 realizations. Because the stacking is made from multiple observations, we consider the counts within a radius varying according to the off-axis angle, corresponding to 90% of the encircled counts. We stacked the 45 objects that lie within the C-COSMOS area, after excluding 1 object that was close to an X-ray source. We found an excess of soft 0.5–2 keV and hard 2–8 keV count rates from the source region at modest levels of $2.2\sigma$ and $2.4\sigma$, respectively. Figure 4.7 shows the results of the stacking in the two energy bands, with the average radii of $3\rlap{.}''4$ and $3\rlap{.}''7$ for comparison, within which no source is noticeable above the background level.

The lack of any obvious source after the stacking suggests that this moderate excess could be in part due to the expected emission from star-forming galaxies, and also from extended source emission (e.g., from a galaxy group). The possibility that a

---

[5]http://cstack.ucsd.edu

few sources dominate the overall count rate is unlikely since (1) the shape of the count rate distribution is that of a unimodal Gaussian and (2) no outliers are present. Therefore, it is doubtful that we are missing a significant fraction of accreting BHs hidden within the population of inactive galaxies undergoing interactions.

**III) No enhanced soft X-ray absorption in merging AGN host galaxies**

As mentioned before, AGN obscuration due to the surrounding gas and dust during a major merger would affect mainly the soft X-ray energy band, while the hard band would remain unobscured. If we observe an AGN hosted by a merging galaxy, and this interaction was responsible for the BH activity, we would expect to observe a hard X-ray spectrum from this source. To trace the obscuration level of our interacting AGN host galaxies, we compute their X-ray hardness ratio (HR). The HR is defined as

$$HR = (H - S)/(H + S),\qquad\qquad(4.4)$$

where H and S stand for the hard (2–10 keV) and soft (0.5–2 keV) counts, respectively. At our redshift range, it is still safe to say that the HR values lower than –0.2 correspond to an unabsorbed, soft spectrum (Hasinger 2008).

From our visual analysis, we have 13 AGN host galaxies regarded as highly distorted with high agreement according to the criteria used before. By computing the HR for these objects, we find that, contrary to what models predict, all of these particular sources present soft X-ray spectra. All of them have HR values $\leq$–0.2, with a mean of –0.53, which shows a low attenuation in the soft band.

It has been argued, however, that the HR diagnostic is rather crude in terms of predicting obscuration, and indeed, bright Compton-thick AGN can feature soft X-ray spectra due to photoionized gas (Levenson et al. 2006). Even so, this is only valid when the AGN is not observed directly, and we can easily establish that at least for the type-1 subsample this would not the case, and that we are certainly looking at active, accreting BHs. Looking only at the seven type-1 objects from these likely merging galaxies, we find that the average HR is –0.56 which indeed suggests a low level of obscuration.

One possible interpretation is that these interactions are not related to the observed AGN episode and that are instead only chance encounters. Dissipationless or gas-poor mergers could account for the lack of obscuration, but then it is unlikely that any strong merging signatures and substantial accretion onto the central BH would take place directly due to these kind of events. Pierce et al. (2007) found the same result

for X-ray-selected AGN hosted by interacting galaxies, suggesting that the observed interactions were not responsible for the fueling of those accreting BHs.

From another perspective, however, the models mentioned earlier are limited by the proposed picture of the merger-ULIRG-feedback-quasar timeline (e.g., Sanders et al. 1988a,b; Hopkins et al. 2008), which is already regarded as oversimplified. The AGN phase is said to happen after coalescence, but observations of large samples of ULIRGs, all of them undergoing interactions, have found a significant scatter in the trends of AGN contribution, accretion rate, and dust obscuration with merging state (Veilleux et al. 2009). Some of these have even been found to be dominated by the AGN in pre-merging state. Chaotic behavior during a merger event can lead to various unpredictable episodes of starburst and nuclear activity. Such episodic behavior can start much earlier than the final coalescence and can be responsible for different periods of gas inflows, obscuration, and visibility, therefore explaining an already unobscured merger-induced AGN still early during the interaction, as traced by the soft spectra observed in our interacting active galaxies. This conclusion, at the same time, contradicts the alternative time lag scenario.

## 4.5.2   Major merging: not the most relevant mechanism

Our analysis has demonstrated that the scenario in which mergers are responsible for triggering AGN after a significant time lag is unlikely. The high fraction of disks, the lack of a hidden significant AGN signal in merging inactive galaxies, and the missing soft X-ray obscuration of interacting AGN hosts all appear to rule out this model as a possible explanation of our results. The absence of any further evidence in support of this scenario leads us to the only remaining possible interpretation of our results: active galaxies are involved in major mergers no more frequently than inactive galaxies, and mergers have not played a leading role in AGN triggering for the last 7.5 Gyr. Our results agree with the few recent studies that have used a control sample (Dunlop et al. 2003; Grogin et al. 2003, 2005; Pierce et al. 2007; Gabor et al. 2009; Reichard et al. 2009; Tal et al. 2009and also with recent results from the E-CDFS by Böhm et al. 2010, submitted), in the sense that the morphologies of the AGN host galaxies are not unusual and do not show a preference for merging systems. Of the studies mentioned earlier which supported a merger-AGN connection, many only provided circumstantial evidence for such a link, without any control sample comparisons.

The lack of enhancement on merging signatures for AGN hosts with respect to the

background level indicates that there is no causal connection between merging and AGN triggering up to $z \sim 1$ and $M_* \sim 10^{11.7} M_\odot$, the galaxies dominating BH growth at these redshifts. It is still a plausible scenario that major mergers could be responsible for some of the brightest quasars; we do not intend to neglect this possibility, but in the context of a clean, large X-ray selected population of AGN, it is certainly not the most relevant mechanism. The large fraction of AGN hosted by disk-dominated galaxies shows that alternative mechanisms, i.e., stochastic processes and minor mergers dominate, for this sample of objects.

The merger-starburst connection has also been widely studied in the same perspective. Both mechanisms share the need for enough cold gas to be brought to the central regions of the galaxy, so it is worth mentioning analogous conclusions from the recent literature: (1) indeed, major mergers *can* trigger strong starbursts (e.g., Mihos & Hernquist 1996; Springel 2000), but (2) *not always*, as seen in models (Di Matteo et al. 2007) and observations (Bergvall et al. 2003), and (3) its overall contribution is relatively modest (Di Matteo et al. 2008a; Jogee et al. 2009), with no more than 10% of star formation in massive galaxies being triggered by major mergers at $z \sim 0.6$ (Robaina et al. 2009).

Different studies (e.g., Ballantyne et al. 2006; Hasinger 2008; Li et al. 2010) have converged on proposing the following scenario: the major merger-driven evolution dominates early in the universe, producing the bulk of the brightest quasars at $z = 2-3$. Around $z \sim 1$ however, a different evolutionary mechanism takes over, with secular processes becoming the main triggers for the BH activity and growth. While our analysis cannot be performed at higher redshifts with the current observational data set, our results appear to fit this picture. Nevertheless, the overall relevance of major merging, even in the early universe, has yet to be determined. Other recent studies suggest that secular processes play a much larger role: observations of massive star-forming galaxies at $z \sim 2$ have shown that their buildup has been dominated by cold rapid accretion and secular processes (Genzel et al. 2008), without the need of major mergers. It has been stated on the basis of dark matter simulations that the likely number of major mergers is insufficient to account for the transformation of star-forming turbulent disks at $z = 2$ into ellipticals at $z = 0$ (Genel et al. 2008). A broader view of the accretion history of dark matter halos by Genel et al. (2010), quantified that ~60% of the dark matter in a given halo is contributed by mergers, with only ~20% being major mergers. Instead, the rest (~40%) of the dark matter would be accreted smoothly. This also agrees with recent work using smooth particle hydrodynamic simulations, stating that galaxies have acquired most of their

baryonic mass through the cold mode of accretion (Kereš et al. 2005, 2009). Furthermore, merger-free models have shown that isolated galaxies can reproduce the quasar duty cycles between $z = 1$ and 3 and feed their BHs with the recycled gas from evolving stars (Ciotti & Ostriker 2007) and even reproduce the observed scaling relations (Lusso & Ciotti 2010). Overall, these studies have shown that secular evolution can be highly relevant, also at the redshifts at which the peak of quasar activity occurs.

## 4.6   Conclusions

In this work, we performed a consistent visual analysis on the *HST*-based morphologies of a sample of 140 X-ray-selected AGN host galaxies over $z \sim 0.3 - 1.0$ and $M_* < 10^{11.7} M_\odot$, and compared them with a matched control sample of inactive galaxies under the same conditions. Our goal was to search for the presence of any significant connection between major merging and BH fueling as suggested by models and observational tests. In summary:

1. From our visual analysis, ~85% of our AGN host galaxies show no strong distortions on their morphologies. Comparison with the control sample shows that the distortion fractions are equal within the 68% central confidence level. Given our sample size, we can state that at a 95% confidence level the highly distorted fraction of AGN hosts is less than 1.9 times that of the inactive galaxies. Mergers and interactions involving AGN hosts are not dominant, and occur no more frequently than for inactive galaxies.

2. Over 55% of the AGN from our sample are hosted by disk-dominated galaxies, implying a triggering mechanism that would not destroy the disk, i.e., not a major merger. This also indicates that it is unlikely that we could be missing major mergers due to strong distortions having already been washed out over a large time lag prior to the ignition of the AGN. The presence of an important fraction of disk-dominated hosts on the AGN brighter than $L_X > 10^{44}$erg s$^{-1}$ suggests that secular fueling mechanisms can be highly efficient as well.

3. Through a detailed stacking analysis of the X-ray data of our inactive galaxies undergoing mergers, we did not find an underlying X-ray signal indicating the presence of a substantial population of obscured AGN.

4. Looking at the hardness of the X-ray emission of our AGN hosts that are clearly undergoing an interaction, we found soft X-ray spectra in all of them, contradicting the expected obscuration in this band predicted by models. This can be either because the observed interactions are not responsible for the BH fueling or the unpredictable output of a merger event allows many accretion phases as well as an unobscured AGN, even during such early stages.

Our work explicitly suggests that, at least for the last 7.5 Gyr, major merging has not been the most relevant mechanism in the triggering of typical AGN, and that the bulk of the BH accretion occurs through internal secular processes and minor interactions. The alternative interpretation of a time lag between merger trigger and AGN onset is unlikely due to the zero enhancement of the distortion fraction, the high incidence of disks, and the absence of a significant X-ray signal in merging inactive galaxies as a potential buried AGN population.

# CHAPTER 5

## SUMMARY

The work presented in this thesis was motivated by the urgent need for additional robust empirical constraints regarding the co-evolution of galaxies and black holes at earlier cosmic times. In particular, for the "second half" of cosmic history, i.e., since $z \sim 1$, we set out to answer two of the still open questions:

1. Is there any evolution in the $M_{\mathrm{BH}} - M_*$ scaling relation?

2. What is the relevance of major merging for the triggering of AGN activity?

Studying of BHs beyond the local universe can only be done while they are actively accreting. The AGN phase is interesting not only because it represents the period in which the BH builds up most of its mass, but also because it is thought it has a direct impact on the evolution of the host galaxy. Most recent theoretical models of galaxy formation *require* AGN feedback to regulate gas cooling and shut down star formation in order to reproduce the observed galaxy properties, color bimodality, and luminosity functions.

Since any significant statement on the evolution of galaxies and BHs requires well-defined samples of AGN and host galaxies, we made use of the best sample available for such a study: the COSMOS survey. The 2 deg$^2$ field has been extensively probed with several space-based and ground-based observatories, covering a vast multiwavelength range from X-ray to radio. The *XMM-Newton* observations provided a clean sample of AGN, confirmed as such from ancillary spectroscopic and photometric

surveys. Perhaps the trademark of the COSMOS survey is that it features the largest contiguous field ever imaged with *HST*, providing high-resolution imaging of hundreds of thousands of galaxies. Because the observations were carried out with the F814W (broad *I*-band) filter, we decided restrict our study below $z = 1$ and hence stay in the optical regime.

We selected a sample of type-1 AGN from COSMOS with the considerations given above, resulting in 87 sources. In order to make quantitative as well as qualitative assessments on the AGN host galaxy properties, we needed to accurately characterize and remove the point-source flux. For this purpose, we created an automated procedure to model and decompose our type-1 AGN sample. We used GALFIT, a highly flexible software package for the modeling of galaxies. Each type-1 AGN was modeled using a PSF and a Sérsic profile to account for the nucleus and galaxy respectively, as it has been shown that, at our resolution and signal-to-noise levels, a two-component model is sufficient to describe a type-1 system. Our pipeline was applied to successfully model and remove the AGN for each source on our sample.

As a standard practice in these kind of procedures, we tested the accuracy of our image decomposition technique by simulating a large sample of type-1 AGN starting from real galaxies. Ten matching inactive galaxies per AGN were selected, and subsequently mocked up using real stars as fake active nuclei, taking care to match the host-to-nucleus ratio of the original AGN. We applied our pipeline on these large sample of over 800 simulated type-1 AGN. When comparing these galaxies before and after this procedure, we found out that our pipeline is able to recover their photometry with an accuracy of $0.03 \pm 0.23$mag. From this test, we concluded that our procedure accurate enough to be applied on the science questions above.

From the sample of type-1 AGN, we drew a subsample of 32 objects at $0.3 < z < 0.9$ with available virial BH mass estimates, covering the range $M_{\mathrm{BH}} \sim 10^{7.2-8.7} \, M_{\odot}$, based on H$\beta$ measurements from the COSMOS Magellan/IMACS survey. With the goal of estimating stellar masses for our 32 type-1 AGN from single-band *HST*/ACS photometry, we built a representative AGN mass-to-light ratio under the assumption that, at these redshifts and luminosities, the line-of-sight unification scheme holds. We used a large sample of ~200 type-2 AGN host galaxies with available stellar masses from an SED fitting, which due to their obscured nature, allow for a more precise assessment of their physical properties. A bivariate fit was used to construct a relation between mass-to-light ratio, redshift, and luminosity. We found that the $M_*/L$ for these intermediately luminous AGN at a given redshift and luminosity

scatters only ~0.25 dex.

With the $M_*/L$ relation in place, we needed accurate measurements of the luminosities of our 32 type-1 AGN. We therefore relied on our image decomposition technique: the nucleus-removed AGN host provided an accurate representation of the underlying host galaxy photometry. The measured luminosity was applied on the derived AGN $M_*/L$, which gave us stellar masses for our sample. Altogether, our error budget on the stellar masses was $\sim 0.35$.

The ratio between $M_{BH}$ and $M_*$ showed a zero offset with respect to the local relation for galactic bulge masses within the scatter, and we also found no evolution in the mass ratio $M_{BH}/M_* \propto (1 + z)^{0.02\pm0.34}$ up to $z \sim 0.9$. Interestingly, at the high-$M_{BH}$ end there was a positive offset from the $z = 0$ relation, which we found it could be fully explained by a mass function bias with a cosmic scatter of $\sigma_\mu = 0.3$, reaffirming that the intrinsic distribution is consistent with zero evolution.

From our results we concluded that since $z \sim 0.9$ no substantial addition of stellar mass is required: the decline in star formation rates and merger activity at $z < 1$ support this scenario. Nevertheless, given that a significant fraction of these galaxies showed a disk component, their bulges indeed are undermassive, and hence these results allow for an evolution with respect to bulge mass, in agreement with previous works. We therefore concluded that for the last 7 Gyr the only essential mechanism required in order that these galaxies obey the $z = 0$ relation is a redistribution of stellar mass from disk to bulge, likely driven by secular processes, i.e., internal instabilities and minor merging.

We then tackled a long-standing question: what is the relevance of major mergers and interactions as triggering mechanisms for AGN activity? Most previous AGN studies addressing this subject suffered from small-number statistics, hand-picked samples, or more importantly, did not establish the actual significance of their findings by comparing them with the merging fraction of the inactive galaxy population.

Our study made use of a large sample of AGN host galaxies: to our original sample of 87 type-1 AGN, we added 53 spectroscopically confirmed type-2 AGN. We analyzed the AGN host galaxies as well as a matched control sample of 1264 inactive galaxies from the same data set. Ten independent classifiers analyzed their morphologies, characterizing the Hubble type as well as the distortion degree, i.e, quantified the signature of recent major mergers which might potentially have been responsible for fueling the AGN.

The visual classification showed that (1) the vast majority (~85%) of the AGN host galaxies do not show strong distortions, and (2) there is no statistically significant difference in the distortion fractions between the active and inactive galaxy samples. These findings are the best direct evidence that, at least since $z \sim 1$, the bulk of the BH growth has not been triggered by major galaxy mergers, arguing that other mechanisms, i.e., internal secular processes and minor interactions, are the leading triggers for the episodes of major BH growth.

We also addressed an alternative interpretation of our results: a substantial time lag between merging and the observability of the AGN phase could wash out the most significant merging signatures, explaining the lack of enhancement of strong distortions on the AGN hosts. We show that this alternative scenario is unlikely due to: (1) recent major mergers being ruled out for the majority of sources due to the high fraction of disk-hosted AGN, (2) the lack of a significant X-ray signal in merging inactive galaxies as a signature of a potential buried AGN, and (3) the low levels of soft X-ray obscuration for AGN hosted by interacting galaxies, in contrast to model predictions.

Put together, these results explicitly indicate that over last 7 billion years, galaxies and BHs have evolved in a secular universe. Is this an outlandish outcome? Certainly not. A direct consequence of the current cosmological model with a hierarchical expanding universe, is that at some point there will be a transition, from a more violent universe at earlier times, to a more passive late one. In the past, galactic evolution was purely dominated by both violent dissipative collapse, as well as hierarchical clustering and merging. As cosmic time goes by and the universe expands, large galaxy clusters assemble and virialize. They get large internal velocity dispersions and galaxy-galaxy encounters become less frequent. It is in this late future, when the universe calms, that secular processes can start to be important. They require undisturbed environments and large periods of time to be able to have a significant relevance in the evolution of galaxies. In this thesis, we showed that the impact of secular mechanisms can be such, that they can have a direct involvement in reproducing the local BH-galaxy scaling relations as well as be responsible for triggering 7 billion years of AGN activity.

# ACKNOWLEDGMENTS

First and foremost, I would like to thank Christian Fendt for doing an amazing job as IMPRS coordinator. Even before being accepted in the program, you feel his support. At a time in which bureaucracy wanted to obstruct my intentions of coming to get graduate education in Heidelberg, he actively participated to make the process of my acceptance possible.

I would like to acknowledge Knud Jahnke, my thesis advisor. I am extremely grateful for his supervision, which many times went beyond the boundaries of science. He never hesitated to back me up when I needed it, and for that I will always be grateful. Regarding research, although in the beginning I was clueless, I think in the end I managed to learn at least a bit from his way of, not only doing science, but also presenting it. He always encouraged me to go to conferences around the world, both to learn from others and show my work. Thanks for the patience, even if I was coming to his office many times per day, and also for pushing me when it was needed. I really hope we get to work together again in the future.

The "Second-in-Command" of our group, Katherine Inskip, had a very important role in the work presented here. She was my IDL-guru, as well as our resident Grammar Police officer. It was great to have her as part of our group, and I thank her for always improving my work with her spot-on comments.

For my slow take-off during the first year, I blame the 4th IMPRS generation. Those after-seminars became a classic. Remember we were once called the "lost genera-tion"? Look at us today: who's laughing now?!... (crickets)... Anyway, being part of this group added the extremely necessary quota of distraction and drama to the PhD

life. I am happy for being part of this generation which definitely set an example for the forthcoming ones.

In particular, I would like to acknowledge my MPIA crew for being a relevant part of my daily life. Bhargav, Gisella, Kasper, Mario, Min, Oliver it's been a pleasure to share every day of the week for three years with you guys. It's been three years complaining about the weather and the canteen food, daily table soccer games, and discussions on whose research is the most problematic. Additional special mentions go to my amazing remaining officemates Vesselina and Somaye, our local bogeyman Roman, fellow groupmember Dading, and lab-partner Alex. Hope to see you all again, either in the next IAU, or at a "someone's" wedding in India, who knows?

The very efficient MPIA staff assisted me many times over these years: Ina Beckmann, Heide Seifert, the Witzels, Uli Hiller, Marco Piroth, Frau Apfel, and the Canteen girls (the food was not their fault).

I would like to thank Thorsten Lisker and Josef Fried for integrating my thesis committee meetings, and also Professors Jochen Heidt, Joachim Wambsganß, and Ulrich Uwer for kindly accepting to integrate my ~~excutioning squad~~ *examination committee*.

While writing a thesis against the clock is stressful, exhausting, and slightly traumatic, it definitely helps to know that there's a good postdoc job waiting for you at the end of the tunnel. Thanks to Johan Knapen and Kartik Sheth for believing in me for this new challenge.

Special thanks to my parents for their support from 12,000 kilometers away, for teaching me the relevance of education, and initiating my way on this path, which 24 years later, I'm more than happy to conclude.

Finally, a very special honorable mention to Sarah, for coping with me during this thesis-writing struggle, being the exact support I needed, and joining me in this new adventure.

# BIBLIOGRAPHY

Abazajian, K., et al. 2003, AJ, 126, 2081

Ammons, S. M., et al. 2011, ApJ, 740, 3

Antonucci, R. 1993, ARA&A, 31, 473

Antonucci, R. R. J., & Miller, J. S. 1985, ApJ, 297, 621

Bahcall, J. N., Kirhakos, S., Saxe, D. H., & Schneider, D. P. 1997, ApJ, 479, 642

Baldry, I. K., Glazebrook, K., Brinkmann, J., Ivezić, Ž., Lupton, R. H., Nichol, R. C., & Szalay, A. S. 2004, ApJ, 600, 681

Ballantyne, D. R., Everett, J. E., & Murray, N. 2006, ApJ, 639, 740

Barnes, J. E., & Hernquist, L. 1996, ApJ, 471, 115

Barnes, J. E., & Hernquist, L. E. 1991, ApJ, 370, L65

Beckwith, S. V. W., et al. 2006, AJ, 132, 1729

Bell, E. F., & de Jong, R. S. 2001, ApJ, 550, 212

Bell, E. F., Phleps, S., Somerville, R. S., Wolf, C., Borch, A., & Meisenheimer, K. 2006, ApJ, 652, 270

Bennert, N., Canalizo, G., Jungwiert, B., Stockton, A., Schweizer, F., Peng, C. Y., & Lacy, M. 2008, ApJ, 677, 846

Bennert, V. N., Auger, M. W., Treu, T., Woo, J.-H., & Malkan, M. A. 2011, ApJL, submitted (ArXiv:1102.1975)

Bennert, V. N., Treu, T., Woo, J.-H., Malkan, M. A., Le Bris, A., Auger, M. W., Gallagher, S., & Blandford, R. D. 2010, ApJ, 708, 1507

Bennett, A. S. 1962, MmRAS, 68, 163

Benson, A. J., Bower, R. G., Frenk, C. S., Lacey, C. G., Baugh, C. M., & Cole, S. 2003, ApJ, 599, 38

Bergvall, N., Laurikainen, E., & Aalto, S. 2003, A&A, 405, 31

Bertin, E., & Arnouts, S. 1996, A&AS, 117, 393

Blanton, M. R., et al. 2003, ApJ, 592, 819

Bongiorno, A., et al. 2010, A&A, 510, A56+

Booth, C. M., & Schaye, J. 2011, MNRAS, 413, 1158

Boroson, T. A., & Green, R. F. 1992, ApJS, 80, 109

Bower, R. G., Benson, A. J., Malbon, R., Helly, J. C., Frenk, C. S., Baugh, C. M., Cole, S., & Lacey, C. G. 2006, MNRAS, 370, 645

Boyle, B. J., & Terlevich, R. J. 1998, MNRAS, 293, L49

Brusa, M., et al. 2007, ApJS, 172, 353

—. 2010, ApJ, 716, 348

Bundy, K., Fukugita, M., Ellis, R. S., Targett, T. A., Belli, S., & Kodama, T. 2009, ApJ, 697, 1369

Bundy, K., et al. 2008, ApJ, 681, 931

—. 2010, ApJ, 719, 1969

Canalizo, G., Bennert, N., Jungwiert, B., Stockton, A., Schweizer, F., Lacy, M., & Peng, C. 2007, ApJ, 669, 801

Canalizo, G., & Stockton, A. 2000, AJ, 120, 1750

—. 2001, ApJ, 555, 719

Capak, P., et al. 2007, ApJS, 172, 99

Cappelluti, N., et al. 2009, A&A, 497, 635

Ciotti, L., & Ostriker, J. P. 2007, ApJ, 665, 1038

Cisternas, M., et al. 2011a, ApJ, 726, 57

—. 2011b, ApJ, 741, L11+

Civano, F., et al. 2010, ApJ, 717, 209

Cole, S., Aragon-Salamanca, A., Frenk, C. S., Navarro, J. F., & Zepf, S. E. 1994, MNRAS, 271, 781

Cole, S., Lacey, C. G., Baugh, C. M., & Frenk, C. S. 2000, MNRAS, 319, 168

Cox, T. J., Dutta, S. N., Di Matteo, T., Hernquist, L., Hopkins, P. F., Robertson, B., & Springel, V. 2006, ApJ, 650, 791

Cox, T. J., Jonsson, P., Somerville, R. S., Primack, J. R., & Dekel, A. 2008, MNRAS, 384, 386

Croton, D. J. 2006, MNRAS, 369, 1808

Croton, D. J., et al. 2006, MNRAS, 365, 11

Daddi, E., et al. 2007, ApJ, 670, 173

de Vaucouleurs, G. 1948, Annales d'Astrophysique, 11, 247

—. 1953, MNRAS, 113, 134

—. 1959, Handbuch der Physik, 53, 311

Decarli, R., Falomo, R., Treves, A., Labita, M., Kotilainen, J. K., & Scarpa, R. 2010, MNRAS, 402, 2453

Di Matteo, P., Bournaud, F., Martig, M., Combes, F., Melchior, A., & Semelin, B. 2008a, A&A, 492, 31

Di Matteo, P., Combes, F., Melchior, A., & Semelin, B. 2007, A&A, 468, 61

Di Matteo, T., Colberg, J., Springel, V., Hernquist, L., & Sijacki, D. 2008b, ApJ, 676, 33

Di Matteo, T., Springel, V., & Hernquist, L. 2005, Nature, 433, 604

Dickinson, M. 1998, in The Hubble Deep Field, ed. M. Livio, S. M. Fall, & P. Madau, 219–+

Disney, M. J., et al. 1995, Nature, 376, 150

Dunlop, J. S., McLure, R. J., Kukula, M. J., Baum, S. A., O'Dea, C. P., & Hughes, D. H. 2003, MNRAS, 340, 1095

Edge, D. O., Shakeshaft, J. R., McAdam, W. B., Baldwin, J. E., & Archer, S. 1959, MmRAS, 68, 37

Elvis, M. 2000, ApJ, 545, 63

Elvis, M., Maccacaro, T., Wilson, A. S., Ward, M. J., Penston, M. V., Fosbury, R. A. E., & Perola, G. C. 1978, MNRAS, 183, 129

Elvis, M., et al. 2009, ApJS, 184, 158

Fath, E. A. 1909, Lick Observatory Bulletin, 5, 71

Feng, J. L. 2010, ARA&A, 48, 495

Ferrarese, L., & Merritt, D. 2000, ApJ, 539, L9

Fiore, F., et al. 2009, ApJ, 693, 447

Fitch, W. S., Pacholczyk, A. G., & Weymann, R. J. 1967, ApJ, 150, L67+

Freeman, K. C. 1970, ApJ, 160, 811

Gabor, J. M., et al. 2009, ApJ, 691, 705

Gebhardt, K., et al. 2000, ApJ, 539, L13

Gehren, T., Fried, J., Wehinger, P. A., & Wyckoff, S. 1984, ApJ, 278, 11

Genel, S., Bouché, N., Naab, T., Sternberg, A., & Genzel, R. 2010, ApJ, 719, 229

Genel, S., et al. 2008, ApJ, 688, 789

Genzel, R., et al. 2008, ApJ, 687, 59

Georgakakis, A., et al. 2009, MNRAS, 397, 623

Ghez, A. M., et al. 2003, ApJ, 586, L127

Giacconi, R., et al. 2001, ApJ, 551, 624

Giavalisco, M., et al. 2004, ApJ, 600, L93

Gilli, R., et al. 2009, A&A, 494, 33

Graham, A. W., Erwin, P., Caon, N., & Trujillo, I. 2001, ApJ, 563, L11

Granato, G. L., De Zotti, G., Silva, L., Bressan, A., & Danese, L. 2004, ApJ, 600, 580

Greene, J. E., et al. 2010, ApJ, 721, 26

Greenstein, J. L., & Matthews, T. A. 1963, AJ, 68, 279

Grogin, N. A., et al. 2003, ApJ, 595, 685

—. 2005, ApJ, 627, L97

Gültekin, K., et al. 2009, ApJ, 698, 198

Gunn, J. E. 1979, in Active Galactic Nuclei, 213–225

Häring, N., & Rix, H. 2004, ApJ, 604, L89

Hasinger, G. 2008, A&A, 490, 905

Hasinger, G., et al. 2007, ApJS, 172, 29

Häussler, B., et al. 2007, ApJS, 172, 615

Hawking, S. W. 1982, Physics Letters B, 115, 295

Heckman, T. M., Bothun, G. D., Balick, B., & Smith, E. P. 1984, AJ, 89, 958

Hernquist, L. 1989, Nature, 340, 687

Ho, L. C. 2007, ApJ, 669, 821

Hopkins, P. F., Cox, T. J., Younger, J. D., & Hernquist, L. 2009, ApJ, 691, 1168

Hopkins, P. F., & Hernquist, L. 2006, ApJS, 166, 1

—. 2009, ApJ, 694, 599

Hopkins, P. F., Hernquist, L., Cox, T. J., Di Matteo, T., Martini, P., Robertson, B., & Springel, V. 2005a, ApJ, 630, 705

Hopkins, P. F., Hernquist, L., Cox, T. J., Di Matteo, T., Robertson, B., & Springel, V. 2006a, ApJS, 163, 1

Hopkins, P. F., Hernquist, L., Cox, T. J., & Kereš, D. 2008, ApJS, 175, 356

Hopkins, P. F., Hernquist, L., Cox, T. J., Robertson, B., & Krause, E. 2007, ApJ, 669, 45

Hopkins, P. F., Hernquist, L., Martini, P., Cox, T. J., Robertson, B., Di Matteo, T., & Springel, V. 2005b, ApJ, 625, L71

Hopkins, P. F., Robertson, B., Krause, E., Hernquist, L., & Cox, T. J. 2006b, ApJ, 652, 107

Hopkins, P. F., et al. 2010, ApJ, 715, 202

Hoyle, F., & Fowler, W. A. 1963, Nature, 197, 533

Hubble, E. P. 1929, ApJ, 69, 103

Hutchings, J. B., Crampton, D., Campbell, B., Duncan, D., & Glendenning, B. 1984, ApJS, 55, 319

Hutchings, J. B., Johnson, I., & Pyke, R. 1988, ApJS, 66, 361

Hutchings, J. B., & Neff, S. G. 1992, AJ, 104, 1

Ilbert, O., et al. 2009, ApJ, 690, 1236

—. 2010, ApJ, 709, 644

Inskip, K. J., Jahnke, K., Rix, H.-W., & van de Ven, G. 2011, ApJ, in press (ArXiv:1103.6026)

Jahnke, K., Kuhlbrodt, B., & Wisotzki, L. 2004a, MNRAS, 352, 399

Jahnke, K., & Macciò, A. V. 2011, ApJ, 734, 92

Jahnke, K., et al. 2004b, ApJ, 614, 568

—. 2009, ApJ, 706, L215

Jogee, S. 2006, in Lecture Notes in Physics, Berlin Springer Verlag, Vol. 693, Physics of Active Galactic Nuclei at all Scales, ed. D. Alloin, 143–+

Jogee, S., et al. 2009, ApJ, 697, 1971

Karim, A., et al. 2011, ApJ, 730, 61

Kartaltepe, J. S., et al. 2010, ApJ, 721, 98

Kaspi, S., Smith, P. S., Netzer, H., Maoz, D., Jannuzi, B. T., & Giveon, U. 2000, ApJ, 533, 631

Kauffmann, G., Colberg, J. M., Diaferio, A., & White, S. D. M. 1999, MNRAS, 303, 188

Kauffmann, G., & Haehnelt, M. 2000, MNRAS, 311, 576

Kauffmann, G., White, S. D. M., & Guiderdoni, B. 1993, MNRAS, 264, 201

Kauffmann, G., et al. 2003, MNRAS, 346, 1055

Kereš, D., Katz, N., Fardal, M., Davé, R., & Weinberg, D. H. 2009, MNRAS, 395, 160

Kereš, D., Katz, N., Weinberg, D. H., & Davé, R. 2005, MNRAS, 363, 2

Khachikian, E. Y., & Weedman, D. W. 1974, ApJ, 192, 581

Kim, M., Ho, L. C., Peng, C. Y., Barth, A. J., & Im, M. 2008, ApJS, 179, 283

Knapen, J. H., Shlosman, I., & Peletier, R. F. 2000, ApJ, 529, 93

Koekemoer, A. M., Fruchter, A. S., Hook, R. N., & Hack, W. 2002, in The 2002 HST Calibration Workshop : Hubble after the Installation of the ACS and the NICMOS Cooling System, ed. S. Arribas, A. Koekemoer, & B. Whitmore, 337–+

Koekemoer, A. M., et al. 2007, ApJS, 172, 196

Komatsu, E., et al. 2011, ApJS, 192, 18

Kormendy, J., & Kennicutt, Jr., R. C. 2004, ARA&A, 42, 603

Kormendy, J., & Richstone, D. 1995, ARA&A, 33, 581

Krist, J. 2003, ACS WFC & HRC fielddependent PSF variations due to optical and

charge diffusion effects, Tech. rep.

Lauer, T. R., Tremaine, S., Richstone, D., & Faber, S. M. 2007, ApJ, 670, 249

Leauthaud, A., et al. 2007, ApJS, 172, 219

Levenson, N. A., Heckman, T. M., Krolik, J. H., Weaver, K. A., & Życki, P. T. 2006, ApJ, 648, 111

Li, Y., Wang, J., Yuan, Y., Hu, C., & Zhang, S. 2010, ApJ, 710, 878

Lilly, S. J., et al. 2007, ApJS, 172, 70

Lin, L., et al. 2008, ApJ, 681, 232

Lintott, C. J., et al. 2008, MNRAS, 389, 1179

Lotz, J. M., Jonsson, P., Cox, T. J., & Primack, J. R. 2008, MNRAS, 391, 1137

Lusso, E., & Ciotti, L. 2010, arXiv:1009.5292

Lusso, E., et al. 2010, A&A, 512, A34+

Lynden-Bell, D. 1969, Nature, 223, 690

Magorrian, J., et al. 1998, AJ, 115, 2285

Mainieri, V., et al. 2007, ApJS, 172, 368

Malkan, M. A., Gorjian, V., & Tam, R. 1998, ApJS, 117, 25

Marconi, A., & Hunt, L. K. 2003, ApJ, 589, L21

Marconi, A., Risaliti, G., Gilli, R., Hunt, L. K., Maiolino, R., & Salvati, M. 2004, MNRAS, 351, 169

Martini, P. 2004a, in Coevolution of Black Holes and Galaxies, ed. L. C. Ho (Cambridge: Cambridge University Press), 169

Martini, P. 2004b, in IAU Symposium, Vol. 222, The Interplay Among Black Holes, Stars and ISM in Galactic Nuclei, ed. T. Storchi-Bergmann, L. C. Ho, & H. R. Schmitt, 235–241

Matthews, T. A., & Sandage, A. R. 1963, ApJ, 138, 30

McLure, R. J., Jarvis, M. J., Targett, T. A., Dunlop, J. S., & Best, P. N. 2006, MNRAS, 368, 1395

Merloni, A., et al. 2010, ApJ, 708, 137

Mihos, J. C., & Hernquist, L. 1996, ApJ, 464, 641

Miller, J. D. 2004, Public Understanding of Science, 13, 273

Miyaji, T., Griffiths, R. E., & C-COSMOS Team. 2008, in AAS/High Energy Astrophysics Division, Vol. 10, AAS/High Energy Astrophysics Division 10, 04.01–+

More, A., Jahnke, K., More, S., Gallazzi, A., Bell, E. F., Barden, M., & Häußler, B. 2011, ApJ, 734, 69

Moustakas, J., & Kennicutt, Jr., R. C. 2006, ApJS, 164, 81

Mushotzky, R. 2004, in Astrophysics and Space Science Library, Vol. 308, Super-

massive Black Holes in the Distant Universe, ed. A. J. Barger, 53–+

Osterbrock, D. E. 1978, Proceedings of the National Academy of Science, 75, 540

Padilla, N. D., & Baugh, C. M. 2003, MNRAS, 343, 796

Parry, O. H., Eke, V. R., & Frenk, C. S. 2009, MNRAS, 396, 1972

Patterson, F. S. 1940, Harvard College Observatory Bulletin, 914, 9

Peacock, J. A. 1991, MNRAS, 253, 1P

Peebles, P. J. E. 1980, The large-scale structure of the universe, ed. Peebles, P. J. E.

Peng, C. Y. 2007, ApJ, 671, 1098

Peng, C. Y., Ho, L. C., Impey, C. D., & Rix, H. 2010, AJ, 139, 2097

Peng, C. Y., Ho, L. C., Impey, C. D., & Rix, H.-W. 2002, AJ, 124, 266

Peng, C. Y., Impey, C. D., Ho, L. C., Barton, E. J., & Rix, H.-W. 2006a, ApJ, 640, 114

Peng, C. Y., Impey, C. D., Rix, H.-W., Kochanek, C. S., Keeton, C. R., Falco, E. E., Lehár, J., & McLeod, B. A. 2006b, ApJ, 649, 616

Percival, W. J., et al. 2007, ApJ, 657, 645

Perlmutter, S., et al. 1999, ApJ, 517, 565

Peterson, B. M. 1993, PASP, 105, 247

Peterson, B. M., et al. 2004, ApJ, 613, 682

Pierce, C. M., et al. 2007, ApJ, 660, L19

Porciani, C., Magliocchetti, M., & Norberg, P. 2004, MNRAS, 355, 1010

Press, W. H., & Schechter, P. 1974, ApJ, 187, 425

Press, W. H., Teukolsky, S. A., Vetterling, W. T., & Flannery, B. P. 1992, Numerical recipes in C (2nd ed.): the art of scientific computing (New York, NY, USA: Cambridge University Press)

Ramos Almeida, C., Tadhunter, C. N., Inskip, K. J., Morganti, R., Holt, J., & Dicken, D. 2011a, MNRAS, 410, 1550

Ramos Almeida, C., et al. 2011b, ApJ, 731, 92

Reichard, T. A., Heckman, T. M., Rudnick, G., Brinchmann, J., Kauffmann, G., & Wild, V. 2009, ApJ, 691, 1005

Rhodes, J. D., et al. 2007, ApJS, 172, 203

Richstone, D., et al. 1998, Nature, 395, A14+

Riess, A. G., et al. 1998, AJ, 116, 1009

Rix, H., et al. 2004, ApJS, 152, 163

Robaina, A. R., Bell, E. F., van der Wel, A., Somerville, R. S., Skelton, R. E., McIntosh, D. H., Meisenheimer, K., & Wolf, C. 2010, ApJ, 719, 844

Robaina, A. R., et al. 2009, ApJ, 704, 324

Robertson, B., Hernquist, L., Cox, T. J., Di Matteo, T., Hopkins, P. F., Martini, P., & Springel, V. 2006, ApJ, 641, 90

Salvato, M., et al. 2009, ApJ, 690, 1250

Salviander, S., Shields, G. A., Gebhardt, K., & Bonning, E. W. 2007, ApJ, 662, 131

Sánchez, S. F., et al. 2004, ApJ, 614, 586

Sanders, D. B., & Mirabel, I. F. 1996, ARA&A, 34, 749

Sanders, D. B., Soifer, B. T., Elias, J. H., Madore, B. F., Matthews, K., Neugebauer, G., & Scoville, N. Z. 1988a, ApJ, 325, 74

Sanders, D. B., Soifer, B. T., Elias, J. H., Neugebauer, G., & Matthews, K. 1988b, ApJ, 328, L35

Scarlata, C., et al. 2007, ApJS, 172, 406

Schade, D. J., Boyle, B. J., & Letawsky, M. 2000, MNRAS, 315, 498

Schawinski, K., Dowlin, N., Thomas, D., Urry, C. M., & Edmondson, E. 2010, ApJ, 714, L108

Schechter, P. 1976, ApJ, 203, 297

Schmidt, M. 1963, Nature, 197, 1040

—. 1969, ARA&A, 7, 527

Schneider, D. P., et al. 2007, AJ, 134, 102

Schödel, R., et al. 2002, Nature, 419, 694

Schramm, M., Wisotzki, L., & Jahnke, K. 2008, A&A, 478, 311

Scoville, N., et al. 2007a, ApJS, 172, 1

—. 2007b, ApJS, 172, 38

Sérsic, J. L. 1968, Atlas de galaxias australes, ed. J. L. Sersic

Seyfert, C. K. 1943, ApJ, 97, 28

Shankar, F., Salucci, P., Granato, G. L., De Zotti, G., & Danese, L. 2004, MNRAS, 354, 1020

Shen, J., Vanden Berk, D. E., Schneider, D. P., & Hall, P. B. 2008, AJ, 135, 928

Shen, Y., et al. 2007, AJ, 133, 2222

Shields, G. A., Gebhardt, K., Salviander, S., Wills, B. J., Xie, B., Brotherton, M. S., Yuan, J., & Dietrich, M. 2003, ApJ, 583, 124

Shields, G. A., Menezes, K. L., Massart, C. A., & Vanden Bout, P. 2006, ApJ, 641, 683

Silk, J., & Rees, M. J. 1998, A&A, 331, L1

Silverman, J. D., et al. 2008, ApJ, 675, 1025

Simard, L., et al. 2002, ApJS, 142, 1

Simkin, S. M., Su, H. J., & Schwarz, M. P. 1980, ApJ, 237, 404

Simmons, B. D., & Urry, C. M. 2008, ApJ, 683, 644

Slipher, V. M. 1917, Lowell Observatory Bulletin, 3, 59

Smoot, G. F., et al. 1992, ApJ, 396, L1

Soltan, A. 1982, MNRAS, 200, 115

Somerville, R. S., Hopkins, P. F., Cox, T. J., Robertson, B. E., & Hernquist, L. 2008, MNRAS, 391, 481

Somerville, R. S., & Primack, J. R. 1999, MNRAS, 310, 1087

Somerville, R. S., Primack, J. R., & Faber, S. M. 2001, MNRAS, 320, 504

Springel, V. 2000, MNRAS, 312, 859

Springel, V., Di Matteo, T., & Hernquist, L. 2005a, MNRAS, 361, 776

Springel, V., & Hernquist, L. 2005, ApJ, 622, L9

Springel, V., et al. 2005b, Nature, 435, 629

Stockton, A. 1982, ApJ, 257, 33

Stockton, A., & Ridgway, S. E. 1991, AJ, 102, 488

Surace, J. A., & Sanders, D. B. 1999, ApJ, 512, 162

Surace, J. A., Sanders, D. B., & Evans, A. S. 2000, ApJ, 529, 170

Surace, J. A., Sanders, D. B., Vacca, W. D., Veilleux, S., & Mazzarella, J. M. 1998, ApJ, 492, 116

Tal, T., van Dokkum, P. G., Nelan, J., & Bezanson, R. 2009, AJ, 138, 1417

Taniguchi, Y. 1999, ApJ, 524, 65

Toomre, A. 1977, in Evolution of Galaxies and Stellar Populations, ed. B. M. Tinsley & R. B. Larson, 401

Toomre, A., & Toomre, J. 1972, ApJ, 178, 623

Treister, E., et al. 2004, ApJ, 616, 123

Tremaine, S., et al. 2002, ApJ, 574, 740

Treu, T., Malkan, M. A., & Blandford, R. D. 2004, ApJ, 615, L97

Treu, T., Woo, J.-H., Malkan, M. A., & Blandford, R. D. 2007, ApJ, 667, 117

Trump, J. R., et al. 2007, ApJS, 172, 383

—. 2009a, ApJ, 696, 1195

—. 2009b, ApJ, 700, 49

—. 2011, ApJ, 733, 60

Ueda, Y., Akiyama, M., Ohta, K., & Miyaji, T. 2003, ApJ, 598, 886

Urrutia, T., Lacy, M., & Becker, R. H. 2008, ApJ, 674, 80

Urry, C. M., & Padovani, P. 1995, PASP, 107, 803

van der Wel, A., Rix, H., Holden, B. P., Bell, E. F., & Robaina, A. R. 2009, ApJ, 706, L120

Veilleux, S., et al. 2009, ApJS, 182, 628

Vestergaard, M., & Peterson, B. M. 2006, ApJ, 641, 689

Volonteri, M., Haardt, F., & Madau, P. 2003, ApJ, 582, 559

Wada, K. 2004, Coevolution of Black Holes and Galaxies, 186

Walter, F., Carilli, C., Bertoldi, F., Menten, K., Cox, P., Lo, K. Y., Fan, X., & Strauss, M. A. 2004, ApJ, 615, L17

Weedman, D. W. 1976, ApJ, 208, 30

Weinzirl, T., Jogee, S., Khochfar, S., Burkert, A., & Kormendy, J. 2009, ApJ, 696, 411

White, S. D. M., & Rees, M. J. 1978, MNRAS, 183, 341

Williams, R. E., et al. 1996, AJ, 112, 1335

Woltjer, L. 1959, ApJ, 130, 38

Woo, J.-H., Treu, T., Malkan, M. A., & Blandford, R. D. 2006, ApJ, 645, 900

—. 2008, ApJ, 681, 925

Wyithe, J. S. B., & Loeb, A. 2003, ApJ, 595, 614

Yu, Q., & Tremaine, S. 2002, MNRAS, 335, 965

Zakamska, N. L., et al. 2006, AJ, 132, 1496

Zel'Dovich, Y. B. 1970, A&A, 5, 84

Zel'Dovich, Y. B., & Novikov, I. D. 1965, Soviet Physics Doklady, 9, 834

Zwicky, F. 1933, Helvetica Physica Acta, 6, 110